Transportable Mass Spectrometry and NMR instruments for in-situ chemical reaction monitoring and real time analysis

CHRISTOPHER ALUN WHITMORE

University of Durham

Department of Chemistry

Transportable Mass Spectrometry and NMR instruments for in-situ chemical reaction monitoring and real time analysis

A thesis submitted in partial fulfilment of the requirements for the degree of Doctor of Philosophy

Christopher Alun Whitmore

2020

Contents

I. Material Abstract

An on-line reaction monitoring system consisting of transportable NMR and MS instruments has been designed and validated for a number of chemical reactions, each reaction posing a different set of analytical challenges. The designed configuration consists of two instruments, a nominal mass single quadrupole electrospray mass spectrometer (QDa, Waters Corp.) and a 43 MHz permanent magnet NMR spectrometer (SpinSolve, Magritek) fitted with flow cell. These two instruments were coupled together with a Mass Rate Attenuator providing the dilution required to bridge the gap between the concentration used in the NMR and that required for the mass spectrometer.

The utility of the system has been demonstrated for a number of chemical reactions, and the capabilities of the system with regard to solvent systems and temperatures of the reaction determined. The benefits of combining two orthogonal analytical techniques for reaction monitoring is clearly demonstrated, with the low field NMR and nominal mass MS instruments each shown to be able to compensate for the limitations of the other. Here, the NMR is shown to detect the presence of, and degree of, ion suppression in the mass spectrometer was demonstrated and validated against standard isotopic labelling based techniques, while methods to overcome the presence of solvent signals in the NMR were trialled.

^{19}F reaction monitoring on the Spinsolve was demonstrated for the first time, with the sensitivity of the instrument for fluorine monitoring established and the results of the monitoring validated against those achieved by mass spectrometry, producing kinetic data which agreed within the margin of error.

A transportable ASAP MS device was trialled for the analysis of toxicological samples and was shown to be capable of identifying compounds in seized drug samples, including mixed samples, and of operating outside of a laboratory environment using ambient air.

II. Abbreviations list

AC - Alternating current

ASAP – Atmospheric Solids Analysis Probe

CEM – Chain Ejection Model

CI – Chemical ionisation

CID – Collision induced dissociation

CRM – Charge Residue Model

DART – Direct Analysis in Real Time

DC - Direct current

EI – Electron ionisation

ESI – Electrospray ionisation

FAB – Fast Atom Bombardment ionisation

FID – Free Induction Decay

FDA – Food and drug administration (USA)

FTICR - Fourier transform-ion cyclotron resonance

GC - Gas chromatography

HPLC - High performance liquid chromatography

IEM – Ion Evaporation Model

IR - Infrared spectroscopy

LC - Liquid chromatography

MALDI- MatrixAssisted Laser Desorption/Ionisation

MIMS – Membrane Introduction Mass Spectrometry

MRA – Mass rate attenuator

MS - Mass spectrometry

MS/MS – Tandem Mass spectrometry

NIR – Near Infrared spectroscopy

NMR - Nuclear magnetic resonance

PEEK - Polyether ether ketone

QqQ - Triple quadrupole

rf - Radio frequency

SIM – Selected Ion Monitoring

TIC – Total Ion Chromatogram

ToF - Time-of-flight

UV-Vis - Ultraviolet-visible spectroscopy

III. Figure list

IV. Declaration

The work presented herein was carried out in the Department of Chemistry at Durham University between October 2015 and June 2019. High field ^{19}F NMR work was carried out at AstraZeneca, Macclesfield over two days. Unless otherwise stated all work is my own and has not been submitted previously for a qualification at this or any other university.

V. Statement of copyright

1 Introduction

1.1 Analytical approaches to chemical reaction monitoring

The area of chemical reaction and chemical process monitoring for pharmaceutical production is, and has been for some time, the focus of much research and an area of great interest to industrial chemists. Traditionally, analysis on pharmaceutical compounds has been conducted off-line, with samples removed to a laboratory and tested using methods with a turnaround time often measured in hours. More recently, however, there has been an increased focus on 'on-line' and 'in-line' analytics. The benefits of rapid and frequent measurements has shown itself useful for process understanding, providing data more representative of conditions in the process itself, and for process control by providing feedback on a timescale that allows control systems to intervene effectively when the process is moving out of specification. These analytics eliminate the requirement for manual handling of the sample and allow for much more frequent sampling. As such, techniques with shorter duty cycles are favourable: while a 15 minute HPLC (High Performance Liquid Chromatography) method may be a perfectly acceptable method for analysis of a sample which has been taken by hand, if sampling is automated then a greater amount of information may be easily obtained by rapid analysis of frequent samples.

The increasing trend towards flow chemistry and continuous manufacturing of compounds has helped place greater importance on the monitoring of processes, and end-of-line testing does not always provide a satisfactory degree of control. In a more traditional batch process, should there be a deviation from desired conditions, it will at worst produce a failed batch. This is not a negligible problem, but remains an acceptable loss in many processes, with the problem being fixed once detected through off-line, *post hoc* testing. In a continuous or flow process, the need for continuous monitoring is much greater as the nature of a continuous process does not allow discrete batches to be differentiated easily, meaning that out of specification conditions can easily persist between

notional batches, and there is no downtime for resetting equipment as there would be in a batch production process.

Process monitoring techniques may be split into the following categories[1]: 'off-line', characterised by manual sampling and transport to an separate laboratory away from the process stream; 'at-line', involving discontinuous or manual sampling and analysis with equipment local to the process stream; 'on-line, involving automated sampling and analysis local to the process stream, and 'in-line' involving the direct measurement of material in the process stream without the need for sampling or transport.

A wide variety of process monitoring techniques have been trialled and implemented, ranging from the most basic process monitors such as temperature and pressure monitors to far more complex and information rich monitoring solutions including a range of light based spectroscopies[2]. The spectroscopic techniques are usually based on calibrations from an external set of reference data, either through tracking of single peaks (e.g. common in Raman, UV and mid-infrared[2]) or through the analysis of multiple peaks or signal regions using multivariate calibrations, used to derive quantitative data for multiple components based on trends which may not be readily recognisable to a manual interrogation of the spectra through the analysis of multiple signals or ranges thereof.

Multivariate models are particularly useful with techniques such as near infrared spectroscopy which do not produce data that is simple to interpret, though such models may be readily applied to many techniques including mid infrared[3], UV-Vis[4] and Raman[5] data. However, there are limitations to such models, in that the information input is often not easily interpreted by a human, with numerous components across wide areas of signal intensity on techniques like near-infrared spectroscopy being used to give quantitative results which may or may not be the direct result of the analyte in question. Developers of such models must therefore take a great deal of care to ensure that regions selected make chemical sense and that they endeavour to understand the connection between

regions which produce models with good predictive capabilities and the actual features of the spectrum which are causing them.

While multivariate calibrations do provide a good opportunity to increase process understanding, they are limited, in that they can only ever analyse information accessible to the reference technique, which, being an off-line method, cannot include any intermediates which are not stable enough to survive quenching and the delay between sampling and off-line measurement. This limits their ability to give an understanding of what is actually happening in the reaction vessel. Mass spectrometry[6] and NMR spectroscopy[7] have been demonstrated as direct solutions for reaction monitoring which are not based on such black box methods.

The use of on- and in-line analytical techniques has been brought to the forefront in pharmaceutical chemistry in part due to the United States Food and Drug Administration (FDA) guidelines on process analytical technology, which they define as *'a system for designing, analyzing, and controlling manufacturing through timely measurements (i.e., during processing) of critical quality and performance attributes of raw and in-process materials and processes, with the goal of ensuring final product quality*.'[8] The FDA definition lends itself to the splitting of process monitoring into two broad categories: firstly monitoring for understanding, a largely laboratory-side process where a great deal of detailed information on the reaction is collected to determine what is actually happening inside the reaction vessel and what critical quality attributes can be determined and monitored; and secondly, monitoring from control where critical quality attributes are monitored and the resulting information is fed back either for regulatory purposes or, preferably, for the purpose of intervention in the process.

Monitoring for control and for understanding, while sharing requirements for certain characteristics including good sensitivity, selectivity, and accuracy[9], place differing importance on certain other characteristics. One example of these differing priorities is the level of downtime required for routine maintenance, as, where a focussed research group may tolerate a system which requires

weekly or monthly shutdowns for cleaning or recalibration, the same requirements could represent an intolerable loss of operating time in a manufacturing plant, especially in continuous manufacturing applications. Conversely, concerns such as instrument cost and instrument flexibility, with regards to responding to a diverse range of processes, are of relatively minor importance for manufacturing solutions. In such cases, capital expenditure budgets are relatively large and can accommodate instruments purchased for dedicated and singular purposes.

1.1.1 Mass spectrometry in reaction monitoring

Mass spectrometry (MS) has been used for on-line monitoring, with magnetic sector based instruments relying on electron ionisation (EI) having been employed in industrial applications since approximately 1975[10]. These systems relied on gas-phase sample introduction and often included gas chromatography (GC) to reduce the complexity of the sample inlet. These sector-based instruments were very large and required highly specialised operation and maintenance, meaning that installing them in a manufacturing environment would represent a significant engineering challenge, requiring skilled operators and modification of the facilities to prevent vibration from industrial equipment from damaging the instrument. The duty cycle, especially when used in conjunction with GC, is significantly slower than that of light-based measurements, on the order of minutes rather than seconds.

The use of EI generally results in multiple signals for each component, an issue which can, in more modern systems where computer power allows, be mitigated by multivariate calibration to deal with the spectral complexity, but which presented a significant barrier to usefulness for of EI prior to this computer power becoming common, as diagnostic ions were not always easily separated from the many ions produced. It is perhaps due to these limitations, along with the size, maintenance requirements, reliability and requirement for highly skilled operators of the sector instruments that lead to a relatively poor uptake of MS in this role relative to light-based techniques over the

following decades. However, as time went on more effort was made to develop MS instruments specifically geared towards process monitoring, notably sacrificing high mass resolution in favour of reliability, robustness and practical considerations on size and cost. By the late 1990s, as computer power increased and smaller, more robust instruments became commercially available, the uptake of MS in process monitoring improved, with quadrupole based instruments becoming the most common in this application[11], though ion traps[12] were also coming into use in these applications. Sample introduction at this point relied mainly on the use of direct capillary inlets for the monitoring of gases and of membrane introduction mass spectrometry (MIMS) for monitoring volatile organic compounds in solution. MIMS functions by flowing analyte containing solution across a semipermeable membrane, allowing volatiles to partition into the membrane, and through that into the gas phase region of the mass spectrometer[13]. MIMS was used in a wide variety of monitoring applications, including monitoring of chemical reactions[14], environmental monitoring[15] and monitoring of bioreactors[12], though MIMS was ultimately constrained by three main factors: firstly, not all compounds would permeate through any given membrane; secondly, the rate at which compounds permeate through the membrane limited temporal resolution and thirdly, the restriction to small volatile analytes common to EI. Attempts were later made to overcome these issues through the use of a hollow fibre membrane interface between the aqueous reaction mixture and a methanol acceptor phase coupled to an electrospray ionisation (ESI) source, allowing less volatile, more polar and larger analytes to be monitored with high sensitivity[16].

Meanwhile, in research applications, a number of techniques were emerging which were capable of coupling liquid reaction mixtures directly to mass spectrometer. Thermospray, a technique based on flowing solvent through a thin heated capillary and ionising the resulting aerosolised droplets with a low-current discharge pin[17], was successfully coupled to electrochemical reactors and used to monitor redox reactions[18,19].

Fast atom bombardment (FAB) ionisation, a technique based on ionisation of samples in a liquid matrix through the impact of a beam of neutral atoms[20], usually xenon or argon, was coupled to biochemical reactors both through the use of a flow injection setup whereby 1 µL aliquots were dosed onto the sample stage of the FAB instrument and by the slow continuous introduction of sample through a narrow bore silica capillary, relying on atmospheric pressure to drive the introduction of the sample rather than involving pumps[21]. The requirement to keep the sample stage 'wet' with liquid matrix meant the technique was particularly well suited to biological reactions where a significant percentage of a viscous compound like glycerol was present in the sample and would prove a limitation in systems with less viscous solvents, though this technique was extremely difficult for even highly skilled users to implement in practice regardless of the reaction under investigation.

Electrospray ionisation mass spectrometry, though first described in 1968 by Malcolm Dole[22] became a widespread and popular technique after the work of John Fenn in the 1980s and 1990s, for which he shared in the 2002 Nobel prize for chemistry[23]. With the ability for electrospray to produce, like FAB, spectra which predominantly contain one ion per analyte representative of intact molecules, though from direct injection of condensed-phase analyte solutions, and to ionise polar species which are not as easily ionised by techniques which rely on moving the analyte into the gas-phase before ionisation occurs, electrospray lends itself well to reaction monitoring.

Sample introduction methods varied widely, from syringe reactors directly attached to the instrument used to monitor protein folding[24] to the development of more complex and versatile systems such as that demonstrated by Dell'Orco and Brum[25,26]. Their system, which served as inspiration for the MS system used in this work, relied on the sampling of reaction liquor into a flow of MS compatible solvent for introduction into the MS instrument. They achieved this by using tubing with different diameters and a pump to provide a make-up solvent such that larger diameter tubing and faster flow from the make-up solvent resulted in a significant dilution of the reaction

liquor prior to its introduction to the instrument. This approach was built upon and refined by Bristow and Ray[27], using a mass rate attenuator, a device for continuously switching small aliquots from one flow path to another, to couple a chip reactor to a small-footprint ESI-MS instrument to monitor the effects of various conditions on the flow reaction.

Numerous other interfaces for on-line ESI reaction monitoring have been developed, with notable examples including ultrasonication of a vial containing a capillary to facilitate the transfer of the sample by Chen *et al.*[28,29]. Sonication provides the energy to push the sample through the ESI capillary and assists in spray formation. The use of inductive ESI by the group of Prof. Graham Cooks[30]to monitor air sensitive systems from a highly concentrated salt solution uses a strong pulsed positive DC voltage and an overpressure of helium gas to generate bursts of charged droplets and transfer them through a capillary into the ESI source.

A number of other ambient ionisation techniques have been used with a huge variety of methods for sample introduction, a particularly ingenious example being the use of pulley systems moving nylon thread through a slurry for transport into a modified Direct Analysis in Real Time ion source (DART), which functioned by bombarding a sample under atmospheric pressure with ionised nitrogen (in place of the more usual dry helium) and atmospheric water through the spraying of metastable high energy carrier gas formed by glow discharge, resulting in chemical ionisation of the sample at atmospheric pressure.[31] This had the advantage of allowing direct sampling from a liquid reaction without the use of any pumping equipment, potentially useful in situations where the reaction medium is not amenable to pump transfer.

Atmospheric Pressure Chemical Ionisation (APCI) has also been used with significant success, with a notable example being the use of on-line APCI to develop a self-optimising reactor system by the group of Prof. Richard Bourne[32]. By coupling an automated flow reactor to the MS instrument and setting the program to vary multiple criteria, it was possible to create a multidimensional model of the factors affecting yield, including dwell times, concentrations of various reagents and

temperature, and then have the system independently establish optimised reaction conditions with results rivalling those of human-run optimisation experiments in a much less labour and time intensive fashion. The use of APCI in this context allows for a wide range of compounds to be ionised, as APCI can ionise less polar analytes more effectively than the more common ESI.

A series of review papers has covered this area in greater detail, with the reviews by Fabris[33] and Ray *et al.*[6] providing between them an excellent summary of the field over the last 20 to 30 years.

1.1.2 NMR in reaction monitoring

NMR has numerous qualities which are desirable to process monitoring. It is a non-invasive, non-destructive technique capable of providing a wealth of chemical information and is amenable to almost all molecules likely to be encountered in a process. Despite these desirable characteristics, NMR has not yet seen widespread use as an in-line industrial sensor[34]. Several explanations are offered for this, including its inherently low sensitivity, the cost and inconvenience of cryogens for superconducting magnets associated with the majority of NMR instruments, and the relatively slow measurement speed, which can be on the order of seconds to minutes depending on the conditions and experiment. NMR has, however, proven to be an excellent tool for off-line process understanding, serving as a, if not the, primary analytical technique for a large proportion of synthetic chemists.

There have been many developments over the years to replace the traditional static NMR tubes with a probe that has the capability to flow a solution through the NMR magnet while emulating the NMR tube in the measurement volume. These include stopped flow adapters for NMR tubes[35] and various specially designed flow cells[36,37]. Both of these approaches enable the use of a high field NMR instrument to monitor a reaction without manual sampling or external sample preparation, though there remain significant issues with conducting a chemical reaction in this fashion. Only chemical reactions that progress at, or close to room temperature can be followed, the reaction cannot be

stirred and cannot easily be conducted inside a fume-hood. If a reaction is not conducive to these restrictions then a significant length of tubing will need to connect the NMR flow tube to an area away from the NMR magnet, which introduces different practical limitations, and does not overcome the issue of temperature sensitive reactions.

The use of high field NMR to obtain a kinetic profile for a reaction has been demonstrated through a number of techniques, including simply conducting the reaction inside a standard NMR tube, and was found to produce markedly different results depending on the nature of the tube or flow cell used[38]. It was suggested that the differences in the reported kinetics were due to the inherent mixing effects, or lack thereof, in tube-based monitoring, monitoring of standard NMR tubes with (ii) periodic inversion of the NMR tube to introduce mixing and (iii) continuous flow adaptation, and it was concluded that the on-line continuous flow technique provided the most accurate kinetic data for the reaction.

The use of smaller footprint, low field NMR instruments for process monitoring has been reported[7,39] which allows for flow NMR to be conducted in a fume hood, in effect allowing the monitoring to be taken to the reaction rather than vice-versa.

Process monitoring by quantitative NMR has also been reported[40], though the requirement for an internal standard and the manual sample preparation involved means that this is, as reported, strictly an off-line or at-line technique.

1.1.3 Combined analytical techniques for reaction monitoring

Combination of multiple techniques can allow for better determination of reaction characteristics. There are reported uses of multiple simultaneous reaction monitoring techniques on a single process to aid process understanding, for example the use of mass spectrometry for headspace gas monitoring and infrared spectroscopy for monitoring of the liquid phase of a distillation for endpoint

determination as described in the review by Chanda *et al.*[41]. Both techniques provided a clear indication of endpoint, and more importantly from an industry perspective, demonstrated a property of the process suitable for determining reaction completion with a simple and robust solution. In the case of the reaction in which mass spectrometry was used to develop process understanding, it was determined that, as the reaction evolved ammonia as a gas, it was possible to monitor reaction completion by simply monitoring the pressure in the reaction vessel, and so the relatively complex mass spectrometric technique used to develop process understanding was then used to validate a much simpler pressure-based monitoring technique to be used once the process was well understood. The concept of using complex instrumentation to provide information rich data at the development stage to gain an understanding of the process understanding which is then used to replace the complex instrumentation with simpler pieces of equipment which are more likely to withstand the rigours of a manufacturing environment demonstrates the differing priorities of the understanding and control functions of monitoring, and the way that the former can feed into the latter.

The combination of multiple techniques was also successfully used to monitor an esterification reaction[42]. In this example in-line mid infrared spectroscopy was combined with a vaporiser connected mass spectrometer designed for gas analysis. Off-line gas chromatography (GC) measurements were used as references for a partial least squares model with the mid-infrared (MIR) spectra, and a separate classical least squares multivariate model using pure component spectra of the reagents, products and catalyst. The mid-infrared and mass spectrometric measurements showed good agreement to each other and to the reference GC method, though the vaporiser method would not be applicable to reactions with components which are either non-volatile or not thermally stable over the temperature range used. The combination of two essentially different ways of looking for a analyte of interest, these being mass based as provided by the mass spectrometer and chemical bond based, as provided by the mid infrared allowed for distinctions not available to a purely bond based monitoring technique, as the ability of the MS instrument to

distinguish between the chosen reagents and products chemically similar contaminants was noted, whereas the mid-infrared method was not able to readily distinguish between ethanol and butan-1-ol.

1.1.4 Transportable instrumentation

The ability to bring analytical instruments out of a dedicated analytical laboratory and to the chemical process to be monitored has found applications beyond the area of reaction monitoring, with transportable analytical systems being deployed throughout modern society, including the ion-mobility based instruments used to detect explosives in airports[43] and a wide variety of portable 'non-laboratory' light based spectroscopic instruments[44]. The goal with such instruments is to produce a rugged instrument which can be quickly deployed in a non-laboratory environment, and so must be tolerant to conditions of ambient temperature, moisture and vibration beyond those which would be normally expected in a laboratory, as well as functioning without access to specialised infrastructure like negative pressure exhausts, specialised power supplies, cooling systems, air compressors or laser safety requirements and needing to be physically small and light enough to allow for transportation without large amounts of specialised equipment.

1.2 Project Aims

The introduction to the market of reliable, transportable MS and NMR systems represents an opportunity to expand the 'toolkit' of available monitoring systems and to allow for a combined monitoring technique not previously explored to be constructed and considered. This work seeks to construct and characterise that combined transportable MS and NMR technique, and in doing so to determine the utility and limitations of such a system as means of process monitoring

2 Instrumentation

2.1 Mass Spectrometry

Mass spectrometry (MS) is a term used for a wide variety of analytical techniques that provide measurement of compounds by the means of separating and detecting charged particles based on their mass-to-charge ratio. One area of great innovation has been in the development of technology to generate these gas-phase ions for the widest range of chemical compounds. To date a large variety of ionisation methods are commercially available, with the most common listed in Figure 2-1.

Figure 2-1 shows an approximate means of characterising these techniques, according to the amount of energy imparted to an analyte molecule during the ionisation process. This ranges from 'hard' ionisation techniques where the energy involved in ionisation causes dissociation of the ion to 'soft' ionisation techniques where the analyte ion remains largely intact.

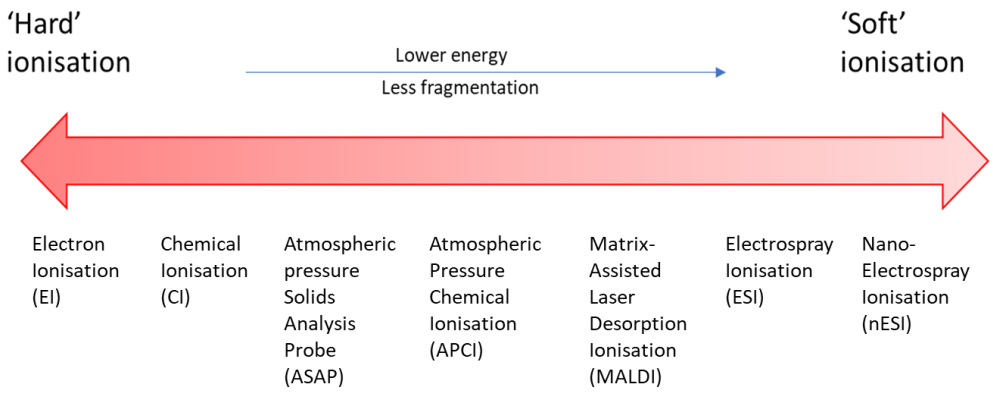

Figure 2-1 Ranking by ionisation 'Hardness' for selected common ionisation methods

Electron ionisation was used with the origins of mass spectrometry in the early part of the 20th Century but it was not until the 1960's that chemical ionisation found use[45]. The drive to facilitate mass spectrometry analysis of larger molecules, and in particular proteins saw the development of Fast Atom Bombardment (FAB) in the 1980s[46] . This technique is no longer in general use and so is

not included in Figure 2-1. The capability that FAB offered has since been replaced by a myriad of atmospheric pressure ionisation (API) techniques. Thermospray offered a means for introduction of liquid samples into the gas phase, though it was largely replaced with the less temperamental and now ubiquitous Electrospray Ionisation for which John Fenn was awarded the Nobel prize in 2002[23]. That year, Koichi Tanaka was also awarded the Nobel prize for soft laser desorption/ ionisation [47], a technique similar in principle to the more widely used Matrix Assisted Laser Desorption/Ionisation developed by Karas and Hillenkamp[48]. In the last two decades, the number of ionisation techniques described in the literature has escalated most heavily in the area of direct analysis[49,50]. The concept of direct analysis is fast and efficient mass spectrometry with minimal or no sample preparation required; a concept that lies at the centre of on-line and in-line reaction monitoring.

2.1.1 Electron ionisation (EI)

Electron ionisation produces ions by direct bombardment of gas-phase molecules with a beam of electrons, usually with an energy of 70 eV. This is far above the first ionisation potential for most instruments, but is a good approximation of the energy at which the greatest number of ions are produced for most organic samples for a given number of analyte molecules[45], and has emerged as a standard energy to allow for comparability of data between different instruments, allowing for the use of library spectra to identify compounds.

Ionisation occurs when the impact of an electron on a molecule imparts sufficient energy to remove an electron from the molecule, resulting in the formation of the radical cation, or less commonly when an electron is captured, creating a radical anion. In both cases the resulting ions are highly unstable. A potential downside of this high energy approach is that significant fragmentation of target molecules, which, while useful for structural analysis and allowing for library matching of fragmentations patterns, can cause difficulties in analysis of mixtures of closely compounds such as a reaction product and the products of side reactions, as it is often difficult to differentiate between

compounds which produce similar fragments. A variety of methods are used to introduce the molecules to the gas phase, most commonly by coupling to gas chromatography, which limits analysis to volatile compounds. LC coupling methods have also been developed[51], but these rely on extremely low flow rates on the order of µL per minute, which would be challenging for a reaction monitoring application.

2.1.2 Chemical Ionisation (CI)

Chemical ionisation is fundamentally similar to EI. In CI a reagent gas such as methane, ammonia or isobutane is ionised by electron bombardment, forming a radical cation as in EI. This then undergoes ion-molecule reactions with the abundant reagent gas molecules, forming a protonated reagent molecule which then either forms an adduct with the neutral analyte or protonates it through proton transfer, the former occurring only with highly polar analytes. The result is a significantly more gentle ionisation process resulting in a lesser, though not always insignificant degree of fragmentation. This often allows for the clear detection of the molecular ion, with some control over fragmentation achievable through variation of the reagent gas[52]. CI has many of the same drawbacks as EI with regards to reaction monitoring, as there is still significant fragmentation which presents significant difficulty in monitoring mixtures of compounds, and analytes must still be volatile for sample introduction.

2.1.3 Atmospheric pressure Solids Analysis Probe (ASAP)

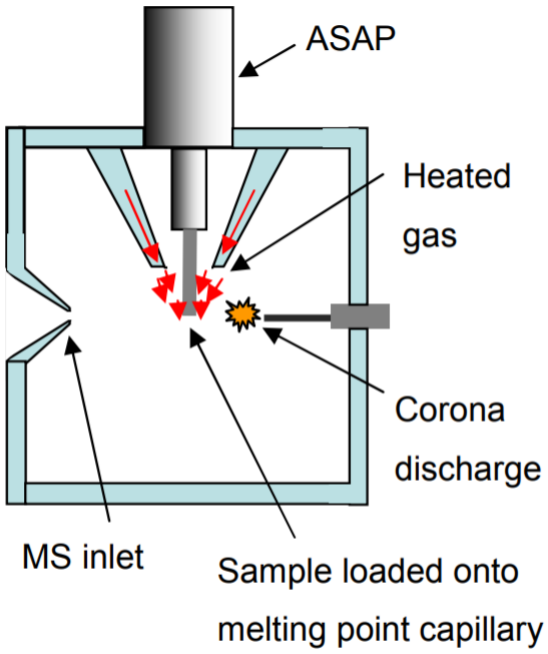

Figure 2-2 Atmospheric pressure solids analysis probe ion source diagram[53]. Reproduced with permission.

The Atmospheric pressure Solids Analysis Probe (ASAP), is relatively recent development, first reported in 2005[54]. It is a desorption-based ionisation method in which a sample loaded onto a capillary rod is placed in the path of a flow of heated gas, usually nitrogen, in the vicinity of a corona discharge pin as shown in Figure 2-2. The flow of hot nitrogen causes neutral analyte molecules to desorb from the rod surface. The electrical discharge ionises the heated nitrogen gas, forming nitrogen radical cations. A cascade of ion-molecule reactions following resulting in a variety of methods of analyte ionisation which can include charge transfer to generate an analyte radical cation, hydride abstraction or protonation of the analyte[55].

ASAP has the advantage of providing a quick method for manual sampling of solids. It takes a matter of seconds to dip a capillary rod into a powder, oil, liquid or solution and then place it into the ion source. This sampling process makes ASAP best suited to an at-line approach to monitoring reactions rather than on-line, as the introduction of sample is not easily automated and would not allow for

continuous introduction of a reaction mixture. ASAP is very rapid, with a typical analysis time on the order of seconds, and is as such well suited to real time analysis.

2.1.4 Atmospheric Pressure Chemical Ionisation (APCI)

Atmospheric pressure chemical ionisation (APCI), a modification of Electrospray Ionisation designed to allow for the ionisation of less polar compounds, uses a corona discharge similar to that used in ASAP, though the sample is introduced through an uncharged capillary with a high temperature (350-500 °C) nebulising gas, usually nitrogen, serving to aerosolise the liquid sample and evaporate the solvent. The corona discharge ionises this nebulising gas and the analytes are ionised by interaction with the nebulising gas ions. APCI is often coupled to liquid chromatography, and shows good potential for continuous reaction monitoring, able to ionise a wide variety of compounds and capable of dealing with continuous sample introduction[56].

2.1.5 Matrix-Assisted Laser Desorption/Ionisation (MALDI)

Matrix-Assisted Laser Desorption/Ionisation (MALDI) involves the mixture of a matrix compound and the analyte on a conductive 'target'. This may be achieved either by pre-mixing of the matrix compound and the sample in solution, or by spotting or spraying individual compounds onto the target. The matrix compound, usually a small organic acid, is selected for its ability to efficiently absorb light at the laser frequency, its volatility and ability to either donate or accept protons depending on whether positive or negative ionisation is desired[57]. The spotted matrix compound is then irradiated with a laser, causing it and the mixed analyte to desorb from the target. The mechanism by which the analyte is then ionised is the subject of some debate, with a variety of models proposed[58] for both primary and secondary ionisation effects. One proposed model for the primary ionisation is the cluster model[59] in which ions are preformed within the solid matrix and by which model a large proportion of such preformed ions are neutralised in the plume after the laser

fires. Another model, known as the 'pooling' model[58] suggests that ionisation occurs due to the migration of energy through the matrix and formation of higher energy complexes by the convergence of multiple 'excitons' (imaginary particles representing excited states of matrix molecules)[60]. The ionisation which results is characterised mainly by the formation of $[M+H]^+$ or $[M+Na]^+$ ions in positive mode, and is 'soft' enough to allow for the intact ionisation of very large molecules.[57] Like ASAP, MALDI is a discrete process, and while it may be possible to automate the spotting process to some degree, this still presents a significant decrease in the time resolution achievable for reaction monitoring.

2.1.6 Electrospray ionisation

One of the softest ionisation techniques, electrospray ionisation (ESI) has the advantage of producing intact molecular ions and minimal fragmentation. The production of intact ions is useful in reaction monitoring, as it reduces the complexity of the spectrum produced, allowing ions of interest to be more easily identified and reducing the likelihood that fragments of one species present might interfere with the monitoring of another species. This is particularly important when monitoring reactions involving the addition or removal of labile groups, as a harder ionisation technique could easily remove those groups in the source, obfuscating the actual reaction progress. In addition, by-products and intermediates are, almost by definition, chemically similar to the reagents and products of the reaction and significant fragmentation is likely to obfuscate the presence of these analytically relevant species. Thus ESI, by producing mainly intact ions represents a much better chance of tracking such species, especially as the signal to noise ratio for individual ions will be better if the ion count is not diminished by being split between different fragments. The ability to use higher voltages in ESI to deliberately induce fragmentation means that fragmentation is available as a tool, but is less likely forced upon the user where it is not useful.

Electrospray ionisation is achieved by flowing an analyte solution through a capillary as shown in Figure 2-3, which has a high potential difference applied between it and a counter electrode, subjecting the solvated analyte molecules to a strong electric field, typically between 1 and 5 KeV[61]. This results in charge accumulation at the liquid surface, deforming the surface from the surface-tension dominated norm of a convex droplet towards that of a Taylor cone. Once a threshold voltage is reached, the electrical field begins to dominate, resulting in a jet of charged liquid being expelled from the surface, and above the threshold voltage, a stable spray may be formed, resulting in a consistent spray of charged droplets into the ion source.

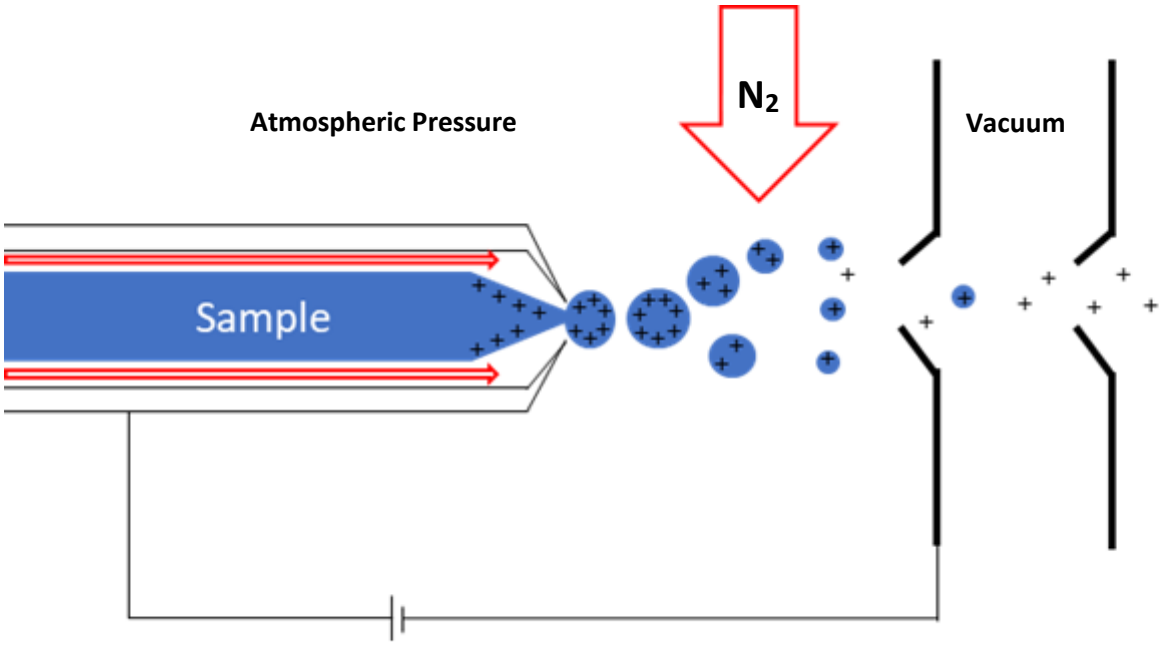

Figure 2-3 -Electrospray diagram showing magnified view of capillary.

Droplet evaporation is then achieved by the assistance from of a heated desolvation gas, as shown in Figure 2-3. As the droplet becomes smaller, so the charge density in a given droplet increasing until the surface tension of the droplet is overcome by the coulombic repulsion between the charged species within that droplet, a threshold known as the Rayleigh limit[62] and defined by Equation 1 for a

droplet of radius α in metres with charge q in coulombs, where ε_0 is the permittivity of free space in Farads per meter and γ is the surface tension of the droplet in Newtons per metre.

Equation 1 - Rayleigh limit

$$q^2 = 64\pi^2\varepsilon_0\gamma\alpha^3$$

Once the Rayleigh limit is reached, the droplet will explode into smaller, more stable droplets, which continue to evaporate[63]. The process repeats until only a very small amount of solvent remains, at which point a number of mechanisms are proposed for the final exit of charged species into the gas phase.

The ion evaporation model (IEM) proposes that the solvated ions are ejected from the nanodroplet when the Rayleigh limit is reached[64] with transient elongation of the droplet in the direction of ejection as the ion. This is believed to be the dominant mechanism for small molecules[65].

The charge residue model (CRM), is based on the theory that a droplet eventually contains just one analyte ion, with evaporation of the solvent continuing until the last of the solvent transfers the charge it holds to the analyte molecule, resulting in a gas phase analyte ion.[65] This is believed to dominate for many larger molecules, especially globular proteins in which the hydrophobic moieties are shielded from interaction with the solvent, allowing the molecule to remain in solution until all the solvent evaporates.

A third model, the chain ejection model (CEM), is proposed for long chain proteins which become unfolded, allowing the solvent to access the hydrophobic groups on the protein chain[63]. Evidence from molecular dynamics simulations and ion mobility spectra[63,66] suggests that this results in the migration of the chain to the surface of the droplet, where one terminus of the chain is ejected from the charged droplet. The repulsive forces between the charged droplet surface and the charged protein chain then result in sequential ejection of the entire chain, leaving the entire chain in the gas phase.

Figure 2-4 summarises the three models graphically.

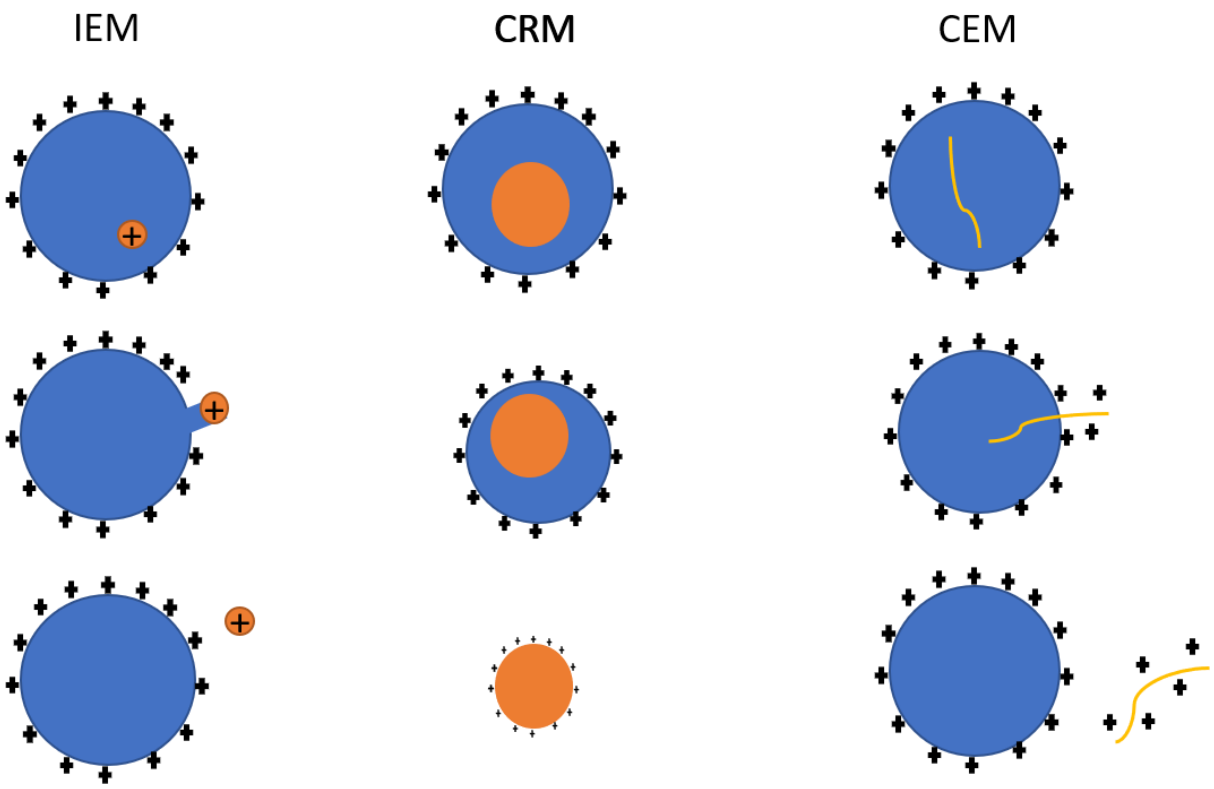

Figure 2-4 Representation of the Ion ejection (IEM), Charge residue (CRM) and Chain ejection models (CEM) of ESI

Once in the gas phase, the charge and vacuum act to transfer the ions into the mass analyser.

2.1.7 Nano Electrospray Ionisation (n-ESI)

Nano Electrospray Ionisation (nESI) is a special case of ESI in which a much smaller aperture capillary (approx. 1-3 micrometer) facilitate the use of much lower flow rates on the order of nanolitres per minute, resulting in smaller initial droplets in the sub 200 nm diameter range[67] as compared to µm for standard ESI[68], consuming less sampled material per unit time. The lower initial droplet size has significant effects on ion formation, with lower susceptibility to salt contamination a particular advantage. However, in situations where the amount of sample available is not a significant constraint on analysis, the requirement for frequent user adjustment to obtain stable spray is a major drawback, especially for the analysis of dynamic systems such as reaction media[69].

2.1.8 Ion Suppression

Ion suppression and enhancement are common issues in mass spectrometry of complex mixtures[70]. The problems arise due to the interactions between multiple analyte species within a droplet during the ESI process. Suppression occurs when the presence of one species causes a decrease in the signal of another; enhancement when the presence of one causes an increase in the signal for another. The mechanisms behind suppression and enhancement effects are complex, with factors including difference in mass between species present[71], the differences in polarities of species[72] and the effects of less volatile compounds on droplet properties[73] all being shown to contribute. As such, the general approach to the problem has been to separate the species prior to ionisation, usually through chromatography[70]. Where this is not possible, methods have been established to calibrate for suppression and enhancement effects through the use of isotopically labelled versions of analyte compounds. When these are present at a known concentration, it is possible to quantify the degree of suppression occurring using the formula in Equation 2

$$[\text{Analyte}] = [\text{Analyte}_{\text{obs}}] \times \frac{[\text{Labelled}]}{[\text{Labelled}_{\text{obs}}]}$$

Equation 2 -Adjustment of suppressed or enhanced signal using isotopically labelled reference

2.1.9 Mass analysers

A relatively small number of mass analysers dominate commercially, with variation of design based on requirements for differing degrees of performance in terms of mass resolution, mass accuracy, sensitivity, duty cycle and dynamic range, as well as functionality in terms of the capability of an instrument to isolate and fragment specific ions iteratively by tandem mass spectrometry (MS^2 or MS^n)[74]. Here, tandem mass spectrometry techniques such as infrared multiphoton dissociation[75], ultraviolet photodissociation[76], collision induced dissociation (CID)[77] and a range of electron-based

dissociation[78,79] can heavily influence the overall configuration and combination of mass analysers in one system. Different scanning modes such as single ion monitoring (SIM) or multi reaction monitoring (MRM) can offer specificity and selectivity, and the ability to rapidly switch between positive and negative mode acquisition broaden the chemical remit. For reaction monitoring, single ion monitoring is particularly attractive functionality as this enables the mass spectrometry to focus on specific ions of interest, thereby improving S/N and duty cycle.

The performance and available functionality for a given instrument broadly tends to scale with physical size and price, with larger, higher performance instruments generally being able to 'bolt on' a far wider variety of ion sources and experimental functionality so as to really benefit from high mass resolution and accuracy. Common mass analysers include quadrupoles, ion traps, time-of-flight, orbitraps and Fourier transform ion cyclotron resonance. While previously common, magnetic sector instruments are rarely in use in modern laboratories.

Fourier transform ion cyclotron resonance mass spectrometers have the highest mass resolving power with upwards of 27,000,000 m/Δm50% reported by Smith *et al.*[80] on an instrument using a 21 T superconducting magnet. Orbitraps[81] and Time-of-Flight[82] mass analysers are also considered capable of high mass resolution with the stability sufficient for exact mass measurement. At the other end of the scale are ion trap and quadrupole mass analysers, which can be found in small rugged benchtop systems.

2.1.10 Quadrupole mass analysis

Quadrupoles function by the generation of a quadrupolar electrical field by passing alternating currents between at least two pairs of either cylindrical or hyperbolic rods, with opposing pairs running parallel to one another. The simplest configuration, that requiring four rods, is constructed as shown in Figure 2-5 where one rod has the applied potential ($U + Vcos(\omega t)$) while the other has

potential of (-(*U + Vcos (ωt)*), where U is a fixed DC offset voltage and V cos(*ωt)* is a variable RF voltage.

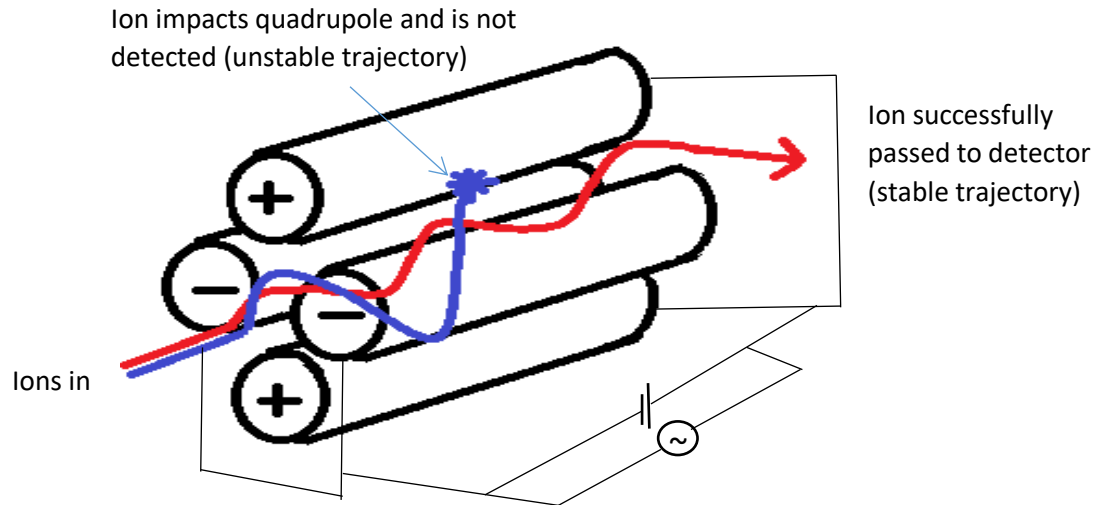

Figure 2-5 Quadrupole diagram showing ion paths

RF voltages of equal magnitude and opposite phase are applied, resulting in a field that oscillates through the centre of the quadrupole propelling the ions through the centre. A DC offset voltage is also applied to all rods. Ions of a specific *m/z* value have a stable trajectory through the quadrupole at a specific ratio of RF and DC voltage; ions of other *m/z* values will not be transmitted as shown in Figure 2-5. Thus only ions at the desired *m/z* are detected. In this way ions of a single *m/z* value can be continually transmitted through the device, filtering out all other erroneous chemical signals and maintaining the highest duty cycle. This optimising the signal-to-noise ratio and the sensitivity, a mode referred to as single ion monitoring (SIM). To obtain a full mass spectrum the RF voltage can be scanned which will result in ions of a different *m/z* to be transmitted in turn as shown in Figure 2-6.

The motion by which ions travel through a quadrupole is described by the Mathieu Equation 3, in which a_u is a function of the magnitude of the DC voltage, q_u is a function of the magnitude of the AC voltage and ξ is a dimensionless parameter of frequency multiplied by time divided by 2.

Equation 3 - Mathieu Equation

$$\frac{d^2u}{d\xi^2} + (a_u - 2q_u \cos 2\xi)\, u = 0$$

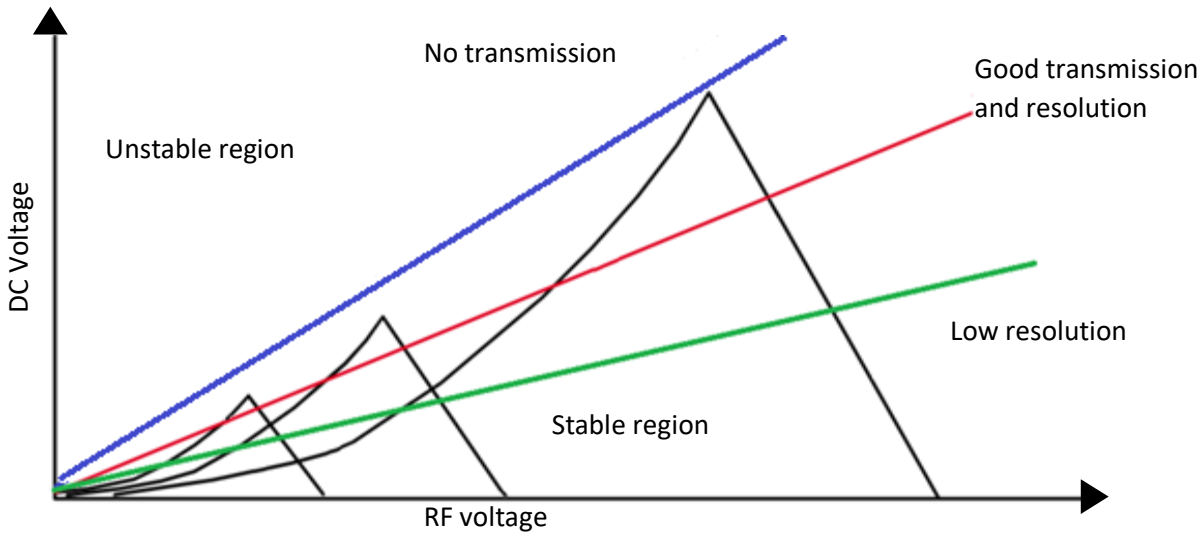

Figure 2-6 Ion stability diagram as function of DC voltage and RF voltage in a quadrupole. Diagram shows regions of stability for 3 different ions in black, of increasing m/z from left to right. The green line represents a scanning setup which provides good transmission for all 3 ions, but would give poor mass resolution, the blue line represents a scan which would not transmit any ions, and the red represents a good balance between transmission and resolution, allowing transmission of all ions without transmitting any 2 at the same time.

The consequence if Equation 3 as the voltages are varied are is demonstrated by Figure 2-6, showing the effect of DC and RF voltage and potential scans through the stable regions.

If no DC offset voltage is applied, ions of all *m/z* values are passed, which allows the quadrupole to be used as an ion guide.

2.1.11 Time-of-Flight mass analysis

Time-of-Flight (ToF) mass analysers function by spatially resolving ions based on the time it takes ions of different *m/z* to travel through a field-free region after the application of a uniform acceleration potential (V), imparting the same kinetic energy to each ion independent of mass.

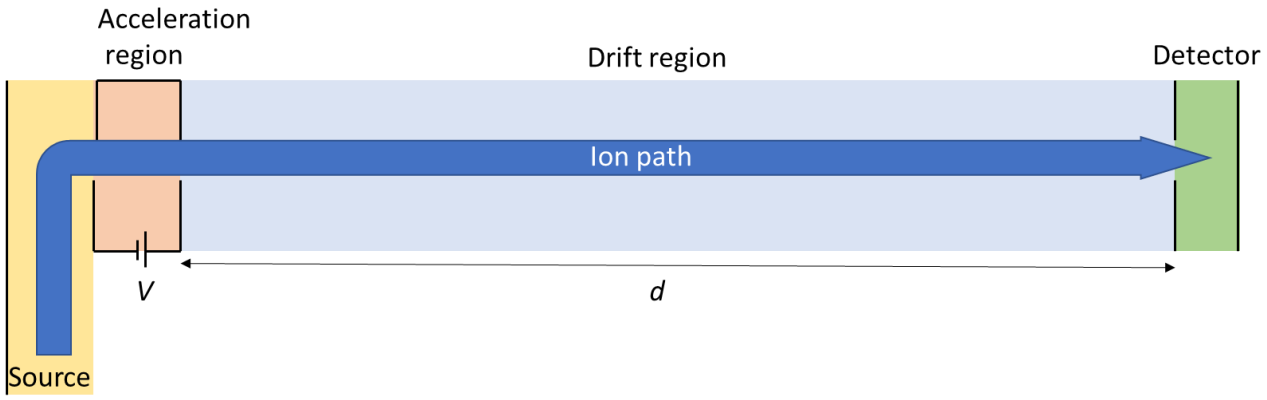

Figure 2-7 Time of Flight mass analyser schematic.

Equation 4 where *z* is the number of unit charges on an ion, *e* is the electron charge, V is the acceleration voltage, and **v** is the resulting velocity, shows the relationship between kinetic energy (E_k) mass and velocity.

Equation 4 - Relationship between velocity, mass and kinetic energy in time-of-flight acceleration region

$$E_{kin} = zeV = \frac{1}{2}mv^2$$

Simple rearrangement of this gives Equation 5, which shows that the velocity of an ion is fixed for a given *m/z* value:

Equation 5 - Rearrangement of equation 4 showing that ion velocity is proportional to m/z

$$v^2 = 2eV\frac{z}{m}$$

Given that $2 \cdot e \cdot V$ is a constant for a given acceleration voltage, and **v** is a function of distance, it can thus be said that the time taken to travel the length of the drift region (d) is proportional to 1 over the square root of the *m/z* value.

As a result of this relationship, the *m/z* of ions in a sample can be analysed by the simple expedient of applying the acceleration voltage at a known time, generating a 'packet' of ions and measuring the time at which signals are received. In order to ensure discrete packets of ions, instruments using ion sources which would otherwise produce a constant supply of ions, such as ESI, orient their intake orthogonally to the flow, taking ions in only when the orthogonal acceleration potential is applied. This also serves to prevent neutral molecules from entering the field-free region, thereby minimising collisions which would result in fragmentation and chemical noise [83].

As well as the accelerating voltage, V, mass resolution in a ToF instrument is directly dependent on the path length d of the drift region, but there are practical limitations to the path length in a reasonably sized instrument. As such, many modern ToF instruments make use of reflectrons to extend the path length possible within the instrument. A reflectron, as shown in Figure 2-8 consists of a series of electrodes with increasing voltages, which divert the ions, with higher *m/z* ions passing further into the electric field while lower *m/z* ions are reflected more quickly, resulting in a longer effective path and thus higher resolution. The reflection also minimises the effect of any aberrations in the kinetic energy imparted across the initial acceleration voltage, as ions of a specific *m/z* but with marginally higher E_k will pass further into the reflectron and thus have a longer path, correcting for the difference in initial kinetic energy[84]. Modern reflectrons use a dual stage configuration, in which an initial high voltage section slows the incoming ions, and then a second lower voltage reflection stage reverses their direction. This two stage approach allows for both a smaller overall reflectron size to achieve the same focusing and the ability to correct 2nd order effects of kinetic energy differences on flight time[85].

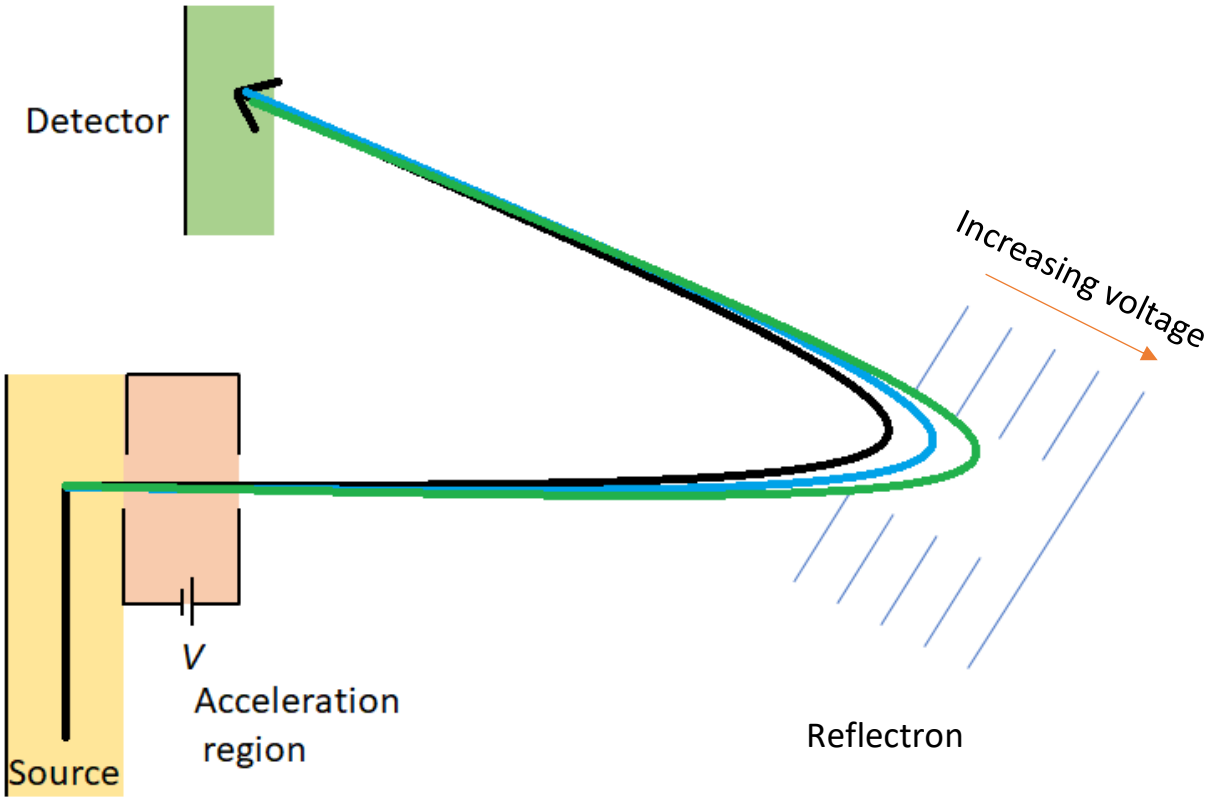

Figure 2-8 Reflectron diagram showing paths for ions of low m/z (black), medium m/z (blue) and high m/z (green)

2.1.12 Stacked ring ion guides.

An alternative to the use of an RF-only quadrupole as a means of transporting ions is the stacked ring ion guide. This consists of a sequence of ring-shaped electrodes, with adjacent rings having opposite phases of RF voltage delivered to them, radially confining ions that pass through the device within the rings and allowing them to be guided through the centre of the rings[86]. Some devices also apply a DC voltage to the rings to generate a travelling wave, allowing for greater control of the transmission of the ions.

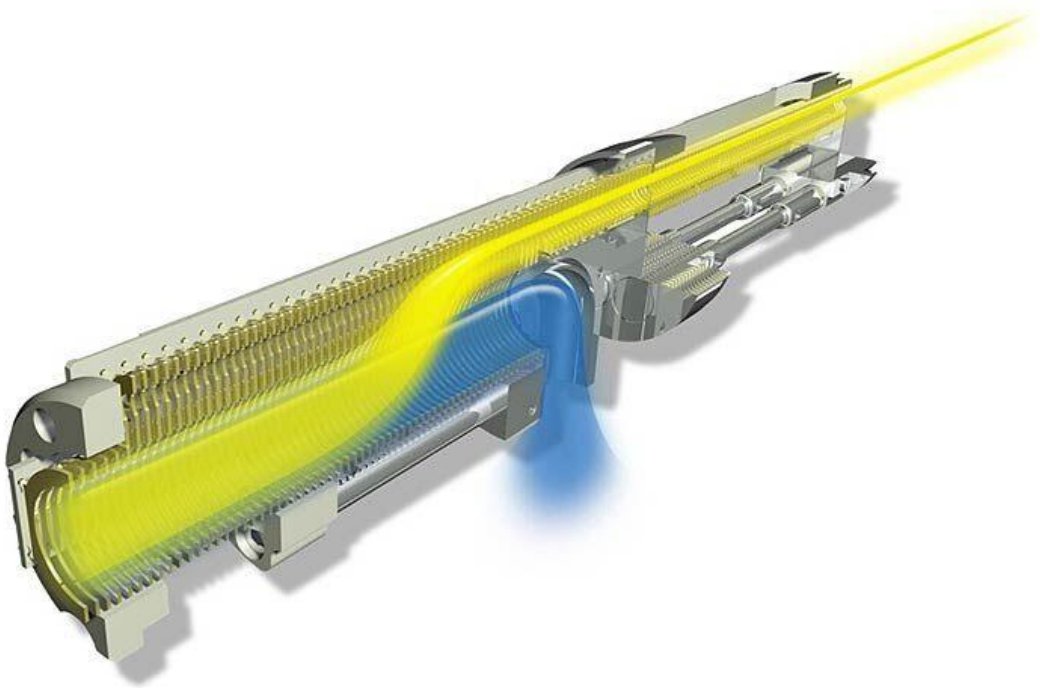

Figure 2-9 StepWave ion guide internal diagram, path of charged species shown in yellow, neutral species in blue. Reproduced from Waters Corp. with permission.

The StepWave, as shown in Figure 2-9, is a specific commercial example of the stacked ring ion guide designed to filter out neutral species by deflecting and focussing the path of charged species into the quadrupole while removing the bulk of the excess solvent molecules, other neutral species and gas, resulting in greater sensitivity and greater robustness, as there is less fouling of the later instrument components by neutral species.

An arrangement similar to the stacked ring ion guide using rings of decreasing size to focus the ion beam is also in use, commonly known as an ion funnel[87]

2.2 Nuclear Magnetic Resonance Spectroscopy

Nuclear Magnetic Resonance (NMR) spectroscopy works on the basis that when nuclei with a non-zero angular momentum (spin) are placed into a magnetic field, their spin characteristic will result in multiple states of alignment with the field at different energy levels.

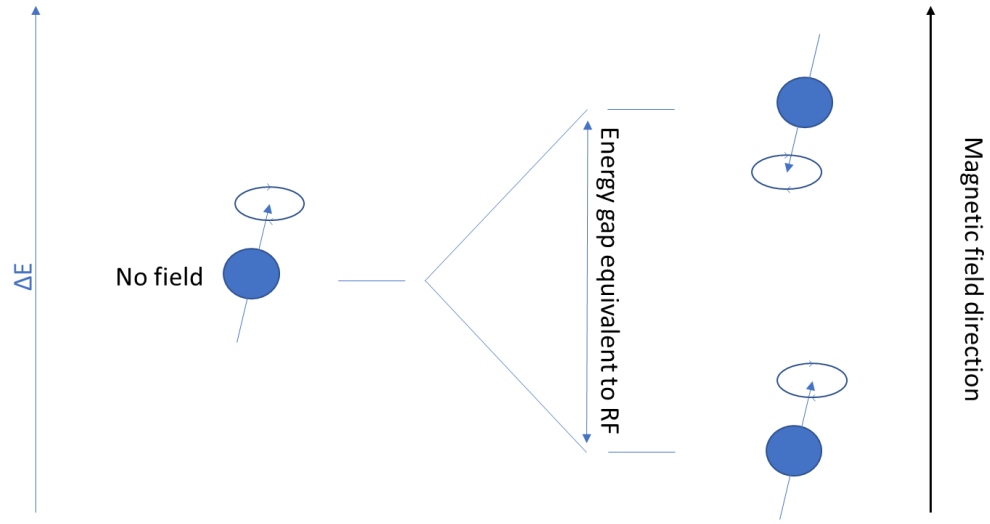

Figure 2-10 Energy level diagram for spin 1/2 nucleus as magnetic field is applied.

As shown in Figure 2-10, for a spin ½ nucleus such as ^{1}H or ^{19}F, there are 2 states as a general rule states that there are 2n+1 where n is the spin quantum number of the nucleus. One state is low energy in which, for a nucleus with a positive magnetogyric ratio, the average spin is aligned with the direction of the field, and the other state has higher energy in which the average spin is aligned opposing the direction of the field[88]. For all realistically achievable magnetic field strengths, the gap between these two energy levels corresponds to the energy of a photon in the RF region of the electromagnetic spectrum. In a sample containing large numbers of nuclei, there is a Boltzmann distribution between the two states, with the more energetically favourable state being the more populated, resulting in a net magnetisation in the direction of the magnetic field. In a frame of reference rotating at the resonant precession frequency (γBo), known as "the rotating frame", this excess of aligned magnetisation appears as a static net magnetisation vector aligned with the magnetic field. The resonance frequency for a given nucleus is dictated primarily by its gyromagnetic ratio γ and the field strength B experienced as shown in equation 6

Equation 6- NMR frequency of a nucleus in a given magnetic field

$$\nu_{NMR} = \frac{|\gamma|B}{2\pi}$$

In the rotating frame, the magnetic component of an on-resonance RF pulse (B_1) appears as a static magnetic field in the plane perpendicular to the applied magnetic field (B_0). The net magnetisation vector precesses about B_0 and its projection onto the xy plane can then be detected by the receiver coil.

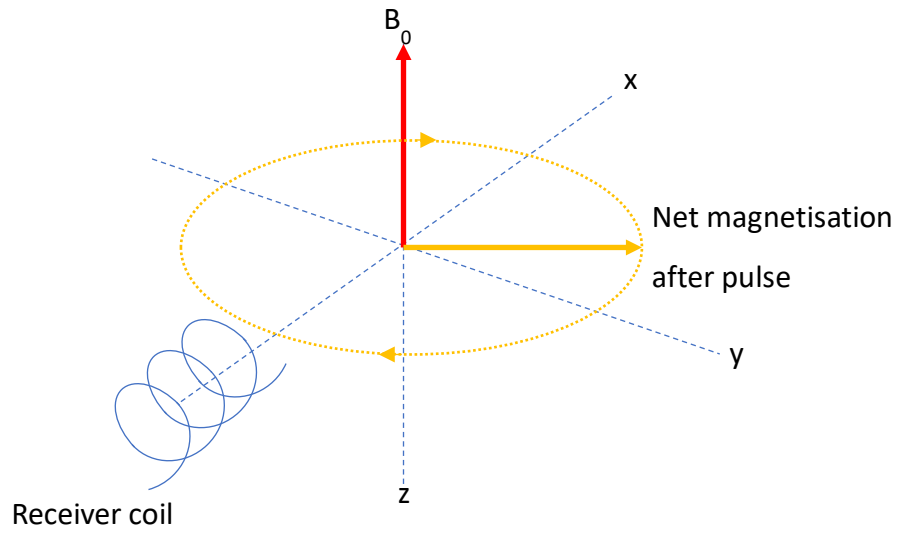

Figure 2-11 Net magnetisation of a spin 1/2 nucleus after application of an RF pulse.

Once an RF pulse is applied, as shown in Figure 2-11, the distribution shifts as nuclei are excited into the higher energy state, the net magnetisation is effectively moved out of the axis of the magnetic field and precesses around that axis, gradually returning to the lower energy state of maximum net magnetisation in the direction of B_0. The process of returning to the ground state is commonly referred to as spin-lattice relaxation, and proceeds through vibrational and rotational transitions[89]. The rate of this relaxation is dependent on the available rotational and vibrational transitions, and thus depends varies widely depending on the physical and chemical properties of the analyte in

question. The current induced in a receiver coil by this precession is measured and results in a ‘free induction decay’ (FID) which is effectively a sum of the decaying signals for the different nuclei, with amplitude of a given wave corresponding to the number of nuclei within the sample resonating at that frequency. The application of a Fourier transform to this FID gives a spectrum with individual signals for each resonance frequency.

The maximum signal is attained when the net magnetisation is moved 90 degrees to the z-axis, the path shown in Figure 2-11 This desired excitation is achieved by using an RF pulse with a power and duration calculated to achieve that excitation for the nucleus in question. The desired ‘rectangular’ pulse shape (on a graph of amplitude against time), when subjected to a Fourier transform yields a cardinal sine function (Figure 2-12) with null points corresponding to the frequencies equal to ±1 pulse width.

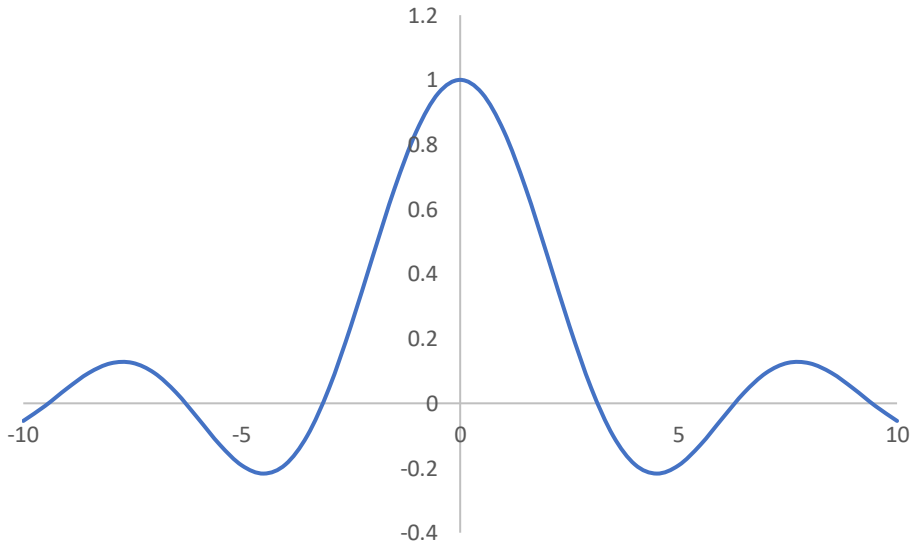

Figure 2-12 Cardinal Sine function (f(x)=sinx/x)

The goal when arranging the pulse width and power is to ensure that the signals of interest fall within the frequency range corresponding to ±¼ pulse widths, as this represents a reasonably even excitation of all such signals. Signals further out can be subject to lower intensities of excitation or even no excitation at all if they occur at null points within the function.

While the magnetic field generated by the NMR instrument is by design uniform in the analysis volume, the magnetic field actually experienced by a given nucleus is affected on a smaller scale by the specific chemical environment in which that nucleus is found, as local electrons are also affected by the applied field B_0, and the induced motion of these electrons acts to generate a small opposing magnetic field B'. This effect is described as 'shielding' as the result is that a portion of the external field is, from the perspective of the nucleus, nullified by the induced field from the electrons, resulting in an experienced field $B= B_0 – B'$, where B' is proportional to B_0. The resulting change in the experienced B, and thus in the resonance frequency per Equation 6 gives rise to the phenomenon of chemical shift, and thus to the analytical utility of NMR, as the resonant frequency of the nuclei in a given sample thus contains information on the chemical environments of those nuclei, with nuclei in environments with higher electron density having greater B' values and thus experiencing lower magnetic field and thus having lower resonance frequency.

This chemical shift is expressed as the difference between the resonant frequency of a reference nucleus, and the observed frequency divided by the frequency of the reference nucleus, given in units of parts per million. IUPAC has set out standard reference nuclei, for example the proton reference is tetramethylsilane in chloroform solvent[90]. As such the chemical shift of a given nucleus is the same regardless of the field strength of the magnet involved.

Another factor which affects signals in NMR is that of spin-spin coupling, wherein the small induced field caused by nearby nuclei and transmitted through partial polarisation of electrons in the intervening bonds affects the field experienced by the nucleus in question. As nuclei exist in a distribution between the two states of alignment with and opposition to the external field, they act to either strengthen or weaken the field experienced by their neighbours depending on their alignment. The overall effect of this is to create a split in the available energy levels, in effect splitting the signal recorded to a degree dictated by the spatial arrangement and proximity of the nuclei. It is important to note that the effect of coupling on the resonant frequency of a nucleus is

independent of the external field applied, and as such the effect on the chemical shift of a given signal is inversely proportional to the strength of the external magnetic field.

2.2.1 Superconducting magnet NMR

The most common design of NMR instrument in modern laboratories employs a superconducting electromagnet operating at extremely low (circa 4 kelvin) temperatures, with cooling provided by liquid helium, insulated with vacuum and liquid nitrogen layers. These cryogens require regular replacement as they are gradually lost through evaporation. Probe assemblies containing the RF coils and receiver coil are placed within the bore of the magnet, with the RF signal generated by a console and amplifier external to the bore.

2.2.2 Benchtop Permanent Magnet NMR

Recently, improvements in the availability, price and crucially in the thermal stability of rare-earth permanent magnets have led to a renaissance in the field of permanent magnet NMR, which had largely been abandoned after superconducting magnets became available, with greater field strengths and a greater uniformity of magnetic field provided by the powerful electromagnets in superconducting magnet instruments[39].

The advent of cheap, reliable rare earth magnets, combined with the implementation of the Halbach cylinder, an arrangement of magnetic blocks which allows for a uniform magnetic field perpendicular to the bore of the cylinder to be formed in the centre of a cylindrical array as shown in Figure 2-13, has resulted in a wave of benchtop permanent magnet instruments, previously not possible due to the bulky cooling systems required to provide the necessary temperature control for ferrite magnets. Temperature control is still necessary for permanent magnets as magnetism depends

strongly on temperature, but the necessary hardware for rare-earth magnet-based designs is significantly smaller.

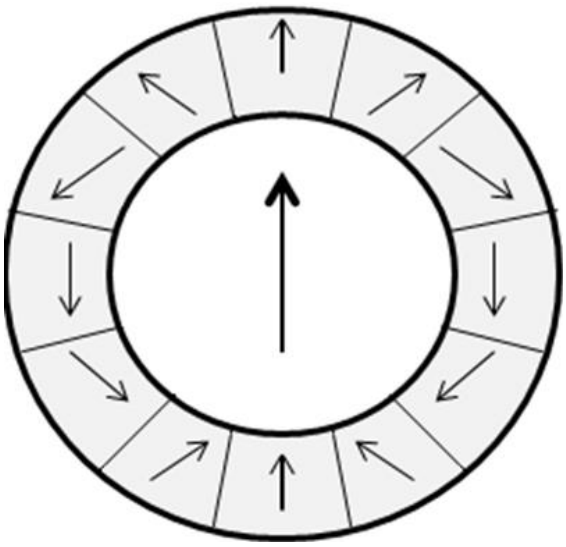

Figure 2-13 Arrangement of magnetic blocks within a cylindrical Halbach array generating a uniform internal field.

The permanent magnet instruments, while having much lower field strength than most commercial superconducting designs, have a number of advantages over them, including that of price, being cheaper to manufacture and maintain, since they do not require the regular supply of cryogens necessary for a superconducting magnet. The Halbach cylinder also results in near-zero external field, meaning that sensitive electronics and magnetic materials do not need to be kept away from the instrument, and the instrument can be freely transported without concerns over health and safety issues such as pacemakers.

For the purpose of reaction monitoring, the relatively small size of these instruments offers additional advantages, as it allows for flow cells with small internal volumes to be used, and for the instrument to be easily situated near whatever equipment is necessary for the reaction, rather than requiring the reaction to be brought to the NMR instrument and connected with long transfer lines.

2.3 Analytical instrumentation investigated for on-line reaction monitoring

A number of analytical instruments were investigated with the view of providing transportable solutions for on-line reaction monitoring and real-time monitoring.

2.3.1 Electrospray ionisation single quadrupole mass spectrometer

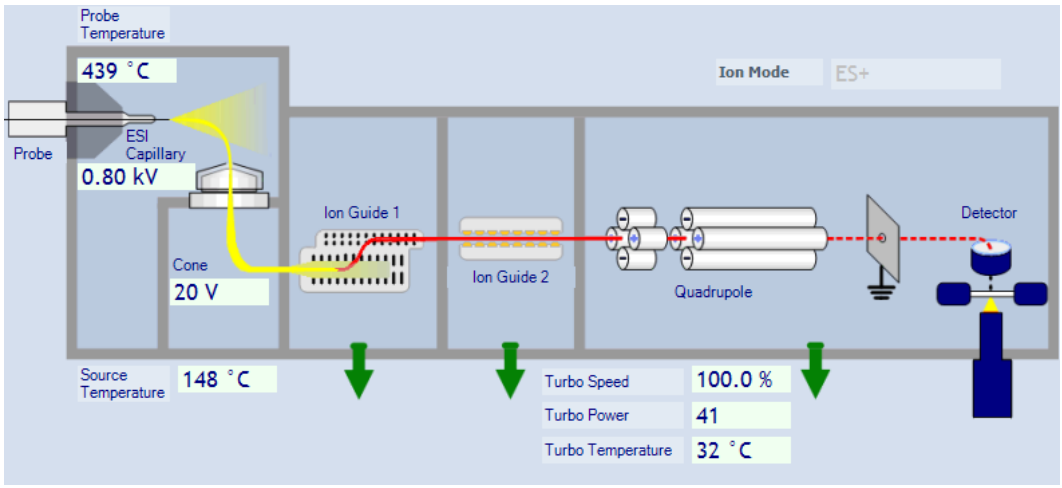

Figure 2-14 Internal diagram of QDa instrument taken from Waters Acquity control software, with permission

A single quadrupole, electrospray ionisation mass spectrometer was chosen for its ease-of-operation, ability to operate in a range of environments and rapid start-up time. The QDa (Waters Corp.) was originally designed and marketed as a detector for liquid chromatography. As such, it has a small footprint (35.3 x 65.0 x 20.0 cm w/d/h) and weighs 34 kg. It is designed to integrate into HPLC stacks on a benchtop rather than being a free-standing instrument. Vacuum is provided by a single turbomolecular pump and, in the standard mode of operation, a small rear-mounted diaphragm pump. This may be replaced with a more powerful rotary pump for use with a larger aperture (0.2 mm as opposed to 0.1 mm for the standard version), allowing for a fivefold increase in sensitivity[91], with the drawback of requiring a larger, heavier, freestanding pump. The internal

layout, as shown in Figure 2-14 is mostly linear, with the source at the front of the instrument passing ions through a StepWave ion guide.

From the StepWave, the ions are passed via a simple ion guide into the quadrupole, which can act in either scanning or single ion monitoring mode to separate ions based on *m/z.* The ions are then detected with a photomultiplier based detector, in which ions entering the detector strike a dynode, releasing electrons which impact a phosphorescent screen. The impact of the electrons on the phosphorescent screen stimulates the emission of photons which then strike a photoanode within a sealed photomultiplier cell, emitting electrons which then pass into an electron multiplier. The electron multiplier amplifies the signal though sequential secondary emissions, whereby one incident higher energy electron striking a surface stimulates the emission of several lower energy electrons, which then strike additional surfaces with an exponential growth in the number of electrons involved, with the necessary energy input being provided by the application of a strong potential between the point of first impact and the point of detection.

The practical upshot of this indirect approach to detection is that it allows for the electron multiplier to be housed in a sealed glass container, preventing fouling of the surfaces involved and thus increasing the durability of the detector.

2.3.2 Electrospray ionisation Time-of-Flight tandem mass spectrometer

The electrospray ionisation time-of-flight mass spectrometer used was the Synapt G2S (Waters Corp.) and combines quadrupoles and ToF analysis to allow for high resolution measurements, MS/MS and ion mobility based experiments[92]. The layout is as shown in Figure 2-15, with one key difference between the Synapt ESI source and that of QDa being that it includes a second capillary for the introduction of a reference mass compound, in this work leucine enkaphalin, sprayed in to provide a known reference 'lockmass' for accurate mass measurement. A rotating baffle ensures that the 'lockspray' does not enter the instrument at the same time as the sample, thus avoiding ion

suppression. Once through the ion source, a StepWave is used to transfer the ions to a quadrupole which can be used to filter ions of a specific *m/z* for fragmentation in the TriWave (essentially acting in SIM mode to deliver only the desired ion), or can be operated in RF only mode to deliver all ions for a full scan. The TriWave section consists of three travelling wave stacked ring ion guide devices which allow for the trapping, fragmentation and ion mobility separation of compounds as desired. The initial trap region can be used to perform either collision induced dissociation or electron transfer dissociation of ions. The transfer region can be used to conduct further collision induced dissociation experiments. The central travelling wave section can be filled with helium and nitrogen to conduct ion mobility separation. Here ions are separated based on their rotationally averaged collisional cross section by passing them through a pressurised area of nitrogen; ions with larger collisional cross sections are slowed more by collisions with the gas. In this work, no fragmentation or ion mobility separation was applied to any of the analyses.

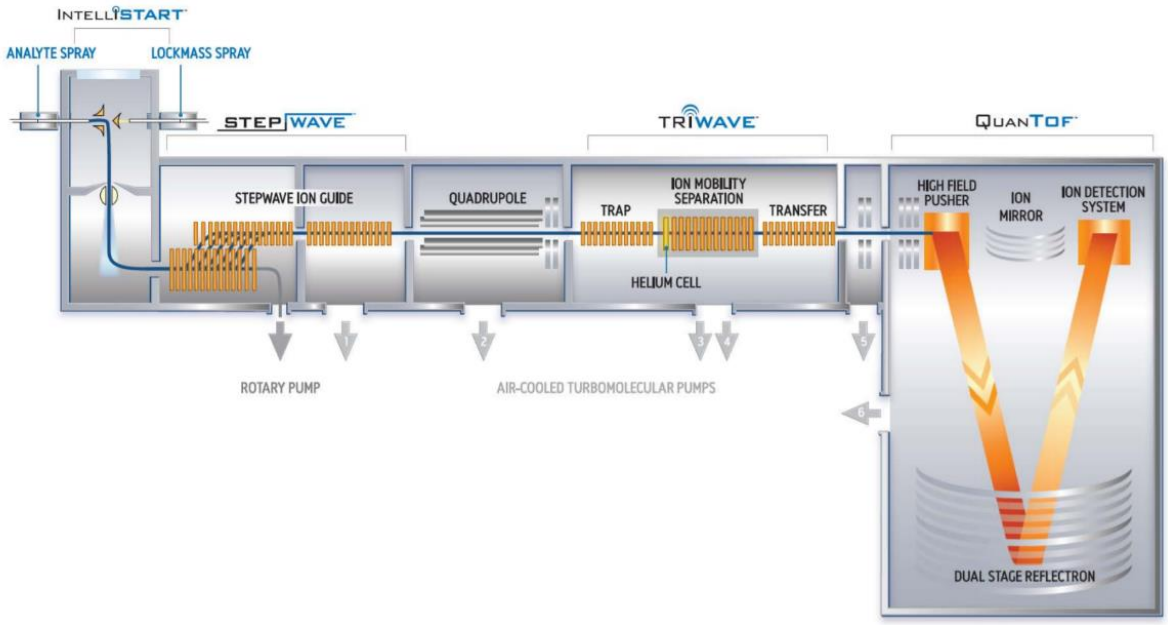

Figure 2-15 Waters Synapt G2S internal diagram, reproduced with permission[93]

Once the ions exit the TriWave section, ToF analysis is conducted, with the choice between a V-shaped single pass on the dual stage reflectron (the path depicted) or a W shaped path using both ion mirrors to achieve an even longer path and thus higher resolution, at the expense of somewhat

lower sensitivity. The detector is an electron multiplier, using a microchannel plate working on the same basic principle as the photomultiplier in the QDa, though without the intervening phosphorescent screen and photoanode.

2.3.3 Selected ion flow tube mass spectrometry

The Voice200Ultra (Syft technologies) uses selected ion flow tube (SIFT) MS to analyse gaseous samples, which works by generation of reactive ions from microwave discharge on moist air, resulting in a selection of reagent ions, namely O^-, O_2^+, O_2^-, OH^-, H_3O^+, NO^+, NO_2^- and NO_3^- A quadrupole is then used to select one of these reagent ions which is passed to the flow tube, through which the sampled gas is passed, with collisions between reagent ions and neutral analytes resulting in charged analytes, which are then passed to a second quadrupole for separation based on their *m/z*, after which they pass to an electron multiplier for detection. A calibrated compound library is used for quantitation for known compounds, though standards have to be run to determine response factors with different precursor ions for any new compounds before quantitation can be achieved. The ability to select reagent ions allows users to tailor the detection towards the compounds they are hoping to analyse, picking the ion which gives the best signal for the compound they wish to monitor. Sample introduction can be achieved either through a 'nose' inlet, which simply sucks in air near the aperture, or by injection from an autosampler attachment as was used in the work described here.

Both the Voice2000Ultra instrument and the autosampler attachment were provided by Anatune Ltd. on a loan basis, and the author would like to take this opportunity to express his gratitude for the loan of the equipment and the support provided by Anatune's staff in its use.

2.3.4 Small footprint NMR (^{1}H and ^{19}F)

The Spinsolve 43 (Magritek) is a small footprint benchtop NMR instrument featuring a 1T Halbach array based permanent magnet capable of analysis of both ^{1}H and ^{19}F nuclei. The model used in this work has an internal lock sample, internal to the instrument, though external to the sample being analysed, which allows a lock to be maintained without the need for deuterated solvent in the sample. The flow system used with the Spinsolve consists of a glass flow cell which is long enough to pass through the bore of the instrument entirely, with a narrow bore which widens to 3mm internal diameter at the approximate position of measurement volume in the instrument. It is connected to peek tubing via fittings on ground glass joints.

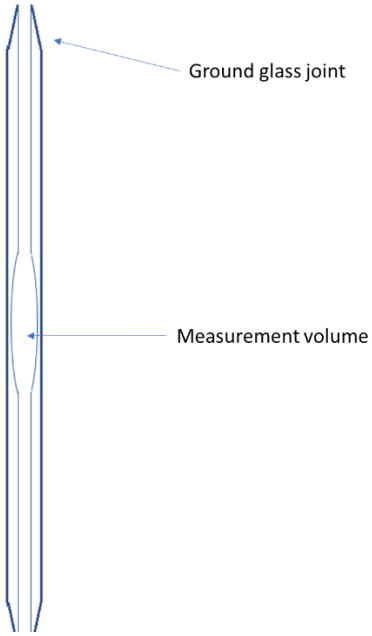

Figure 2-16 Magritek flow cell diagram. The flow cell passes completely through the bore of the magnet.

2.3.5 High-Field NMR instruments

Several superconducting magnet NMR instruments were used, including a ^{1}H 200 MHz (Oxford Instruments), a ^{1}H 400MHz (Bruker, GmBH) and a ^{1}H 700 MHz (Varian) at Durham University and a ^{19}F 470 MHz (Bruker, GmBH) instrument at AstraZeneca Macclesfield.

All reaction monitoring experiments using high-field NMR instruments conducted at Durham University, were performed in an NMR tube, which has been noted to produce different results to those seen for flow measurements due to the lack of mixing effects.[38]

At AstraZeneca, the Bruker InsightMR flow monitoring system was used, which consists of a flow tube and a long insulated connector to allow the reaction to be conducted at a sufficient distance from the instrument to avoid concerns over external field and a tube which, as shown in Figure 2-17, seeks to approximate a standard 5 mm NMR tube, which reaction mixture flowing in through an inner tube and then being forced back up the outside and into the outlet tubing.

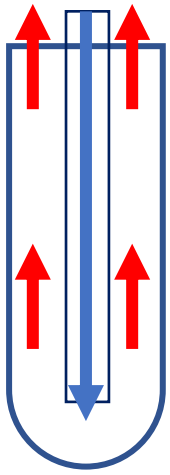

Figure 2-17 Flow cell for InsightMR system. Analyte flows in through a central tube into a cell mimicking a standard 5mm NMR tube before being forced out through the exterior tubing into an outle

3 System development and validation

3.1 Chapter Abstract

For the first time, a system was assembled using a small permanent magnet NMR instrument and a small footprint ESI-MS instrument. Testing was conducted in an off-line fashion to establish instrument performance, and then moved on-line with gradual troubleshooting and improvement of both online systems before their eventual combination into a single system. A robust combined setup was established which could be used to monitor a range of reactions.

3.2 Validation of a chemical reaction by ^{1}H NMR and ESI MS in preparation for on-line experimental design.

3.2.1 Establishing chemical reduction of acetanisole as a model system.

The reaction selected for the initial development work was a borohydride reduction of 1-(4-methoxyphenyl)ethanone (acetanisole) to 1-(4-methoxyphenyl)ethanol. Such reductions are a staple of organic chemistry, with borohydride reductions having been a go-to means of reducing aldehydes and ketones to alcohols for over 50 years[94] This reaction was chosen for convenience as it could be performed at 20 °C by a simple mixing of the reagents on the open bench (i.e. did not require the containment of a fumehood) and because it proceeded over a timescale suitable to developing and evaluating methodologies with these systems, in the order of tens of minutes, at a concentration which was compatible with the NMR instrumentation, though notably this concentration was approximately 3 orders of magnitude greater than that which would be desirable for MS analysis, necessitating a dilution step between the two instruments.

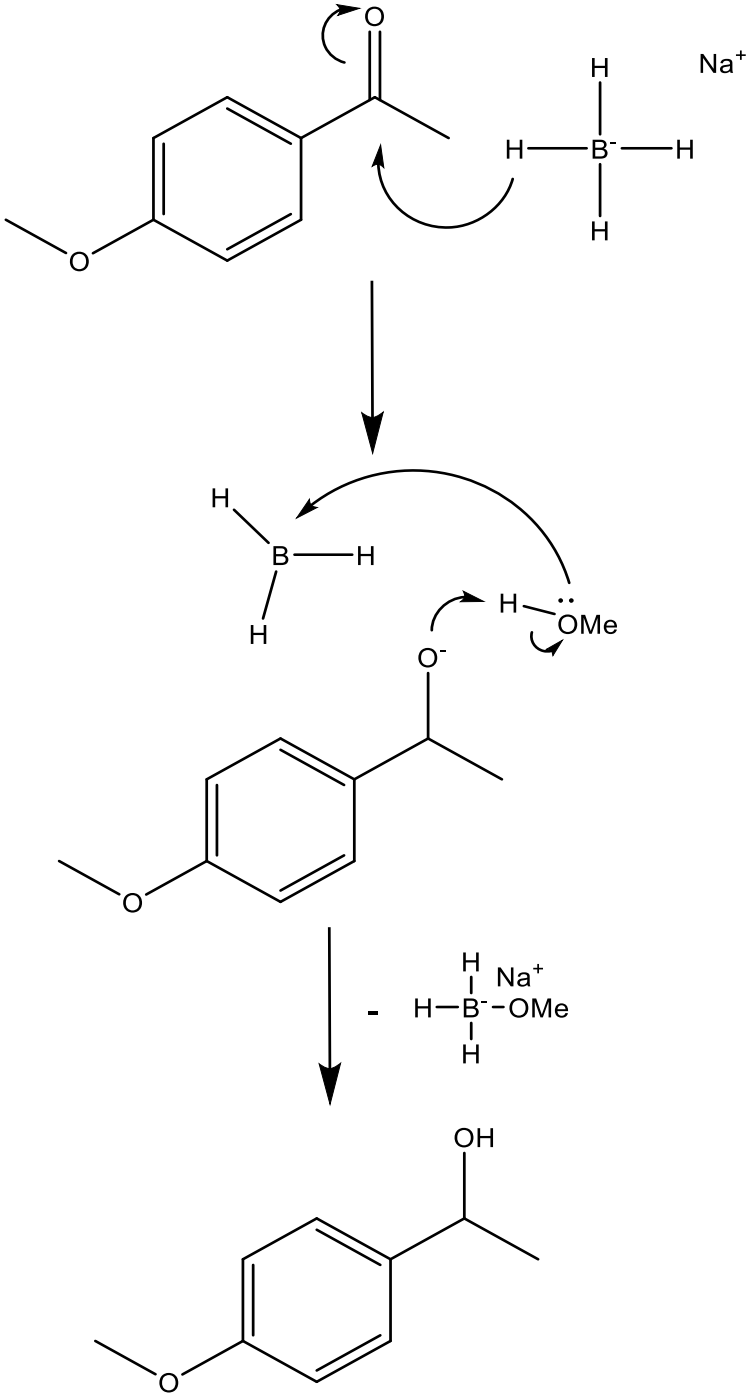

Figure 3-1. Borohydride reduction of acetanisole to 1-(4-methoxyphenyl)ethanol

The reaction proceeds as shown in Figure 3-1, with each equivalent of sodium borohydride capable of providing four equivalents of hydride for reduction. The sodium borohydride also undergoes a slow side reaction with the methanol solvent[95], though this does not proceed sufficiently rapidly to consume the excess of borohydride used in each reaction.

3.2.2 Mass spectrometry analysis of the borohydride reduction of acetanisole.

A solution containing acetanisole and 1-(4-methoxyphenyl)ethanol was prepared and analysed through flow injection analysis. The positive ion mass spectrum shown in Figure 3-2 indicated signals at *m/z* 151 and *m/z* 135. These are identified as the protonated molecule for acetanisole and $[M+H-H_2O]^+$ from the 1-(4-methoxyphenyl)ethanol respectively. These peaks are deemed ideal to follow the chemical reaction outlined in Figure 3-1.

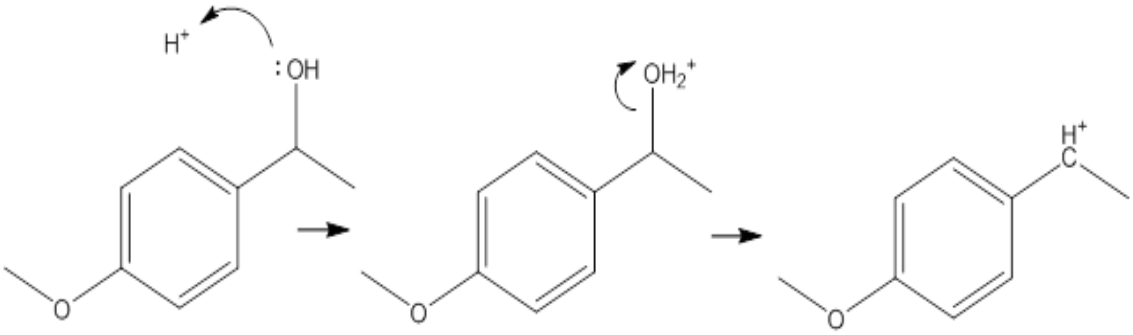

Figure 3-2 Proposed mechanism for 1-4(methoxyphenyl)ethanol product ion formation

The proposed dissociation of protonated acetanisole, through water loss to 1-(4-meyhoxyphenyl)ethanol is given in Figure 3-2 series of injections were analysed on whereby the concentration of acetanisole covered a range of 0.1 µg/mL to 20 µg/mL. From this full scan MS experiment, a concentration of 6 µg/L was deemed to be a good starting point for the acetanisolesuch that the signal at *m/z* 151 for acetanisole $[M+H]^+$ was clearly observed via a SIM channel at a S/N of 366:1 whilst at the same time enabling detection of $[M+H-H_2O]^+$ for 1-(4-

methoxyphenyl)ethanol at *m/z* 135 with S/N 209:1. Full scan data was first used to observe the ions if any and then SIM channels were added to the method to target ions of interest.

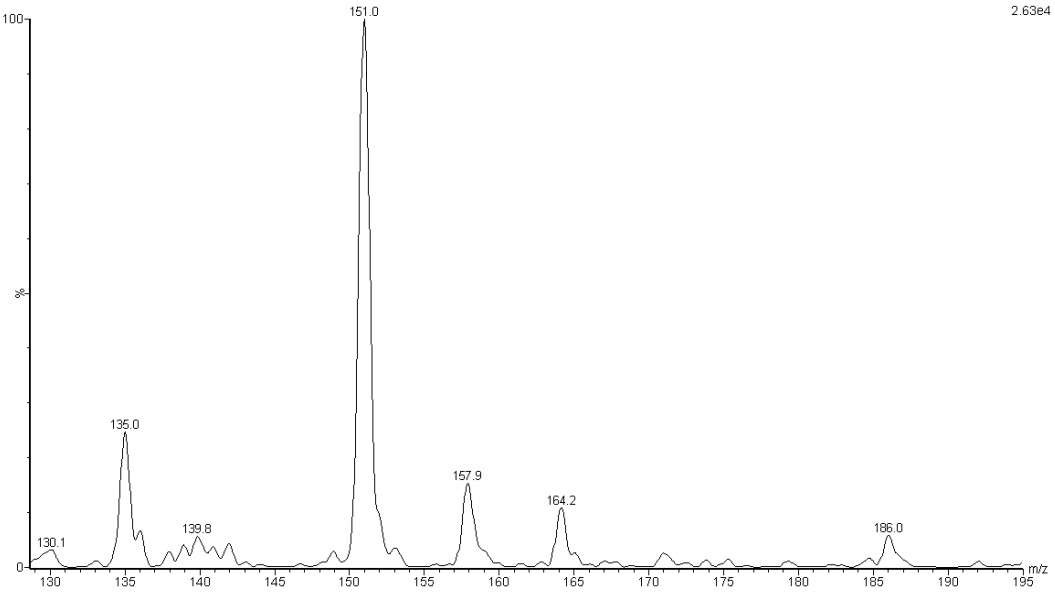

Figure 3-3. Example mass spectrum for the injection from an off-line reaction after 45 minutes, showing signals for m/z 151 (protonated acetanisole) and m/z 135 (1-(4-methoxyphenyl)ethanol [M+H-H_2O]$^+$) Other signals visible were present in blank backgrounds at similar levels, and are believed to be residual within the instrument due to contamination from other experiments run at extremely high concentrations on the shared instrument.

To test the monitoring capability of the QDa for this reaction, a reaction was conducted with off-line monitoring using a commercial HPLC (Aglient) for flow induction analysis before establishing a dedicated reaction monitoring system, achieved by manually removing 1 µL aliquots from the reaction vessel approximately every 3 minutes, diluting them 1:4000 into 50:50 acetonitrile:water with 0.1% formic acid, and injecting them into a flow of the same solvent. The presence of water in the solvent used for dilution acts to quench the reduction reaction by rapidly reacting with the sodium borohydride present and consuming it. The presence of acetonitrile with the water helps maintain a stable electrospray signal and the 0.1% formic acid assists protonation; this is a very common solvent system for electrospray mass spectrometry.

Figure 3-4 shows the ESI MS results from the manual sampling. Here the peak area of the SIM scan traces for *m/z* 135 is plotted as a function of the sum of the peak areas of the SIM scan traces for *m/z*

151 and *m/z* 135. The reaction can be seen to progress well over the first 1000 seconds, beyond which the graph begins to plateau, indicating that the reaction reaches completion at around 2000 seconds.

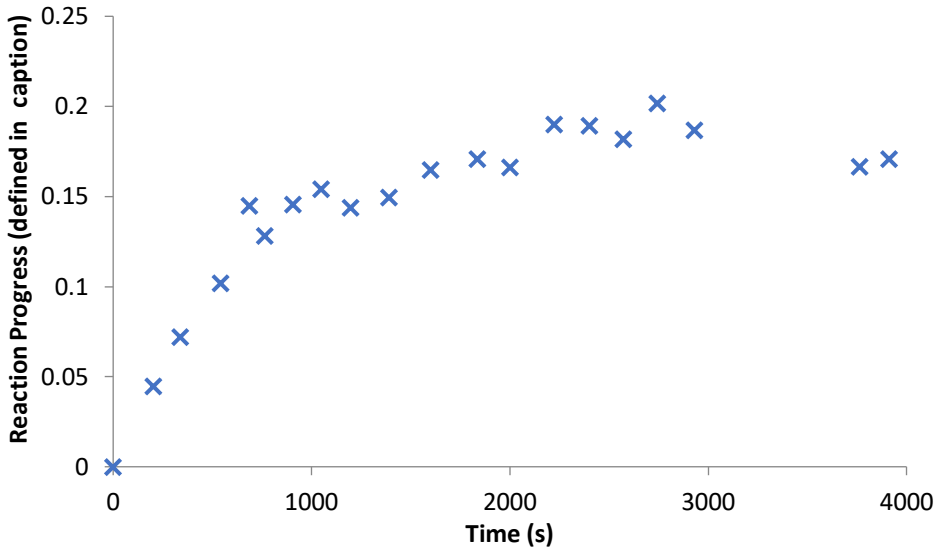

Figure 3-4. Reaction progress, equal to the m/z 135 signal area divided by the sum of the m/z 135 and m/z 151 signal areas.

From these results, it could be concluded that the reduction of acetanisole proceeds over an appropriate time frame and at an optimal concentration range, achieved through acceptable dilution, for MS monitoring and is suitable to be used as the initial target reaction for the on-line system.

3.2.3 NMR analysis of the borohydride reduction of acetanisole

In preparation for monitoring the reduction of acetanisole by low field ^{1}H NMR, a reference spectrum of the acetanisole starting material was taken. Figure 3-5 shows the ^{1}H NMR spectrum of a $CDCl_3$ solution measured on a 400 MHz superconducting magnet instrument (Bruker), showing 2 distinct singlets at 2.55 ppm and 3.85 ppm corresponding to 3 protons each for the methyl groups, and 2 distinct doublets at 6.95 ppm and 7.95 ppm corresponding to 2 protons each for the two different proton environments on the ring.

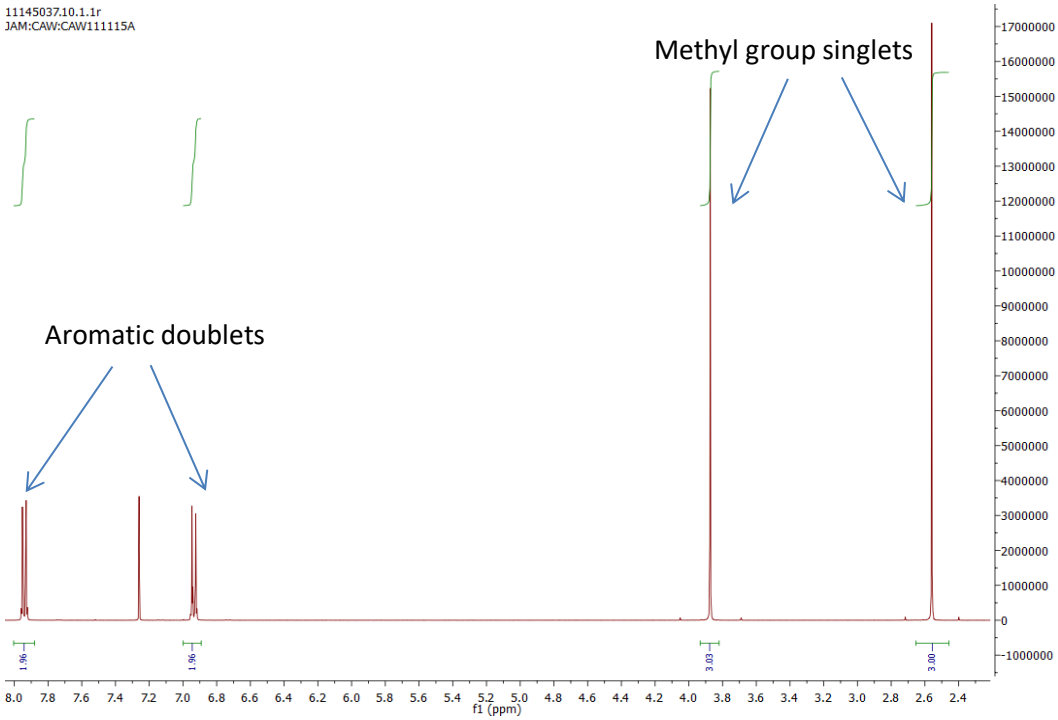

Figure 3-5. ^{1}H NMR spectrum of acetanisole (400 MHz, $CDCl_3$, non-flow)

The signal from the methoxy group (3.85 ppm) was discounted as a prospect for monitoring, as the reaction was to be conducted in methanol which itself has strong methyl signal at 3.31 ppm and considered likely to interfere with acetanisole's methoxy signal .

The feasibility of monitoring the reduction from signals indicative of acetanisole and 1-(4-methyoxyphenyl)ethanol in a protonated solvent was investigated by taking a sample of the reaction mixture 30 minutes after the addition of the $NaBH_4$. A standard 5 mm NMR tube with vented cap as the side reaction between $NaBH_4$ and methanol results in a slow release of hydrogen gas. A ^{1}H NMR spectrum, Figure 3-6, was then recorded on a 200 MHz superconducting magnet instrument (Oxford instruments)

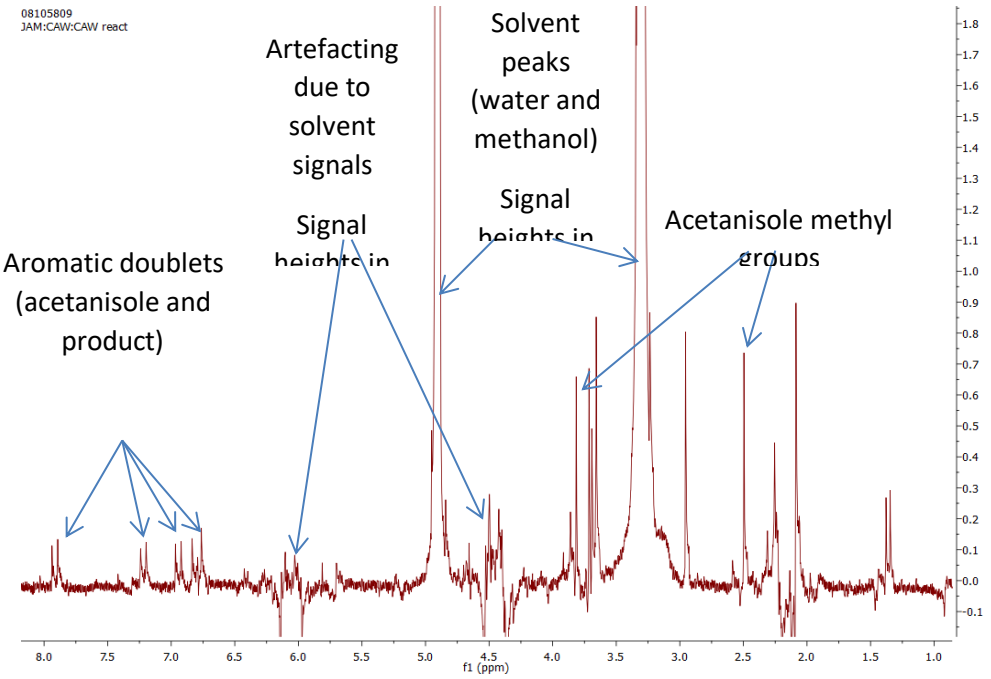

Figure 3-6. ^{1}H NMR of reaction sample (200 MHz, CD_3OD, non-flow) taken mid-reaction.

As the pulse sequence was originally designed for relatively small concentrations of proton-containing sample in a deuterated solvent, it was necessary to reduce the pulse angle in order to avoid overloading the detector. In addition, automatic shimming was not used due to the absence of a deuterated solvent signal to lock on to. This led to non-ideal peak shape as can be seen in Figure 3-6. The strong methanol signal also caused artefacts which further distorted the sample. As the concentration of the methanol was much greater than those of the reactants, the signal-to-noise ratio is poor, with the relevant peaks close to the baseline noise in intensity.

Nevertheless, as can be seen in Figure 3-6 the aromatic doublets shown in 3-5 have shifted over the course of the reaction, resulting in 4 sets of doublets being visible in that region (2 arising from the acetanisole, 2 from the 1-(4-methoxyphenyl)ethanol and are not in an area of the spectrum with which the methanol signals are interfering, making them the best targets for monitoring.

The reaction was then monitored in CD_3OD with a ^{1}H 500 MHz instrument (Varian). This produced two results of note. Firstly the signals for sodium borohydride were clearly visible, as shown in Figure 3-7, showing as a widely split doublet of doublets between -0.125 and -0.375 ppm. The smaller

triplet signals adjacent to each signal are due to H-D exchange with the deuterated solvent which show a decline as the reaction progresses. The $NaBH_4$ was not observed in the ^1H NMR spectrum in methanol recorded at 200 MHz as the region observed was narrowed in an attempt to improve instrument performance, nor was this visible in the positive ion electrospray mass spectrum as the sodium concentration is insufficient to see clusters and the borohydride ion would not have sufficient mass to be detected.

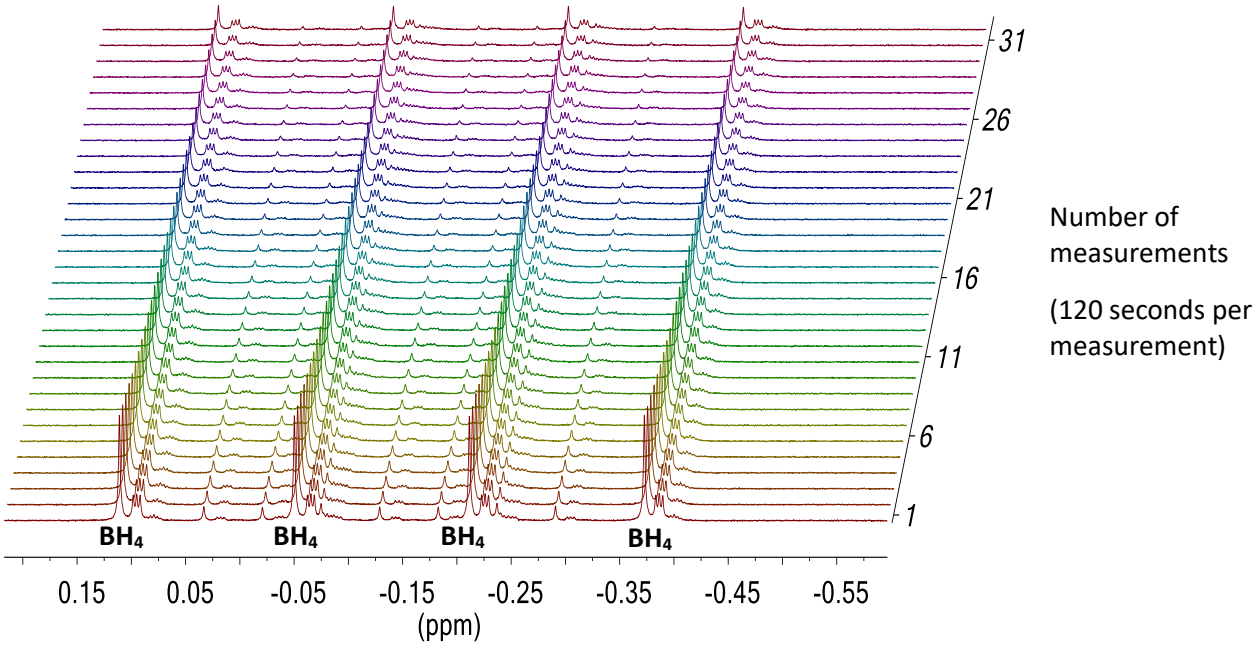

Figure 3-7. Borohydride signal over time (500 MHz, CD_3OD, earliest at bottom, 1 minute 4 seconds per spectrum).

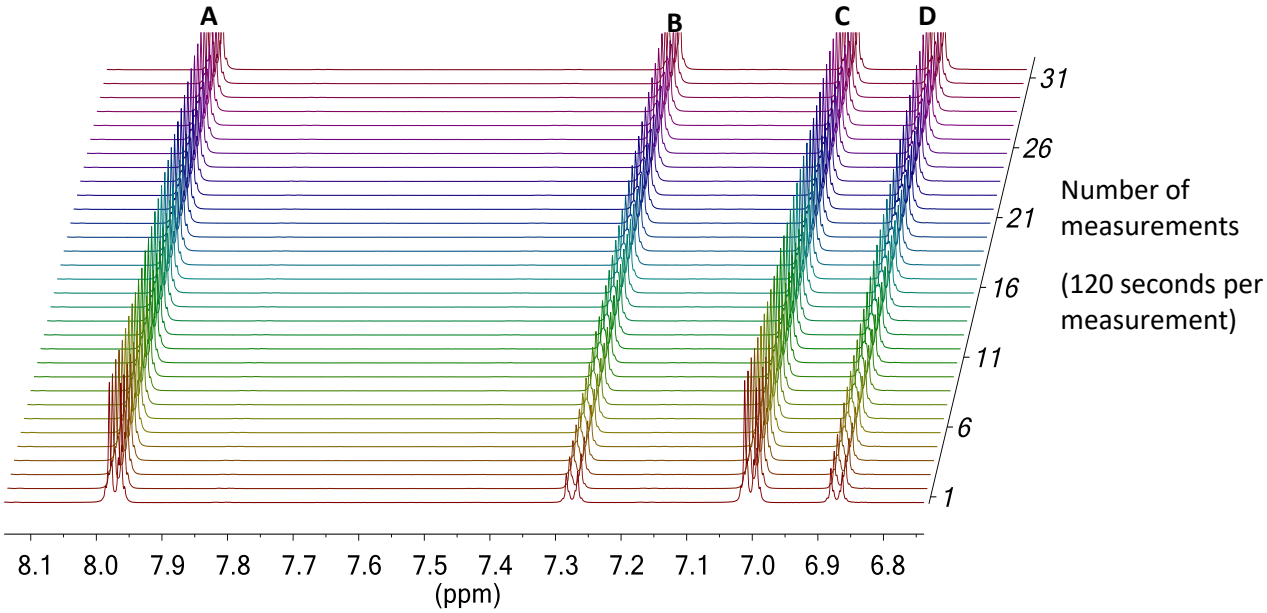

Figure 3-8. Aromatic region, (^1H NMR 500 MHz, CD_3OD, earliest at bottom, 1 minute 4 seconds per spectrum). Signals A and C result from aromatic protons on acetanisole, while Signals B and D are from 1-(4-methoxyphenyl)ethanol

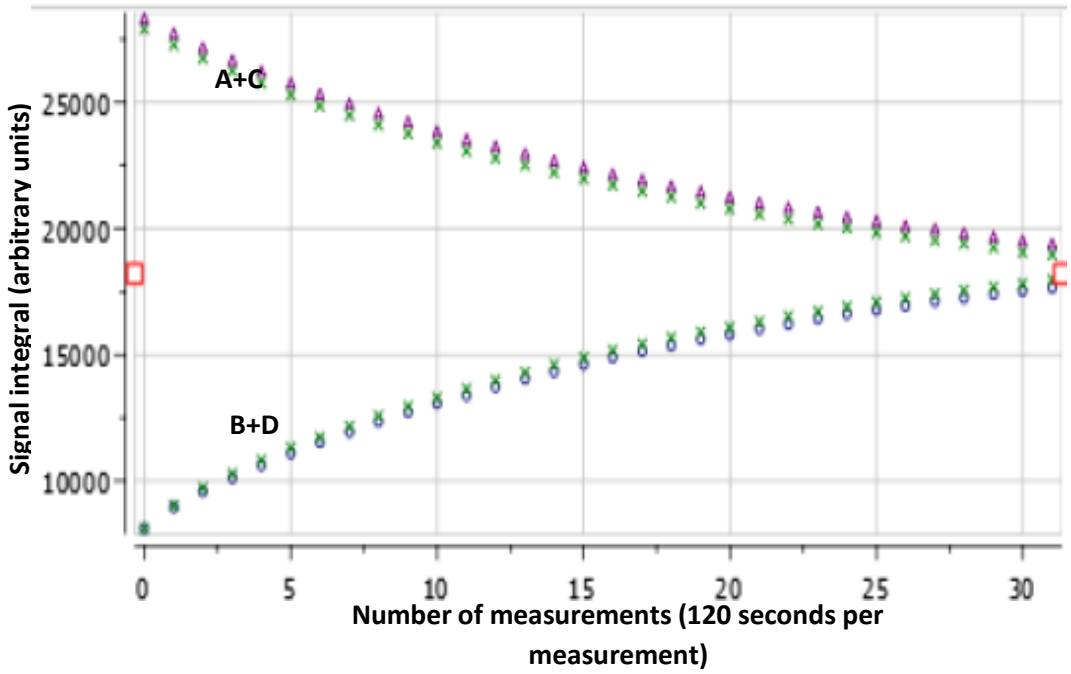

Figure 3-9 Integration values of aromatic signals over time (500 MHz 1 minute 4 seconds per scan). Signals A and C result from aromatic protons on acetanisole, while Signals B and D are from 1-(4-methoxyphenyl)ethanol

The second observation was that the signals in the aromatic region identified as potential targets for reaction monitoring were sufficiently clear and well defined such that changes in each of the signals was successfully plotted, as Figure 3-9 shows. The trends are paired with the signals for acetanisole (**A** + **C**) showing matching decline while the equivalent signals (**B** + **D**) show a reciprocal increase, as can be seen in Figure 3-9

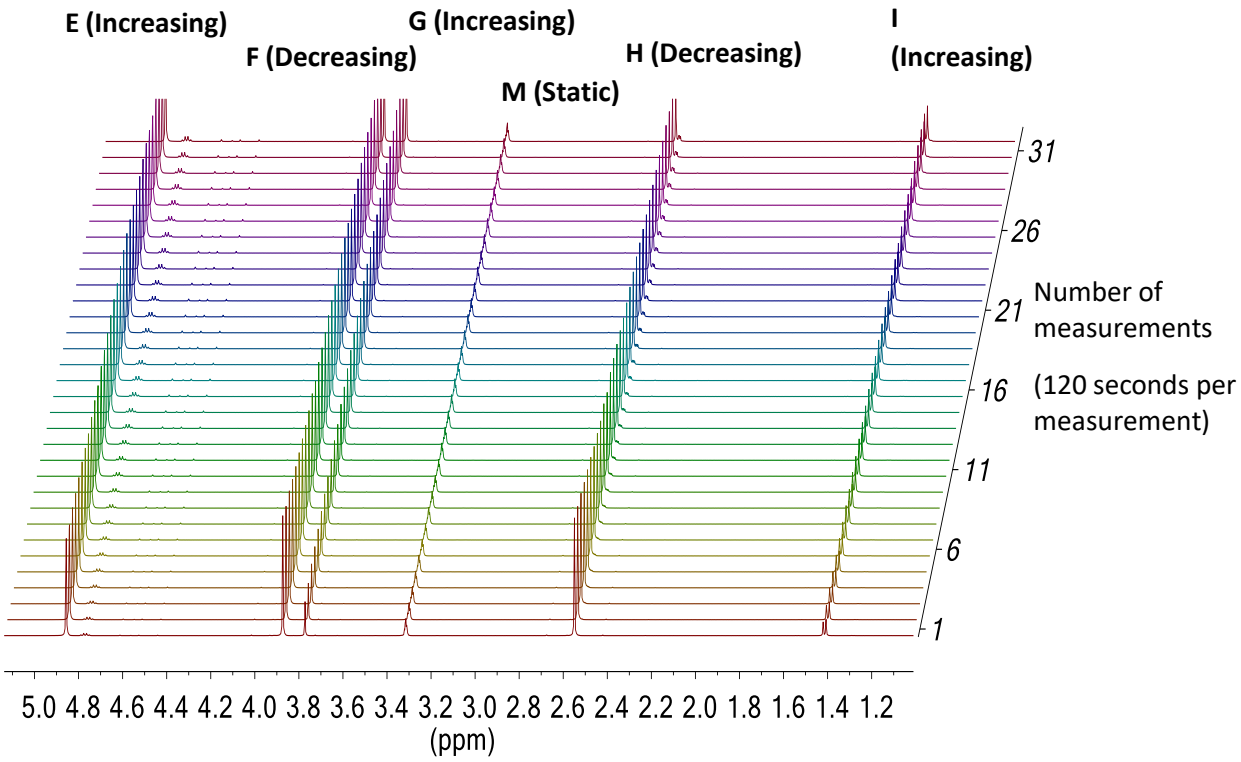

Figure 3-10.[1]H NMR(500 MHz CD_3OD) signals between 1 and 5 ppm from reaction over time (earliest at bottom) 1 minute 4 seconds (64 sec) per spectrum. Signals E G and I arise from 1-(4-methoxyphenyl)ethanol, Signals F and H from Acetanisole, while signal M is from CD_3OH formed by proton exchange between CD_3OD solvent and exchangeable protons on the analytes.

.

The signals observed between 1 ppm and 5 ppm, shown in Figure 3-10, range fall into 3 groups, with **E** (4.9ppm), **G** 3.8ppm and **I** (1.5ppm) arising from 1-(4-methoxyphenyl)ethanol, **F** (3.9ppm) and **H** (2.5 ppm) arising from acetanisole and **M** (3.35 ppm) which arises from CD_3OH formed from proton exchange between the analytes and the deuterated solvent[96], and which remains consistent across the reaction period. Signal **M** serves as a useful reminder of the approximate position that a methanol OH signal would appear at in a reaction without deuterated solvent, and as a consequence, the proximity of the signals labelled **F**, **G** and **H** lead them to be ruled out as prospects for monitoring, despite giving clearly observable trends in this experiment.

A reaction was then conducted under the same conditions in a static tube using a low-field NMR instrument operating at 43 MHz (Magritek) to monitor the proton signal for 50 minutes, acquiring 1 spectrum every 30 seconds. The level of noise was noted to be significantly greater than in the high-field instrument. This was expected as only a single pulse acquisition per spectrum was possible, whereas it is common practice for multiple acquisitions to be averaged on higher field instruments.

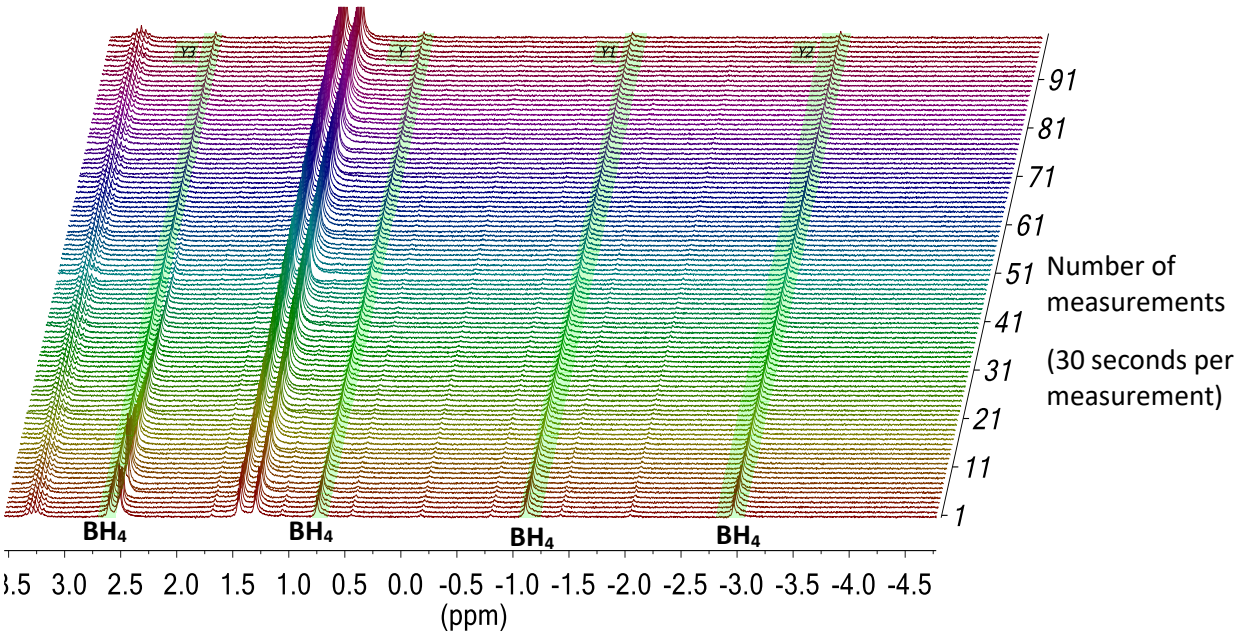

Figure 3-11. Borohydride signal over time (^{1}H 43 MHz, CD_3OD, non-flow, earliest at bottom, 30 seconds per spectrum).

Another significant difference was noted in the borohydride signals, which, as can be seen in Figure 3-11 are splitting over a range of 5.5 ppm. This is an inherent feature of lower field-strength NMRs as the splitting frequencies are field independent, and in this case are 161 Hz and 84 Hz. The split in ppm terms is proportional to $1/B_0$, with this 161 Hz coupling resulting in a split of 3.75 ppm and the 84 Hz coupling resulting in a further split of 1.95 ppm on this 43 MHz instrument, though the same couplings on a 500 MHz instrument would represent splits of 0.32 and 0.17 ppm respectively . While the BH_4 signal is a particularly dramatic example of this issue, all protons with splitting will see similarly increased splits in ppm terms.

The impact here in practice is that there is some overlap between the portion of the BH_4 signal at 2.65 ppm and signal **H** from the acetanisole starting material, meaning that the data from both of

those will be suboptimal. However, for monitoring BH_4, any of the other signals are sufficient, though as can be seen in Figure 3-12 the data produced even from those has a significant amount of noise due to baseline fluctuations.

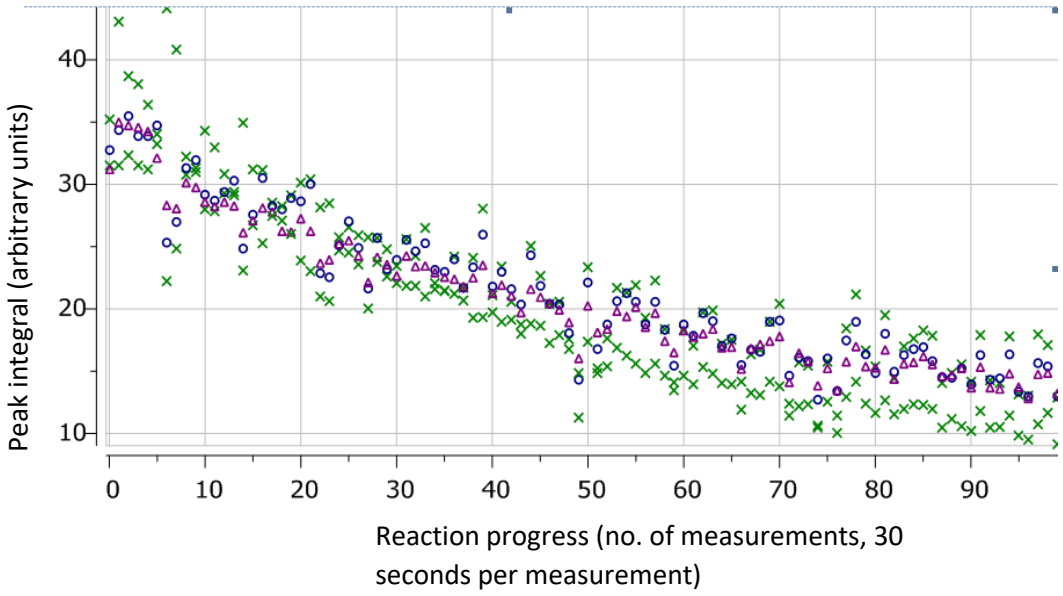

Figure 3-12 - Integration values of borohydride signals at 2.6 ppm (green), -1.1 ppm (blue) and -2.9ppm over time (^{1}H 43 MHz, CD_3OD, non-flow, 30 seconds per measurement)

The aromatic signals (Figure 3-13) were also more split in ppm terms due to the lower field, resulting in overlap between signals. As such it was decided to treat each half of each doublet as an individual signal, labelled **A_1** and **A_2**, **C_1** and **C_2** for the aromatic protons from acetanisole and **X_1** and **X_2**, **Y_1** and **Y_2** for the aromatic protons from 1-(4-methoxyphenyl)ethanol, since most had some degree of overlap.

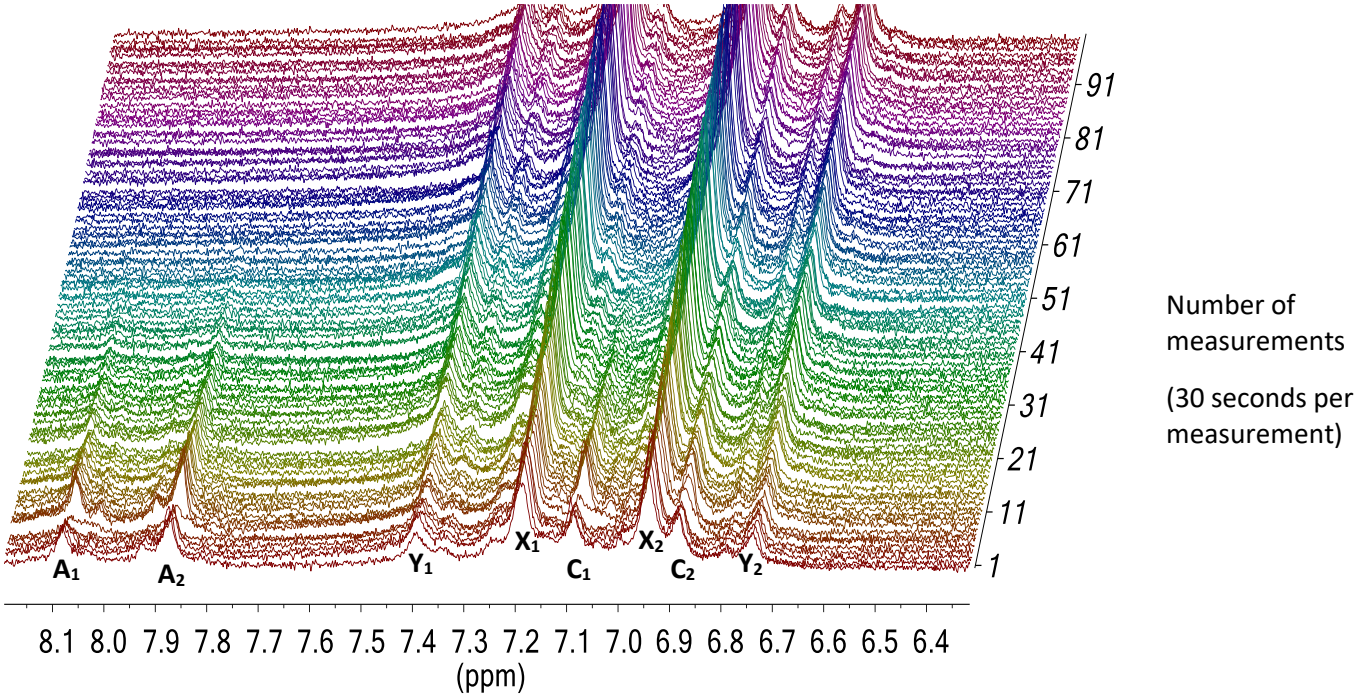

Figure 3-13- Aromatic signals over time (^{1}H 43 MHz, CD_3OD, non-flow earliest at bottom, 30 seconds per spectrum)

The aromatic signals from the acetanisole, namely **A_1, A_2** and **C_1**, are clearly separated and show decreases across the course of the reaction (Figure 3-13) which, while showing fluctuation in peak integral due to baseline interference, are broadly consistent with the decreases observed from the reaction in the 500 MHz instrument. Integrals of the three signals, **A_1, A_2** and **C_1,** are given in Figure 3.14 where a marked dip in signal is clearly visible at 5 min, believed to be due to a gas bubble passing through the measurement volume, following which the reduction of acetanisole settles into the same rate of consumption as shown in Figure 3-9 for the high-field NMR measurements.

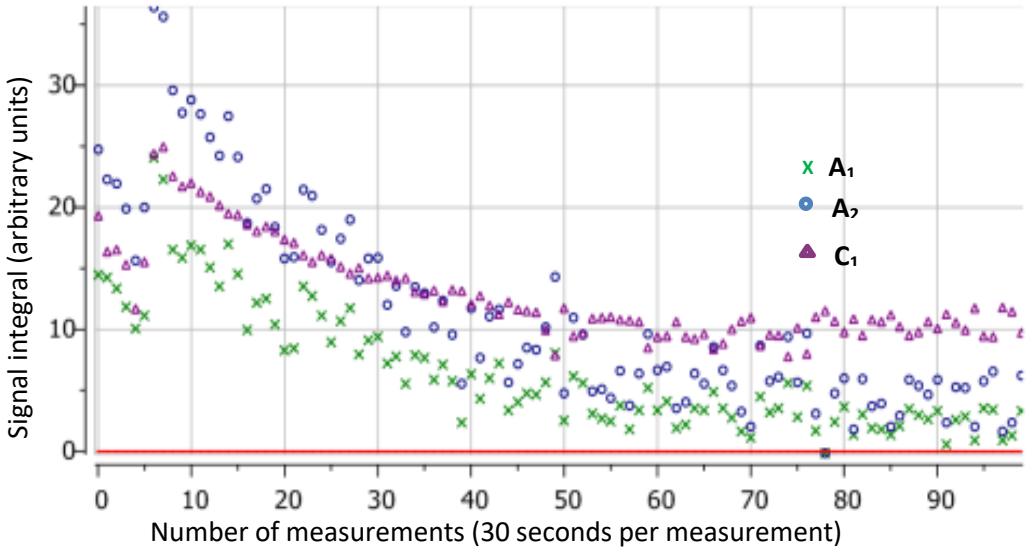

Figure 3-14- Acetanisole aromatic signal integrations over time (^{1}H 43 MHz, CD_3OD, non-flow, 30 seconds per scan)

The change in integral over the course of the reaction is smaller in the 43 MHz dataset than in the 500 MHz dataset. This is proposed to be due to a slow side reaction between methanol and sodium borohydride during a delay of around 20 minutes between the dissolution of the sodium borohydride and its addition to the reaction in the 500 MHz experiment, the effective starting concentration of sodium borohydride in the 500 MHz experiment was smaller and there was thus more acetanisole unreduced by the time the monitoring could be commenced, there being a short additional delay for the loading of the sample and the start of the experiment.

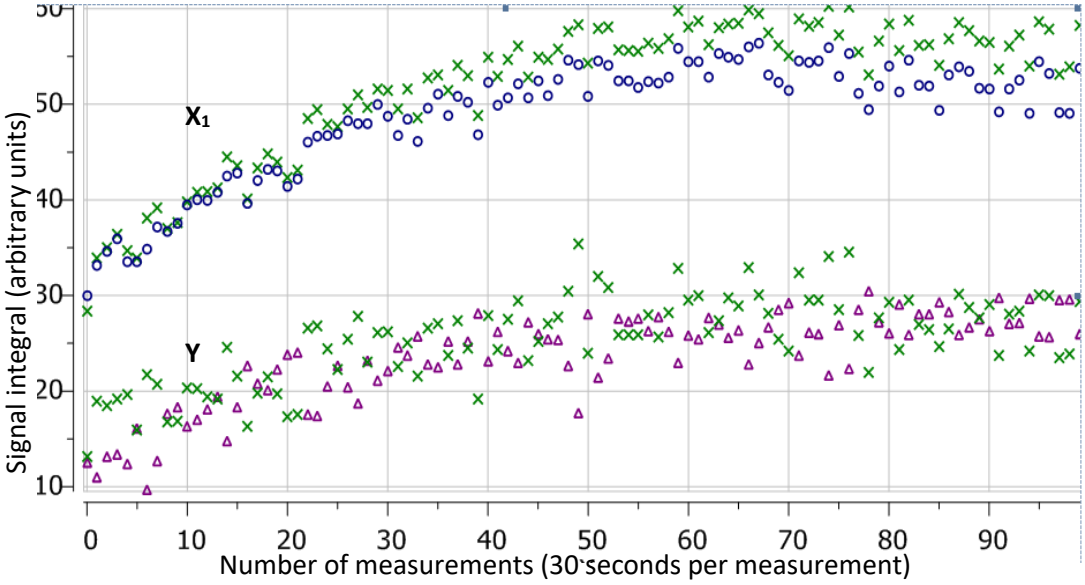

Figure 3-15. 1-(4-methoxyphenyl)ethanol aromatic signal integrations as a function of time (43 MHz, methanol, flow, 30 seconds per scan).

The signals corresponding to the aromatic protons on the 1-(4-methoxyphenyl)ethanol also have been split into two groups, **X** and **Y.** based on trends produced (Figure 3-15), with group **X** showing approximately the same increase as **Y**, as expected given that both are aromatic signals from though with the **X** signals starting at higher integration values. It would appear that other peaks are interfering with the **X** values, as a fairly consistent positive offset of approximately 20 units results.

The remaining signals from 0 ppm to 5 ppm (Figure 3-16) again fall into two broad groups of behaviour, with **F**and **H** mirroring the behaviour seen in Figure 3-14 for $\mathbf{A_1}$, $\mathbf{A_2}$ and $\mathbf{C_1}$, though in the case of **H** with some offset due to slight overlap with the adjacent BH_4 signal, while **E**, **G** and the doublet of **I** mirrors the pattern seen in Figure 3-15 for **Y**, lacking the interference from overlapping signals seen in the signals labelled **X.**

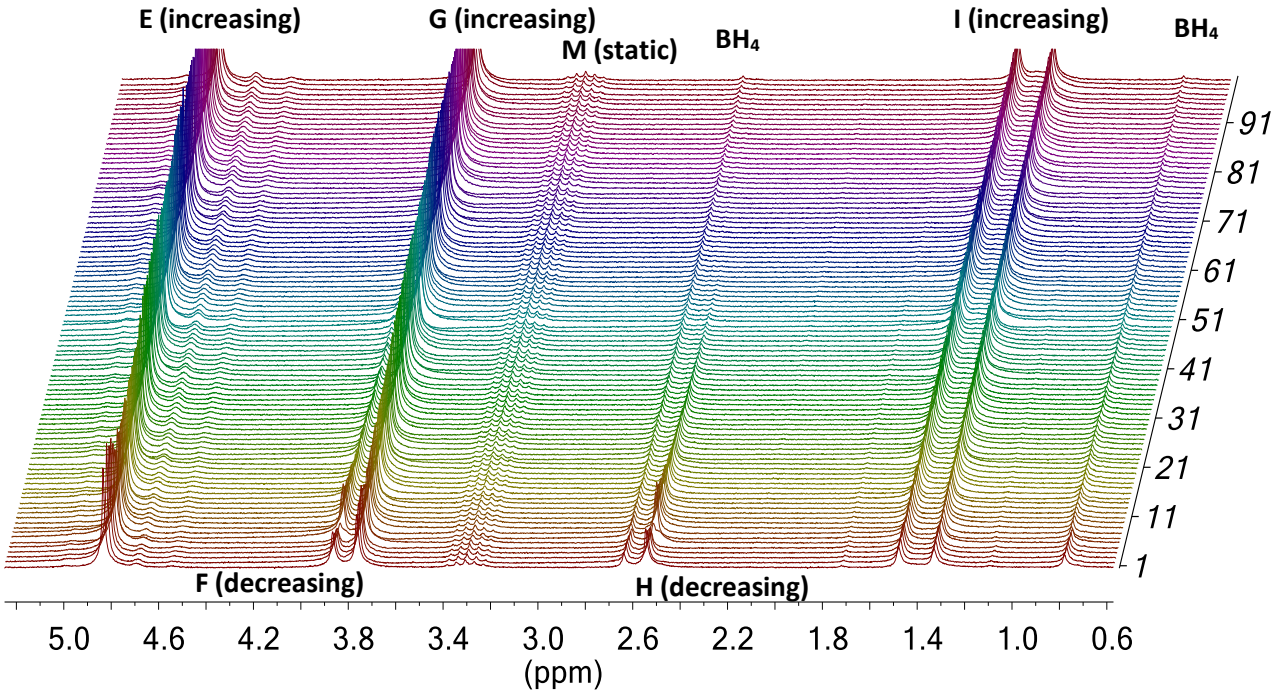

Figure 3-16- ^1H NMR (43 MHz, CD_3OD, flow) signals between 0.6 and 5 ppm from reaction over time (earliest at bottom) 30 seconds per spectrum.

3.2.4 Summary

Through these experiments, an understanding was gained for the ions observed in the mass spectrometer. Only one peak was observed for the starting material, and this corresponded to protonated acetanisole, $[M+H]^+$. Only one peak was observed for the generated material and this corresponded to the dehydrated product ion of protonated 1-(4-methoxyphenyl)ethanol, $[M+H-H_2O]^+$. These signals are clearly distinct from each other and are not compromised by any interfering signals, which inherently simplifies reaction monitoring process. In addition, an appropriate concentration range for MS monitoring starting from a concentration of 6.25 μg/mL, the effect of methanol solvent on the NMR spectrum established and appropriate monitoring signals for the NMR in the aromatic region identified, with additional signals for the product and starting material identified but judged to be poor candidates for monitoring due to their proximity to methanol solvent signals.

3.3 Developments in MS configuration towards an on-line detection system

3.3.1 Integrating a mass rate attenuator to manage on-line dilution

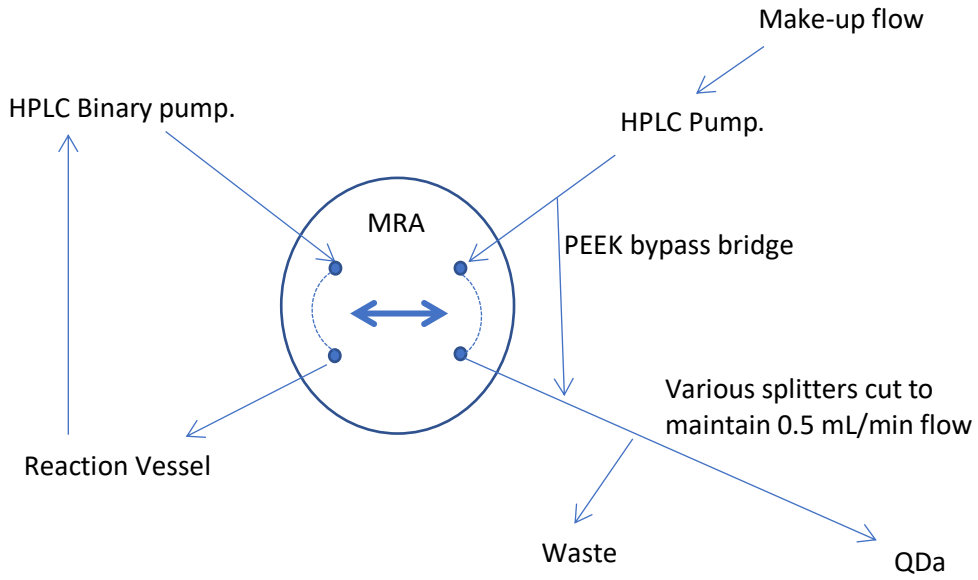

Figure 3-17- Reaction setup used for MS-only reaction monitoring

The analytical solution for reaction monitoring was initially assembled as two separate loops, with the NMR and MS instruments each designed, tested and validated independently by monitoring a reaction on-line. The dilution required to reduce the concentration of acetanisole and 1-(4-methoxyphenyl)ethanol to a level suitable for analysis by the mass spectrometer was achieved through the use of a Mass Rate Attenuator (MRA) (Rheodyne). This device uses a rotor system in which two flow channels pass through fixed volume channels on the rotor (Figure 3-17), with options for 300, 100 or 22 nL volume channels. When the rotor cycles, an aliquot of the selected volume is switched between flow paths. By controlling the flow rate of the channel passing into the mass spectrometer, the channel used and the frequency of the rotor cycling, it is possible to achieve a fixed dilution of the analyte. For a full list of switching rates for each channel, see appendix 1.

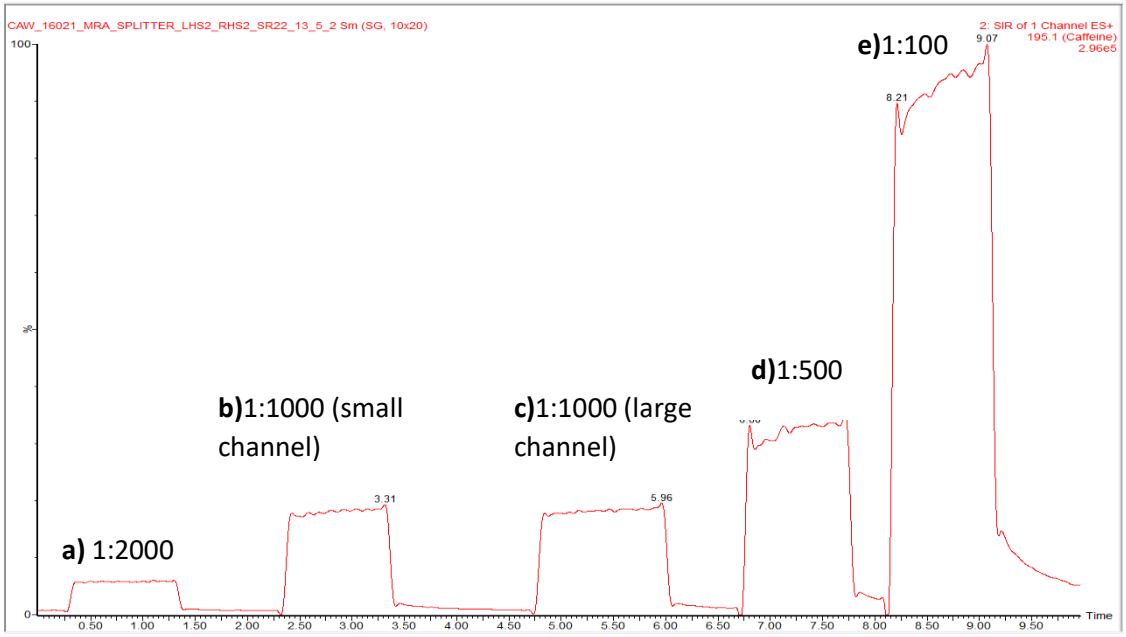

Figure 3-18 Investigation into five MRA settings. 1 mg/mL caffeine diluted by the indicated proportions, with the first 1:1000 dilution using a higher sampling frequency but lower sampling volume than the second.

Using a 1 mg/mL solution of caffeine in 50:50 acetonitrile:water and monitoring the $[M+H]^+$ peak at *m/z* 195, the ability of the MRA to provide suitable dilution for MS analysis was investigated. Figure 3-18 shows 5 different MRA settings, from **a),** SR (switching rate) 22 (22 nL) sampling at 0.303 Hz into a 1 mL/min make-up flow of 50:50 water:acetonitrile diluting the caffeine by 2000 times, through to **e),** SR 31 (300 nL) sampling at a frequency of 2.22 Hz.

The MRA was capable of two configurations capable of delivering a split ratio of 1:1000 as shown in Figure 3-18, one with the 100 nL volume, at a lower frequency, the other using the 22 nL volume at a higher frequency. Despite the absence of dedicated mixing volume, these produce near identical results, indicating that the dead volume inherent in between the MRA and MS is serving to smooth out the signal at this scale.

There is no significant difference in the rate of signal build-up between the faster and slower switching conditions for the 1:1000 dilution, indicating that the overall rate of flow into the mass spectrometer determines the rate of signal appearance, rather than an artefact of the MRA dilution.

Signal drop-off after the end of MRA cycling is near immediate, though there is visible tailing from sample build-up especially at higher concentration, as shown in Figure 3.17 for sample **e)** at a 1:100 dilution. Here, the caffeine signal shows a clear increase from 90% to 100% relative abundance between 8.0 min and 9.0 min; followed by a rapid decrease at 9 min, the signal only drops to 20% and takes a further minute to reach 10% suggesting that caffeine is building up, most likely inside the ion source of the MS instrument. This would therefore not be suitable for use in monitoring as the gradual buildup of caffeine would mask or alter any change in concentration caused by a reaction. This phenomenon was found to be a general issue with the instrumentation, with similar buildup found after uses of high concentrations of lactose and paracetamol.

The maximum dilution factor possible with the MRA is 1/2000th of the flow rate in mL/min. The optimal flow rate for the QDa mass spectrometer operating in 'standard mode' (see section 2.3.1) is 0.5 mL/min and the maximum stable flow rate of the make-up pump is 4 mL/min. To examine make-up pump flow rates greater than 0.5 mL/min, a T-piece was introduced to divert a proportion of the flow to waste. The proportion of flow diverted to waste was managed by choice of PEEK tube length, with lengths of 1/16th inch I.D. tubing cut to length to balance the backpressure provided by the QDa capillary and associated tubing. These were determined manually by measuring flow rates using a stopwatch and measuring cylinder. Consequently, the maximum dilution that could be achieved through this combination of equipment is 1:8000, delivered by the make-up pump operating at 4 mL/min and the MRA switching 22 nL at 0.303 Hz. The T-piece was plumbed in to deliver a 1:7 split of solvent with 0.5 mL/min reaching the mass spectrometer and 3.5 mL/min to waste.

3.3.2 Investigation of flow interruption due to cycling

A close inspection of a total ion chromatogram shows pulsing when 22 nL aliquots of methanol are sampled into a makeup flow of methanol at 0.303 Hz (Figure 3.19 (a)), despite this effectively being a solvent blank. These negative spikes are thought to be due to a short interruption of the make-up solvent flow while the rotor is between the fill and transfer positions. In an experiment to overcome

the pulsing, a bypass line of 0.05” internal diameter PEEK tubing (shown in Figure 3-17) allowing a flow to pass to the mass spectrometer, even when flow from the reaction vessel through the MRA was interrupted. The narrow diameter was used to ensure that when both paths are open, the majority of the flow will be via the MRA, which has an internal diameter of 0.1”. The split was calculated as 240:1 in favour of the MRA path using a passive flow split calculator provided by Waters Corporation[97]

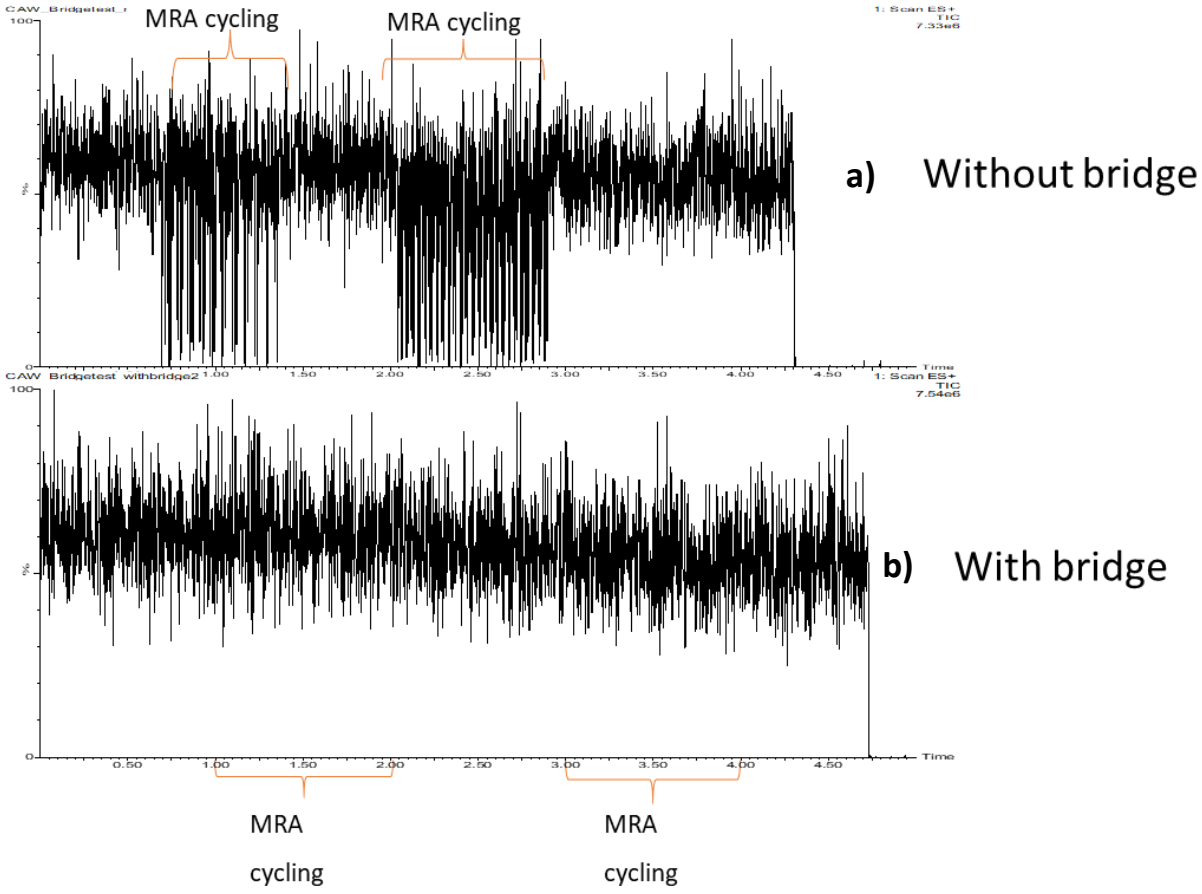

Figure 3-19 Effects of MRA cycling on signal for methanol a) with and b) without bridge.

As may be seen in Figure 3-19 (b), the negative spiking ceased once the bridge was added. This configuration was retained for all future experiments.

One further consequence of the MRA operation must be considered. When aliquots of reaction mixture are switched into the flow from the make-up pump, at the same time, the same volume of make-up solvent will be switched into the flow that is returning to the reaction vessel. It is important to return the flow to the reaction vessel because the volume of sample consumed over the course of a reaction would otherwise be the full amount removed for NMR and MS analysis (in the order of 1 mL/min) rather than the 400 nL/min transferred via the MRA when cycling the 22nL volume at 0.303 Hz and the volume of reaction mixture required and the loss of product to monitoring would thus be much larger however, it should be appreciated that adding small quantities of make-up solvent to the reaction vessel may have an effect on the reaction. For example, for the reaction shown in Figure 3-1, the use of the 50:50 acetonitrile:water mixture would cause significant problems as the $NaBH_4$ reacts rapidly with water (see section 3.2.2 where inclusion of water was used to quench the reaction). Regular dosing of even nL of water into the reaction vessel would have the cumulative effect of depleting the available $NaBH_4$. This was overcome for the on-line MS analysis of sodium borohydride reduction of acetanisole by using methanol as the make-up flow, however, make-up solvent(s) compatibility with the reaction under investigation remains an ongoing factor that must be considered in experimental design.

3.3.3 Evaluating the On-line ESI MS configuration by monitoring the reduction of acetanisole.

3.3.3.1 Experimental setup

Dry methanol was used for the make-up solvent. The flow rate was 2 mL/min with an initial 1:1 split delivering solvent at 1 mL/min to the QDa. While 1 mL/min is above the optimal value for the QDa, the dry methanol entering the mass spectrometer is more volatile and far more easily desolvated than aqueous solvent systems, and so this flow rate did not present any problems in this particular case and gave good steady signal response.

The MRA was set to switching ratio 22 0.22 nL at 0.385 Hz (see appendix 1), delivering the greatest split ratio possible for a make-up flow of 2 mL/min and resulting in a dilution of 1:4000, as had been used in the offline monitoring experiment. The QDa was operated simultaneously in two modes (channels). SIM scans were performed on ions at *m/z* 135 and 151 and full scan MS measurements made over *m/z* 100-1000. These channels were set to collect at 10 Hz, which was automatically reduced to 8.81 Hz to balance the channels within the capabilities of the quadrupole scan rate. The reaction was monitored for 1 hour.

3.3.3.2 MS Data processing

The analysis of the online MS data presented something of a challenge, as the data from each from a SIM channel consisted of some 31,716 data points detailing some 1386 separate cycles of the MRA, each the equivalent of one injection in an off-line method.

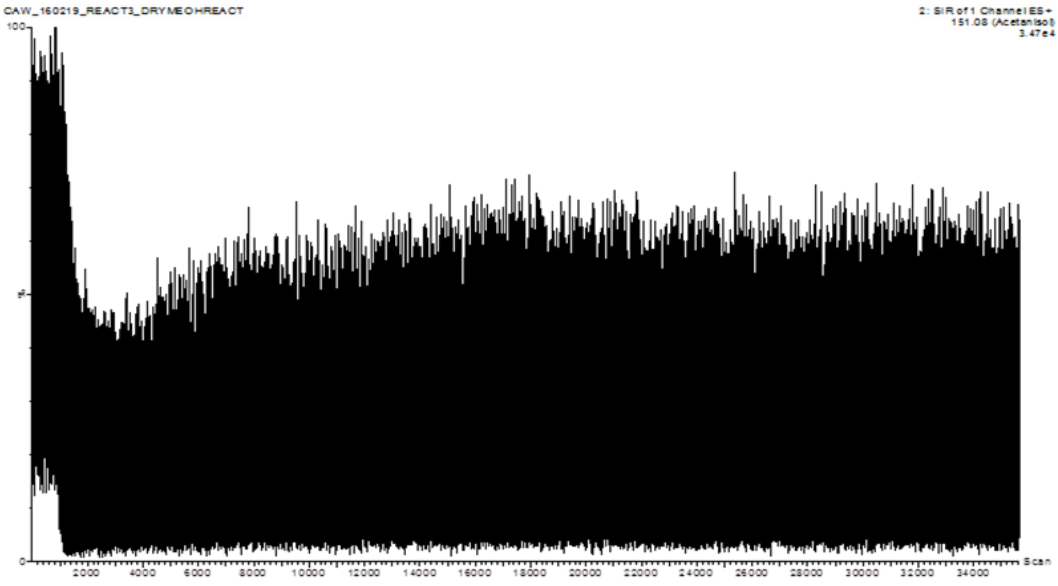

Figure 3-20. m/z 151 SIM chromatogram for acetanisole reduction reaction. MRA cycling rate 0.303 Hz,

Expansion of the region 950 to 1450 scans is shown in Figure 3-21, shows that at this MRA cycle rate, the signals for each 'injection' of the reaction mixture can be clearly resolved. This represents the greatest degree of resolution possible with the MRA, derived from the slowest cycling frequency,

and the high flow rate of make-up solvent and was chosen so as to deliver the greatest possible dilution and thus wash the reaction mixture through the ion source as quickly as possible.

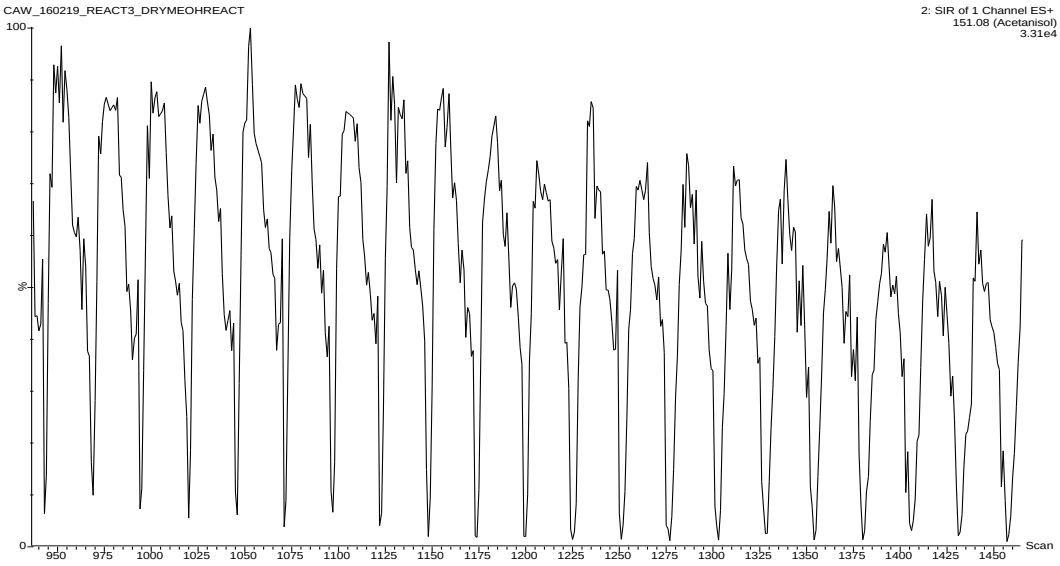

Figure 3-21. m/z 151 selected ion chromatogram (expanded view)

To extract usable information from these datasets, three methods of data processing were considered and evaluated: (1) moving average, (2) peak area analysis and (3) peak apex analysis.

3.3.3.2.1 Moving average

One method proposed for data processing was to take a simple moving average of the entire TIC using Microsoft excel, averaging across a period large enough to ensure that the fluctuation caused by the injections is damped out, in this case a 50 point (5 second) moving average. The outcome of this is shown in Figure 3.22 (a) for the SIM scan data of protonated acetanisole and (b) for the SIM scan data of 1-(4-methoxyphenyl)ethanol.

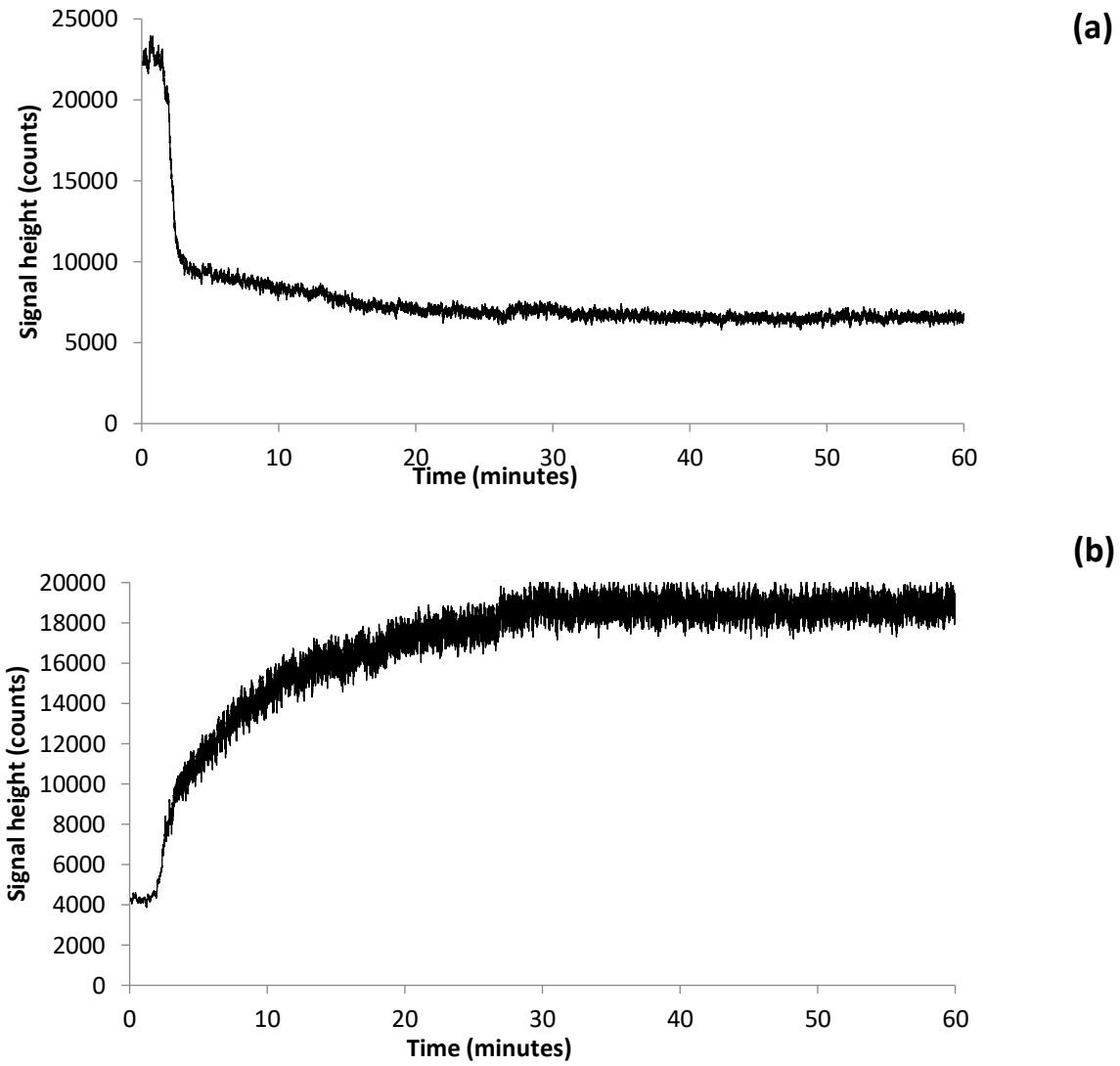

*Figure 3-22 SIM signals over time, with trend line indicating a 50 point moving average for **(a)** m/z 151 (acetanisole) and **(b)** m/z 135 (1-(4-methoxyphenyl)ethanol*

This produced, with an extremely simple processing method, a clear trendline for both *m/z* 151 and *m/z* 135, with the acetanisole being gradually consumed and the 1-(4-methoxyphenyl)ethanol generated as expected from the offline validation. One disadvantage of this approach is that the temporal resolution is limited by the size of the period averaged, in this case 5 sec.

3.3.3.2.2 Peak area

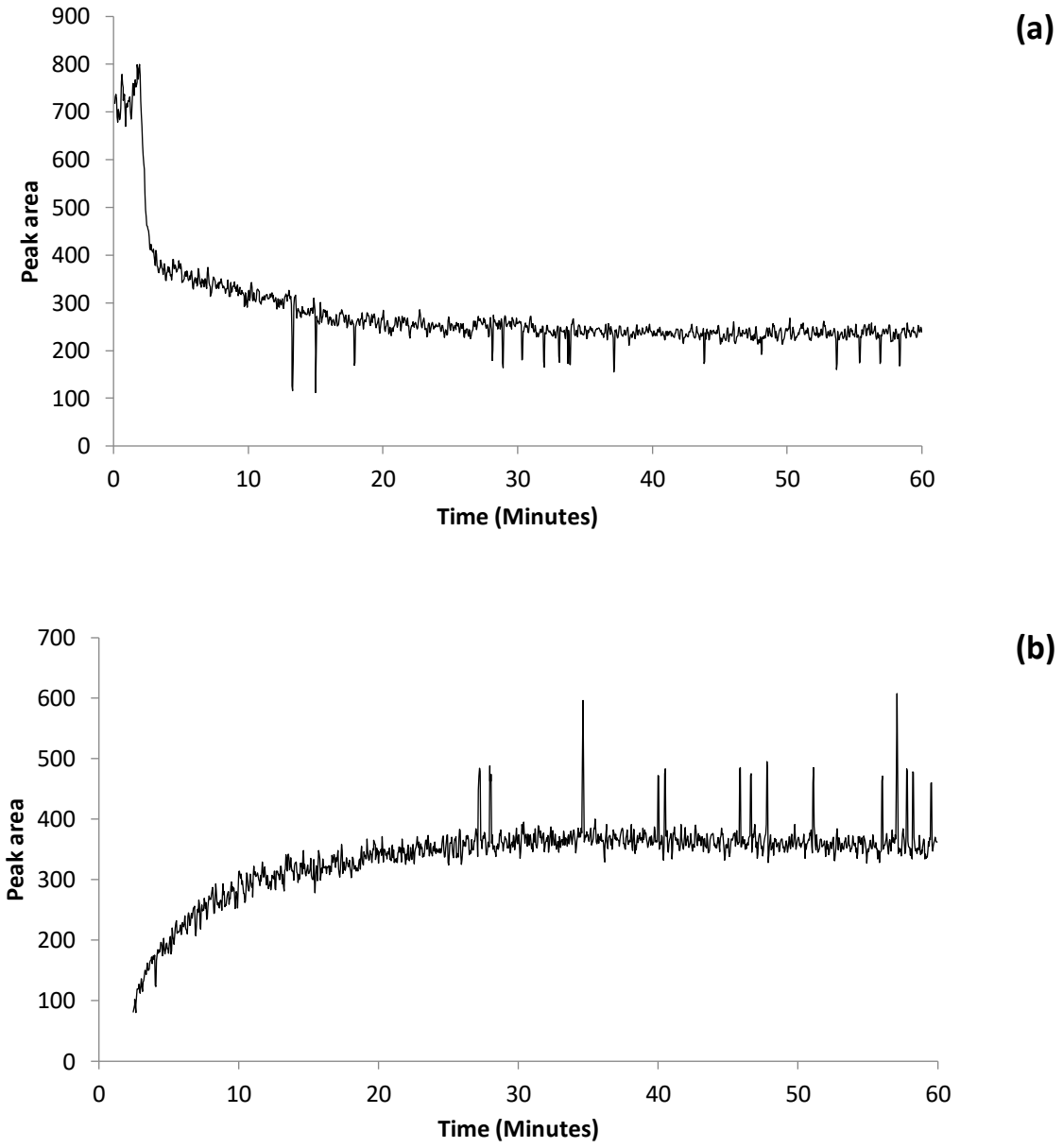

*Figure 3-23. MRA injection peak integration vs time for the SIM scan of **(a)** m/z 151 (acetanisole) and **(b)** m/z 130 (1-4-methoxyphenylethanol) using a 2 point average trendline. Negative spikes are outliers produced due to the misidentification of a single injection*

The second data processing method investigated was analysis by peak area, using the inbuilt peak integration within MassLynx 4.1. (Waters Corp.). This had the advantage of reducing the number of data points to be processed in excel significantly as it reduces the number of data points to be considered by a factor of 33, assuming the 0.303 Hz switching ratio. This makes the raw data easier

to manipulate in widely available software packages such as Excel (Microsoft), but was hindered by the limitations of the MassLynx software, which contains algorithms designed to identify and integrate the more gaussian shaped peaks generated in a chromatographic method, resulting in a tendency to identify partially overlapping peaks as a single peak, and to split those peaks with non-ideal shape into two separate signals, as would be desirable when processing a chromatograph of two compounds eluting at nearly the same time. In an attempt to correct for these occurrences, a moving average was employed. This still resulted in some negative spikes when misidentification of peaks occurred, as seen in Figures 3-25 (a) and (b). For consistency, the presented data is shown with a 2-point moving average, as this covers the same time 5 second period as the 50-point average used in Figure 3-22 for the moving average method and the trendlines produced with the peak area method were consistent with those from the moving average method, with the exception of the spiking.

3.3.3.2.3 Peak apex analysis

The third method investigated was the use of IF functions in Excel (Microsoft) to identify the apex of each peak. Working on the principle that, as the cycling frequency of the MRA is known, there is a defined period within which the local maximum must therefore be the apex of an injection peak. As such, the values were tested against the maximum for 10 scans in either direction, representing a window matching the known time of a single MRA cycle, and if they were found to be the largest value over that period, were passed forward as the apex of a peak.

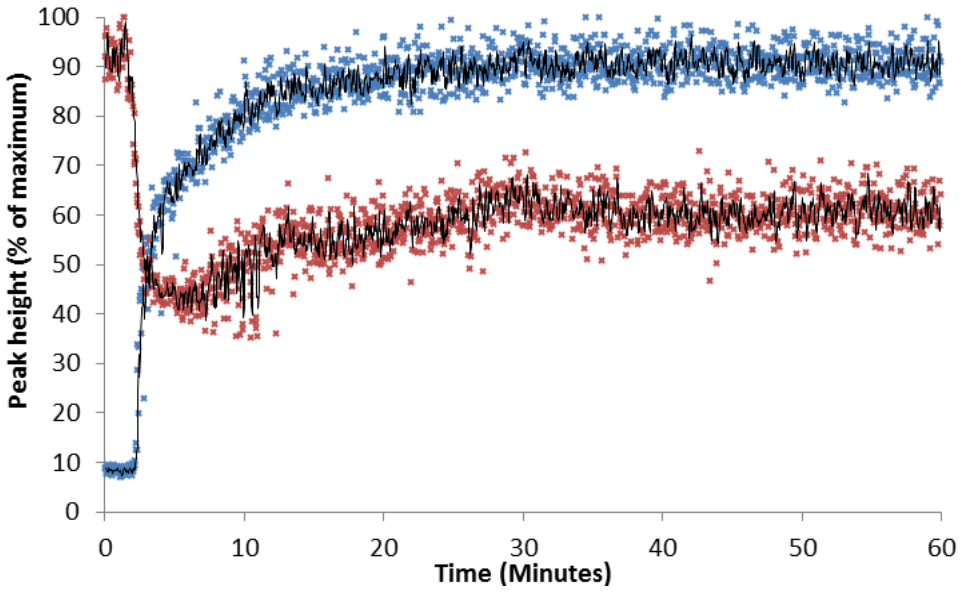

Figure 3-24. - Intensity of peak apex vs time. m/z 151 in red, m/z 135 in blue, 2 point average trendline

The peak apex method shows the same initial drop in intensity for *m/z* 151 as the moving average and peak area methods. This drop is then followed by a slight increase in *m/z* 151 between 8 and 28 minutes. The slight increase is not apparent in any of the other data analysis methods, and both the simple moving average and peak integration approaches show comparable rapid decrease that becomes more gradual as the reaction nears completion. There is no commensurate drop in the *m/z* 135 peak heights in this method, which show the same pattern as the other analysis methods.

As the apparent increase in the *m/z* 151 after the initial drop does not match with any other analysis method, nor with the off-line methods, nor with what one would reasonably expect to see, it appears that this apex based analysis method is falling prey to the issue that it assumes uniform peak shapes, which were not found in this case.

3.3.3.3 Conclusions

Both the moving average approach and the peak integration approach to processing this type of data produced fit-for-purpose trends. The moving average method has the advantages of simplicity, robustness against non-gaussian peak shape and compatibility with any MRA cycling rate as it does

not require clearly resolved injection peaks of uniformly gaussian shape. As such, the moving average method was used for future analyses, with some variation in the period of the averaging, which seemed to be best used at between 50 and 100 points depending on the degree of noise in the data. Figure 3-25 shows that a 100 point moving average does not introduce artefacts, though the duration of the period being averaged should be carefully considered on a case-by-case basis with reference to the rate of the reaction in question.

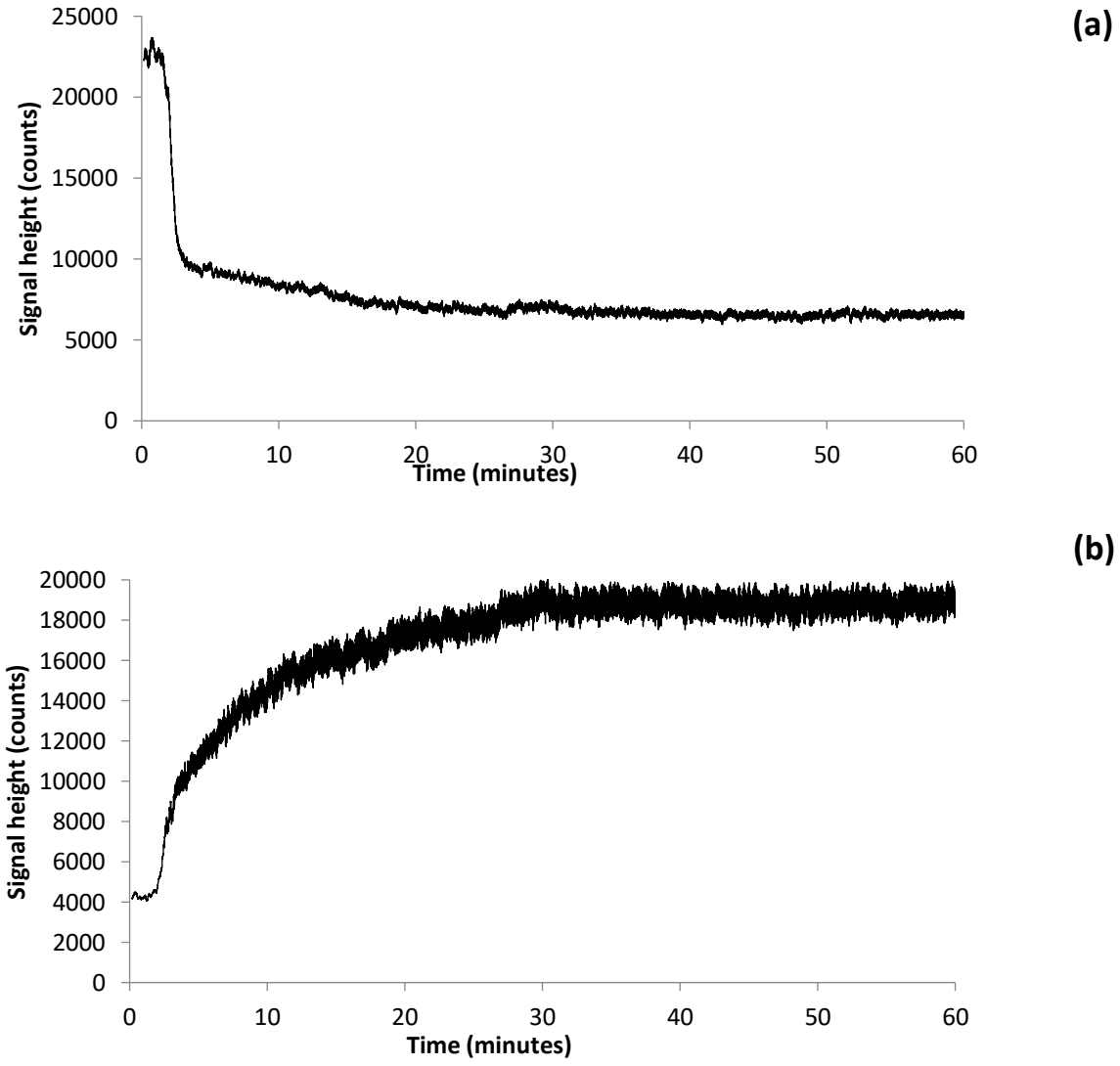

Figure 3-25 SIM signals over time, with trend line indicating a 100 point moving average for (a) m/z 151 (acetanisole) and (b) m/z 135 (1-(4-methoxyphenyl)ethanol)

3.4 Validating low field flow ^{1}H NMR for the operational conditions required.

3.4.1 T_1 Considerations

In order to determine the rapidity of measurement possible for online NMR it was necessary to determine the T_1 relaxation times for the compound. The T_1 spin-lattice relaxation time was measured by the simple expedient of introducing a pulse to align the magnetization to a plane at 90° to the field through the magnet, and then recording the time taken for the signal to recover. T_1, the time constant for this recovery, is the time taken for the magnetization to recover to [1-(1/e)] of its maximum. As a rule of thumb, an acquisition time of no less than $2T_1$ is advisable to allow magnetisation to fully recover before a new pulse is introduced in an experiment.

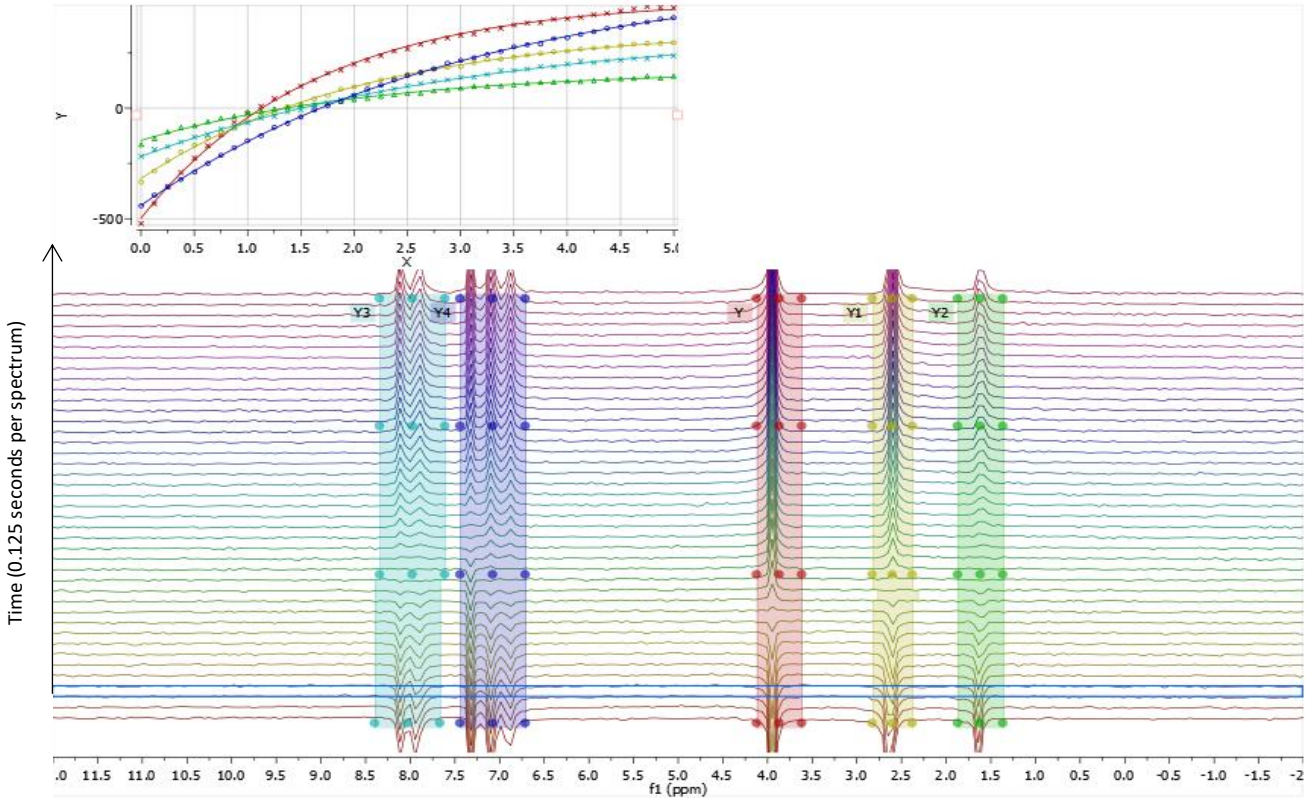

Figure 3-26 T_1 monitoring experiment results

A 3 factor exponential fit, shown by the trendline on the graph inset to Figure 3-27, is applied to the integrals of each signal, with the generic formula where B is the integral when the signal has fully aligned (t→∞), F is the difference between the starting and final integral, approximately 2B if the experiment was allowed to run for sufficient time, and G is equal to $1/T_1$. From this the T_1 values for each signal can be determined.

$$y = B + Fe^{(-xG)}$$

Equation 3-1. T_1 fit equation

The T_1 values produced for acetanisole and 1-(4-methoxyphenyl)ethanol ranged from 1.595 to 3.101 seconds. As such, a pulse program was selected that produced a spectrum by averaging 4 acquisitions per spectrum, each of 7 second duration, resulting in one spectrum every 30 seconds, with a 2 second delay after the 4th acquisition.

3.4.2 NMR permanent magnet temperature sensitivity.

Permanent magnets are extremely temperature sensitive, with the effect of temperature on the strength of the magnet being defined by two factors. Firstly, the magnet strength decreases as temperature increases in a reversible fashion due to the competition between thermal motion of the atoms in the magnetic material and the tendency towards the low-energy state in which the dipoles of the material align. Secondly, above the Curie point, there is a phase transition at which point the dipoles become incapable of spontaneous alignment, and as such all ferromagnetic behaviour ceases.

The practical implications of this, for a Halbach array-based NMR instrument, are that a uniform magnet temperature must be maintained. Any deviation in temperature will result in sections of the magnet heating or cooling, cause local changes in field strength and a loss of field homogeneity. To maintain a robust uniform temperature, such magnets are held just above room temperature. This

presents a potential issue for the use of flow NMR for reaction monitoring in such instruments as reactions are rarely conducted at the specific temperature to which the magnet is heated. In addition, the flow of reaction mixture through the magnet has the potential to heat or cool the magnet, or indeed be heated or cooled by the magnet itself. The latter would cause significant problems in temperature sensitive reactions.

To investigate the effect of temperature on the magnet stability and the reaction of acetanisole with sodium borohydride, liquid flow was set up for a range of temperature values, using methanol for 20 °C and below and ethylene glycol for temperatures above 20 °C. The peak drift from the initial frequency was measured, as was the increase in peak width (Figure 3-27).

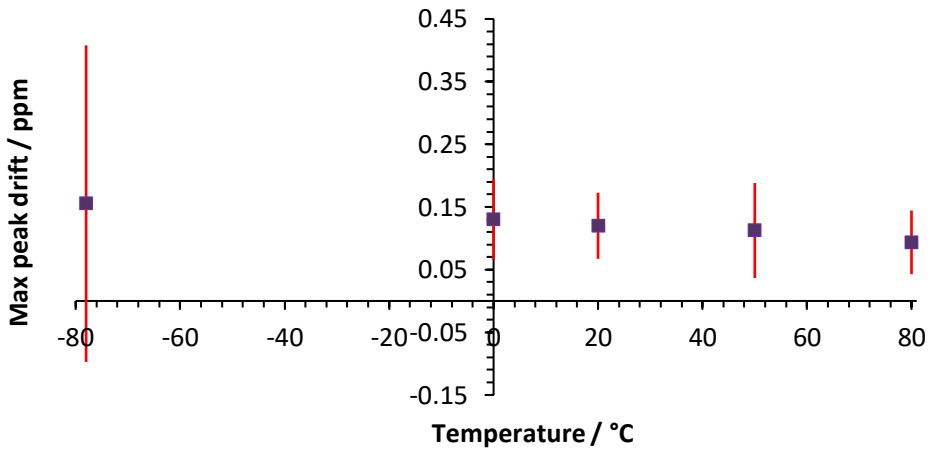

Figure 3-27. Peak drift (■)and peak broadening (red line) resulting from magnet cooling, measured with methanol (for 20 °C and below) and ethylene glycol (for 40 °C and above) at 1 mL/min

Methanol at -80 °C caused the greatest peak drift (almost 0.16 ppm) and peak broadening (almost 0.5 ppm), and the magnet was quickly cooled to the point that the internal lock signal was lost, after which the spectra produced were unusable. The instrument displayed minimal signal drift and retained lock for over an hour with flows close to its 28 °C operating temperature, as would be expected. Figure 3-30 shows the time taken for the lock signal to be lost at each temperature. All of the analyses at or above 0 °C were successfully monitored 1 mL/min for over 1 hour before signal lock was lost.

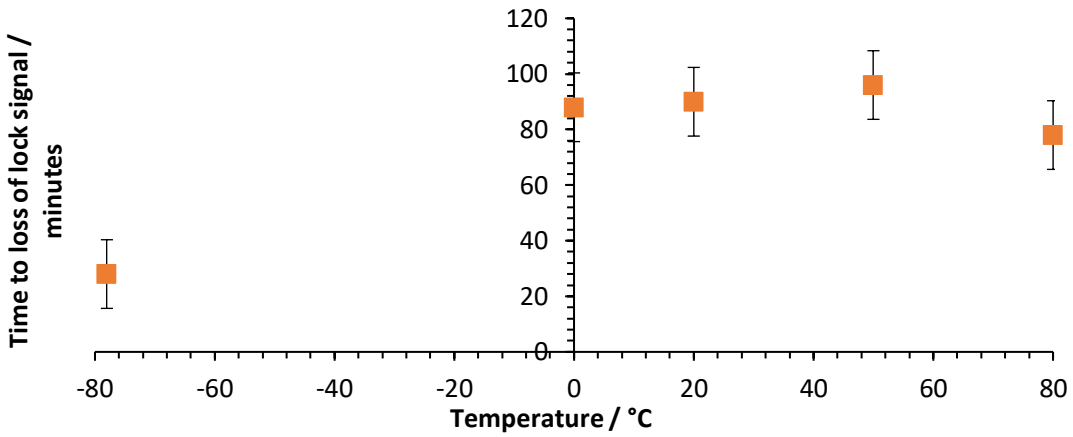

Figure 3-28. Time taken for loss of lock signal at 1 mL/min flow rate

The use of methanol and ethylene glycol, as well as providing liquid flow which would remain liquid at the temperatures evaluated, were chosen as they allow the temperature of the substance being monitored by NMR to be calculated, such that these compounds both have pairs of NMR peaks which shift relative to one another depending on the temperature, allowing for the temperature of the liquids to be empirically determined at point of measurement. The use of these two compounds as an 'NMR thermometer' is well established[98] method of determining the temperature of an NMR sample, with ethylene glycol shown in Equation 3-2, showing a linear relationship over the range in question, while the relationship for methanol is quadratic, as shown in Equation 3-3 (where $\Delta\sigma$ is the change in the peak position in ppm)

$$\mathrm{T\,[K]} = 466.50 - 102.00\Delta\sigma$$

Equation 3-2 Ethylene Glycol Thermometer equation

$$T\,[K] = 409.0 - 36.54\,\Delta\sigma - 21.85\,(\Delta\sigma)^2$$

Equation 3-3 Methanol Thermometer equation

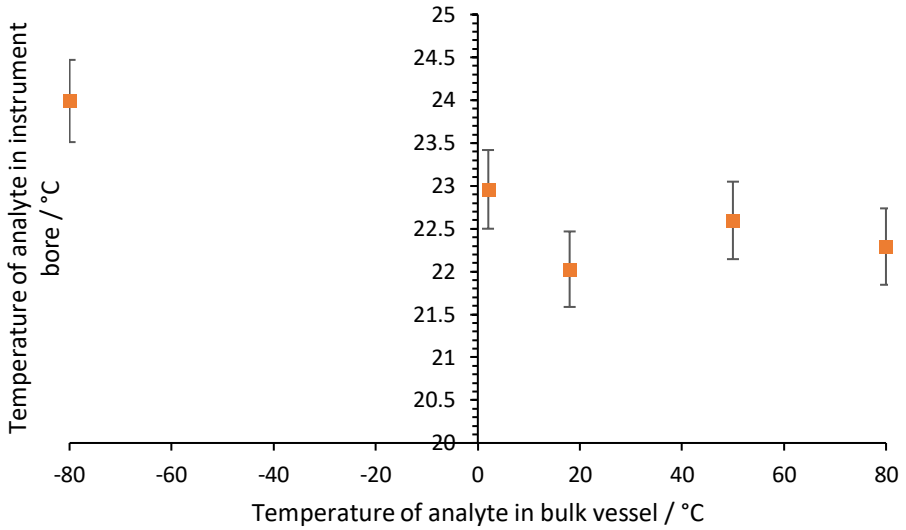

Figure 3-29. Temperature of analyte in measurement volume vs bulk temperature.

Using the NMR thermometers, Figure 3-29 shows that in every case examined, the temperature of the analyte when measured was found to be between the 20 °C room temperature and the 28 °C operating temperature of the instrument, suggesting that the majority of heating or cooling occurs before the sample reaches the measurement region of the magnet, which is expected given that the sample first passes through the pump, 60 cm of PEEK tubing and a significant portion of the NMR instrument.

Interestingly, the analyte appears to be slightly hotter in the lower temperature samples. It is hypothesised that this is due to the heating element in the instrument working harder to heat the bulk of the magnet as it is cooled faster by the colder bulk sample. It is notable that all of the samples were above the ambient temperature of the room (climate controlled to 20 °C), but below the operating temperature of the magnet itself (26 °C)

These experiments show that the instrument is robust for reactions between 0 and 80 °C for time periods up to one hour at 1 mL/min and for extended periods at lower flow rates. The effects of heating/cooling on the signal have been characterised and the standard procedures adjusted to avoid such problems.

3.4.3 Evaluating on-line NMR for the reduction of acetanisole.

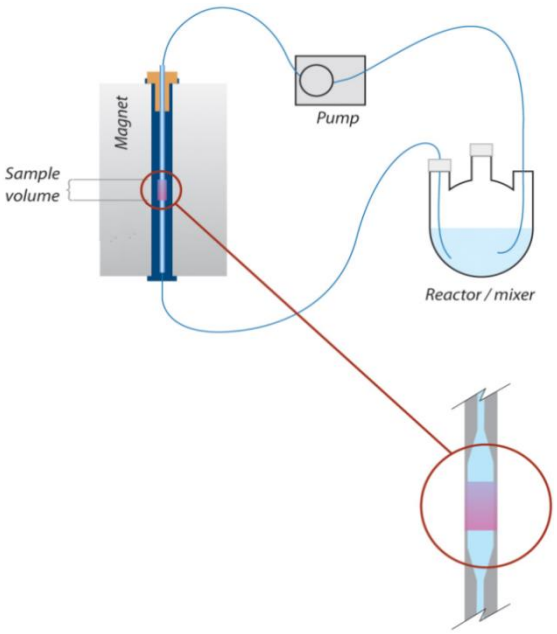

Figure 3-30. NMR reaction monitoring flow cell diagram (image courtesy of Magritek)

The reduction of acetanisole was initially monitored using an experimental approach suggested by Magritek (shown in Figure 3-30), with a single pump used to circulate the acetanisole dissolved in CH_3OH at 25 mg/mL and flowing at 1 mL/min. From the data collected, peaks corresponding to acetanisole could clearly be discerned as shown in Figure 3.31.

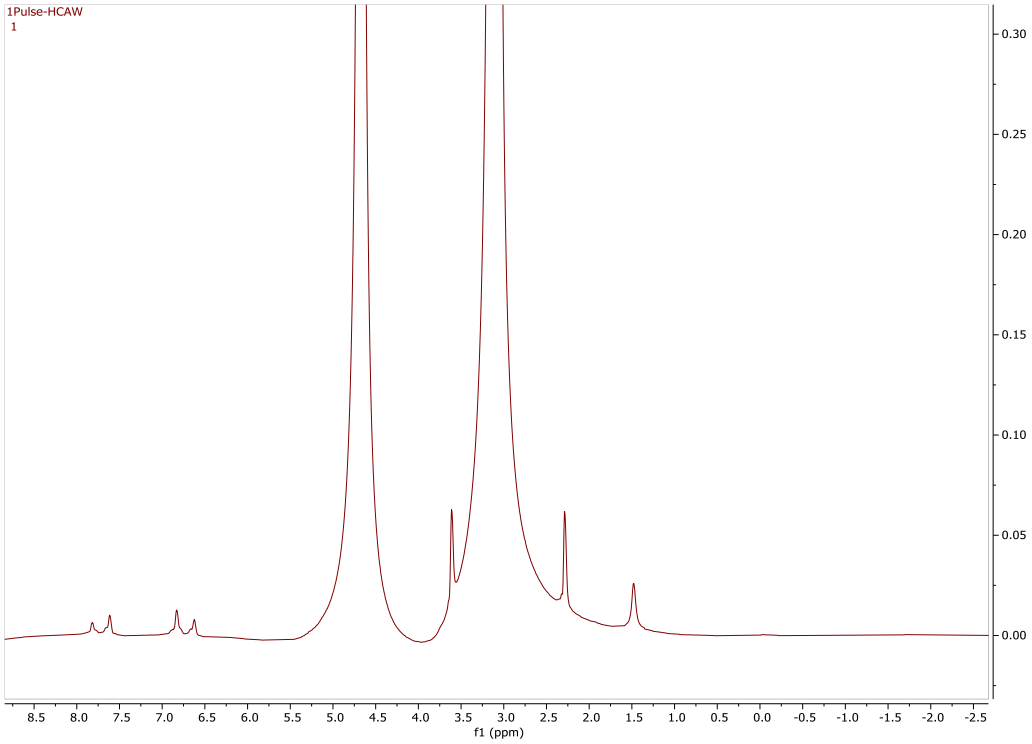

Figure 3-31 NMR spectrum of reaction start concentration (25 mg/mL) acetanisole in flow cell (^{1}H, 43 MHz, CH_3OH, 1 mL/min). Note large solvent signals at 3.0 and 4.7 ppm

The strong methanol signals can be seen at 3.0 ppm for C**H$_3$**OH and 4.7 ppm for CH$_3$O**H**, while the aromatic signals at 6.75 ppm and 7.75ppm and one methyl signal at 1.4 ppm for the acetanisole are clearly resolved from those large solvent signals.

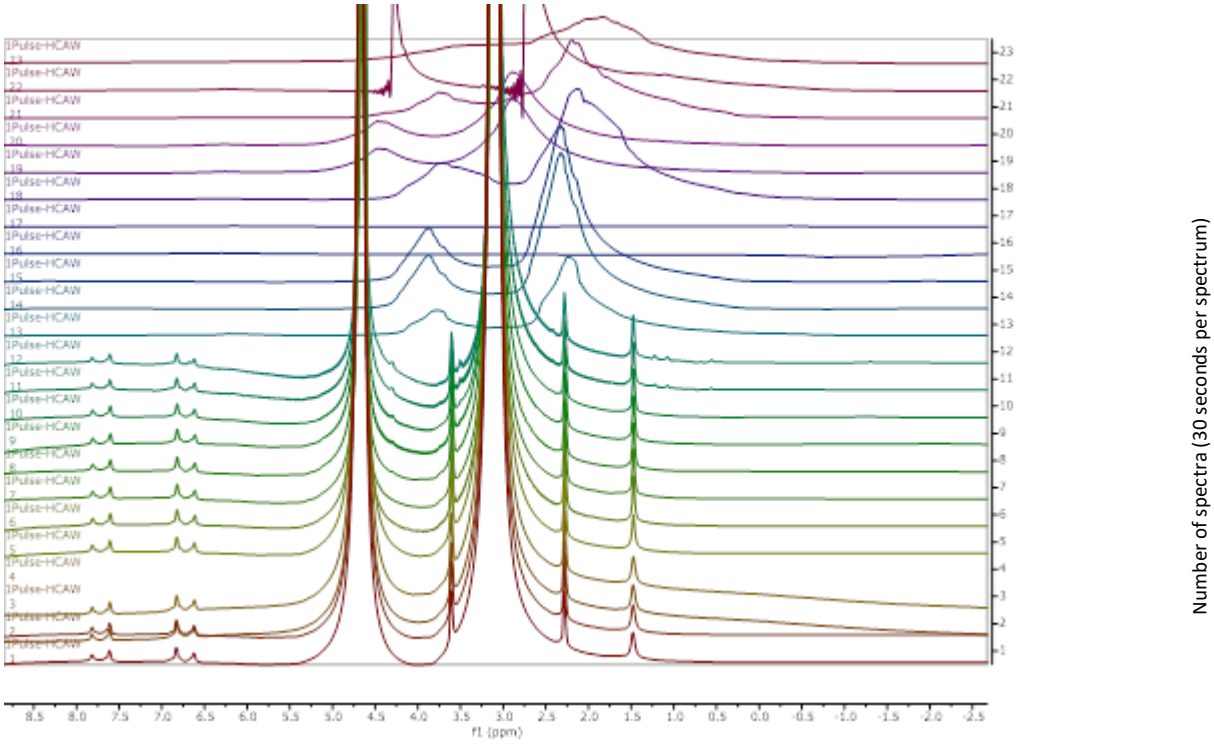

Figure 3-32 ^{1}H NMR (43 MHz, CH_3OH, 1 mL/min) of acetanisole reaction. Note the entrance of a bubble into the measurement volume degrading spectra from 13 onwards.

When the experimental design outlined in Figure 3-30 was used to monitor the reduction of acetanisole by sodium borohydride, the formation of hydrogen bubbles within the flow cell was found to cause near total signal loss, as may be seen from spectrum 13 onwards in Figure 3-32. This experimental approach was then modified in an attempt to avoid gaseous reaction products from becoming trapped in the bulbous section of the NMR flow cell. The solvent flow was reversed, entering at the base of the magnet and exiting at the top. Unfortunately the bubbles were still frequent enough to prevent the small footprint NMR being used in-flow for the monitoring of this reaction, and it was determined that reactions which produce significant quantities of gas as a by-product are not suitable for monitoring with this system. As such, an alternative reaction was sought to allow development to continue.

3.5 Developments to bring ESI MS and NMR together to monitor progress from one reaction vessel.

All the developmental work conducted thus far enabled the two systems to be bought together in the experimental design shown in Figure 3.33 A photograph of the equipment in use is shown in Figure 3-34. In connecting the two instruments a T-piece was used to split the reaction mixture flow between the NMR and MRA. Tubing lengths were selected such that the amount flows into the NMR and MRA were equal to within a measured tolerance of less than ±5%.

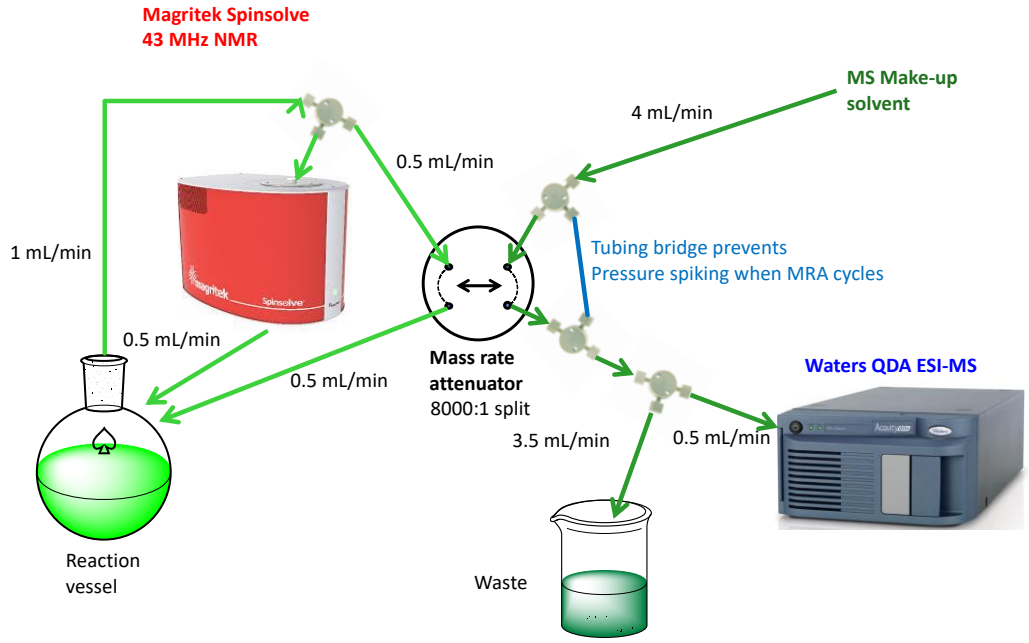

Figure 3-33. Combined MS and NMR system schematic.

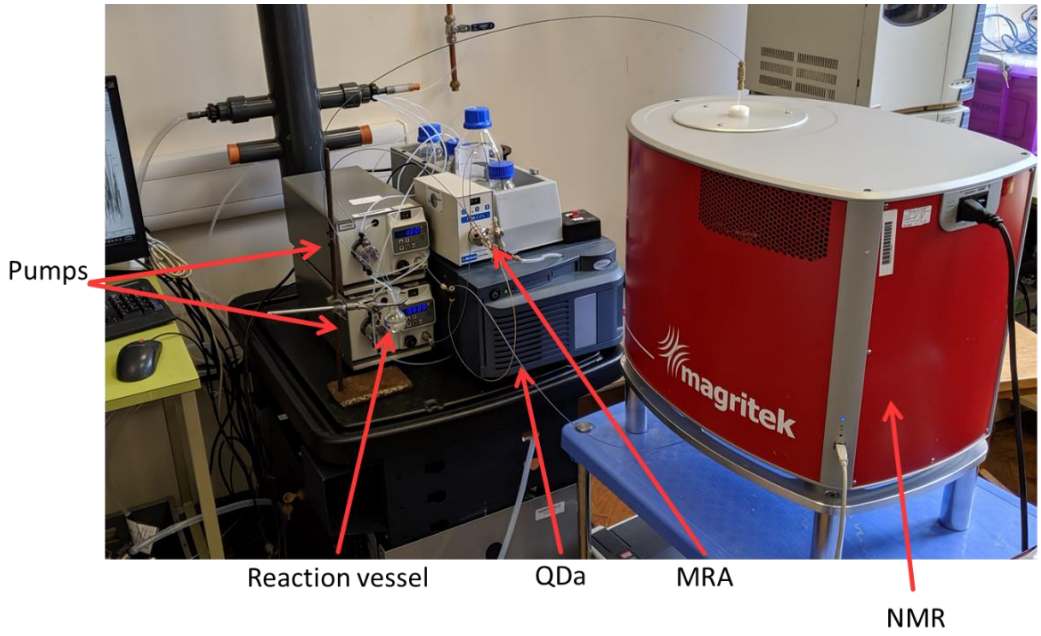

Figure 3-34. Combined monitoring system in use.

3.6 Conclusions

With the construction and validation of a combined on-line MS and NMR system for reaction monitoring, a number of points of interest have been demonstrated, including the necessity of selecting techniques suitable to the reaction, and in particular the issues arising from any reaction which produces gas being monitored by flow cell NMR in this configuration. In addition to this, the necessity of selecting a dilution solvent for the MS which does not interfere with the reaction was highlighted, a point which applies both to this system in particular and more generally where switching valve based dilution systems are used for on-line dilution of reaction mixtures. Information was also gained with regard to the robustness of the NMR system when dealing with reactions conducted at high or low temperatures, and with regard to the suitability of this method for monitoring temperature sensitive reactions. This chapter also provides an outline of the necessary protocol for applying this system to monitoring of a new reaction, both in terms of the required points of consideration and the necessity of validating the techniques with more established high performance techniques.

4 Ion Suppression in Mass Spectrometry

4.1 Chapter Abstract

For the first time, signal suppression in ESI MS was observed and qualified by simultaneous measurement by on-line NMR operating in parallel. The degree of suppression was determined with NMR measurements, and this technique was verified against measurements a high-resolution MS instrument using a well-established MS based method involving isotopically labelled compounds.

4.2 Establishing reaction conditions for formation of L-thioproline

The reaction in question was the formation of L-thioproline from L-cysteine and formaldehyde in aqueous solution at room temperature, as shown in Figure 4-1.

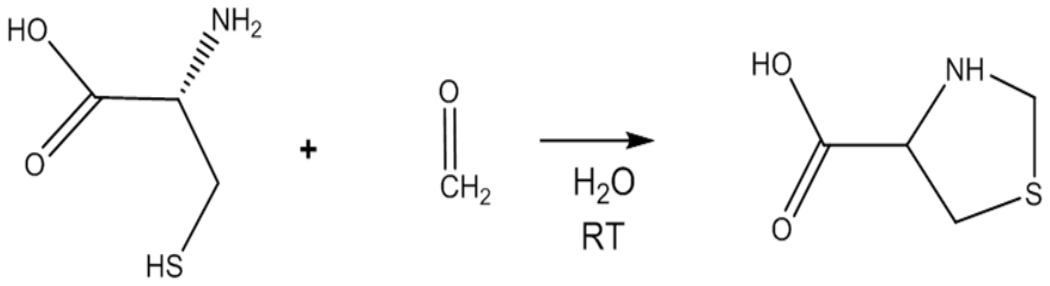

Figure 4-1 Reaction scheme for the synthesis of L-thioproline from cysteine and formaldehyde

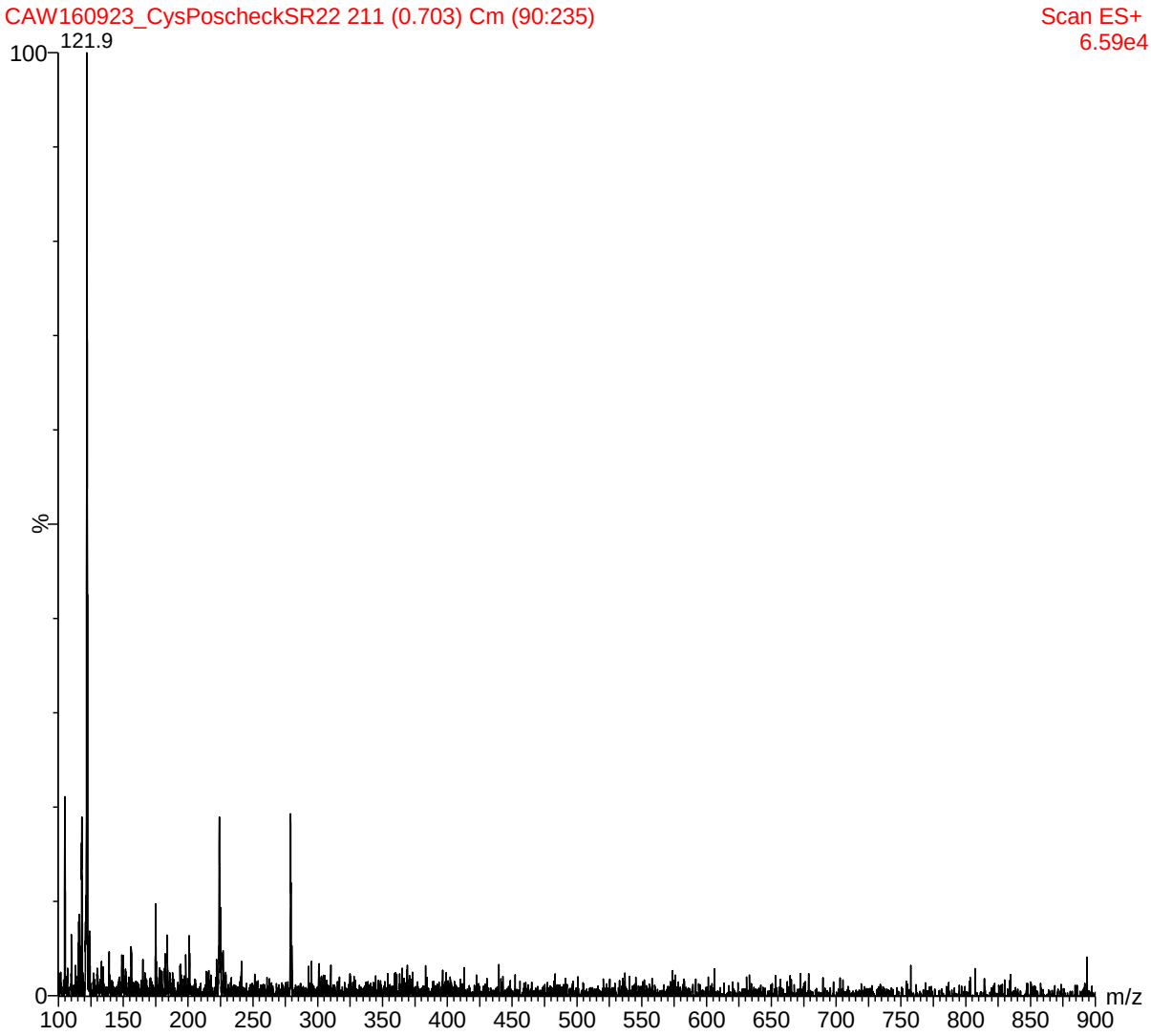

Figure 4-2 Mass spectrum for cysteine in aqueous solution at 6 mg/mL. Signals at m/z 224 and 279 are contaminants present in solvent background at comparable levels.

Positive mode on the QDa was used to identify suitable ions for monitoring the reaction given in Scheme 1. For L-cysteine and L-thioproline, $[M+H]^+$ were found to be most abundant at *m/z* 122 and *m/z* 134 respectively, and subsequently used as the targets in SIM MS measurements.

No positive or negative ions were observed by the QDa for formaldehyde, as was to be expected for such a small volatile compound when studied by electrospray ionisation. Likewise, water was not expected to be observed.

Suitable ions for monitoring the cysteine and L-thioproline having been identified, a reaction monitoring method was created with SIM channels set for *m/z* 122 and 134, alternating with a full

scan in order to allow data to be interrogated for any potential intermediates or side reactions that may occur. This allowed for a duty cycle of 8 Hz with the 3 channels.

^{1}H NMR (43 MHz, D_2O) signals at 2.91 ppm for cysteine and 3.26 ppm for L-thioproline were identified as showing good monitoring potential, as they were well clear of the area in which the water signal would be expected to appear.

4.3 Considerations in the monitoring of the formation of L-thioproline from formaldehyde

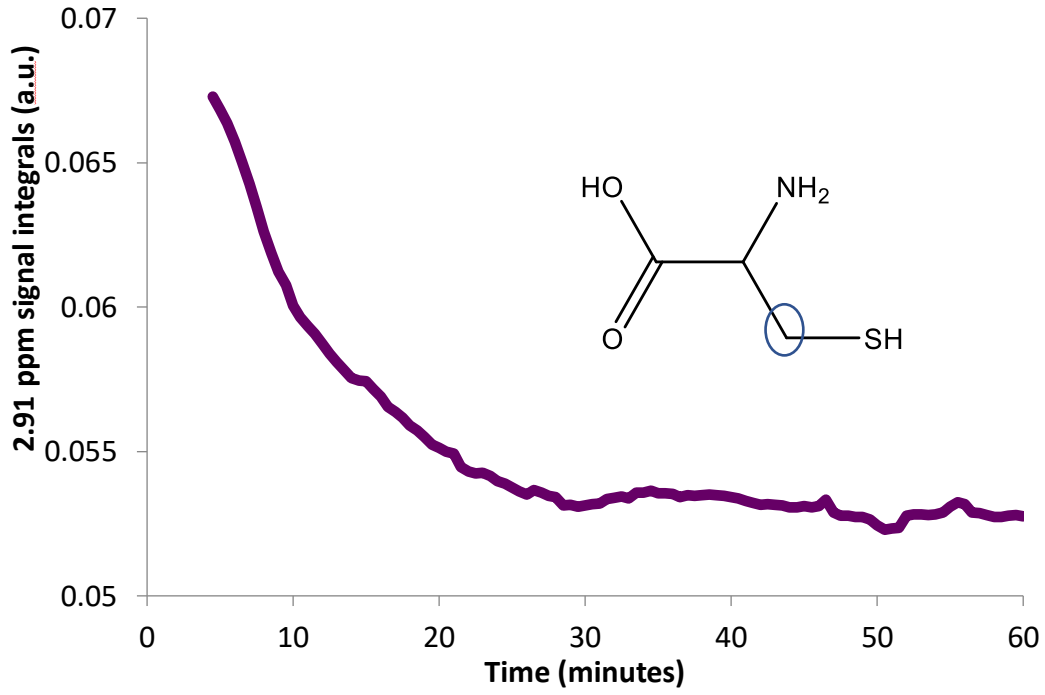

Figure 4-3- ^{1}H NMR 2.91 ppm (cysteine) signal trace for initial reaction. Circled carbon indicates the position of the protons giving rise to the signal.

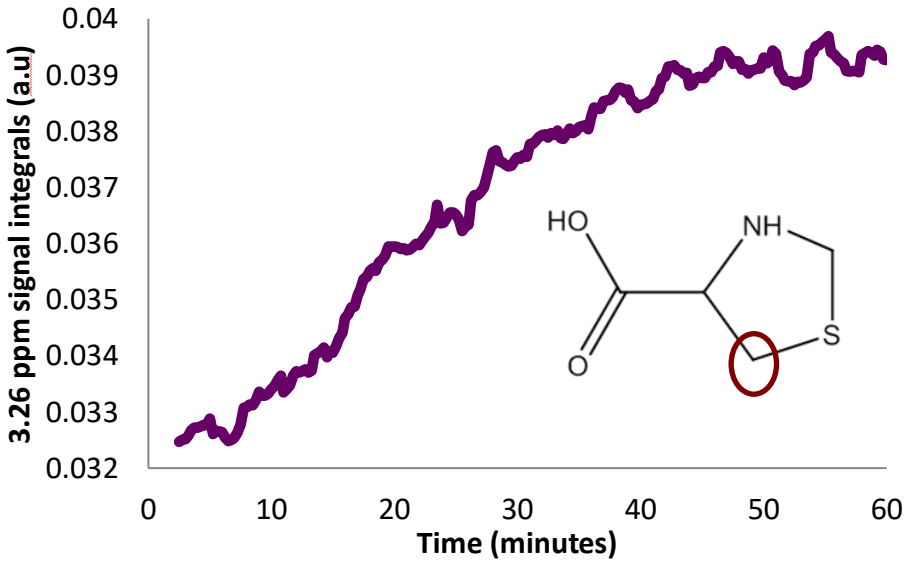

Figure 4-4- ^{1}H NMR in water solvent following signal at 3.26 ppm (L-thioproline methylene at circled position) signal trace for initial reaction.

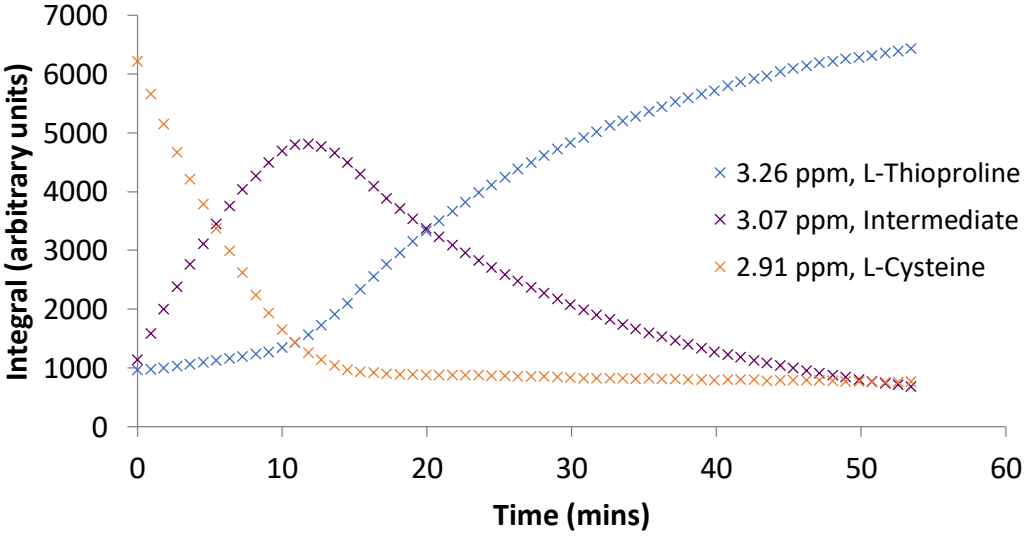

Figure 4-5 NMR signals monitored in deuterated solvent in 500 MHz NMR

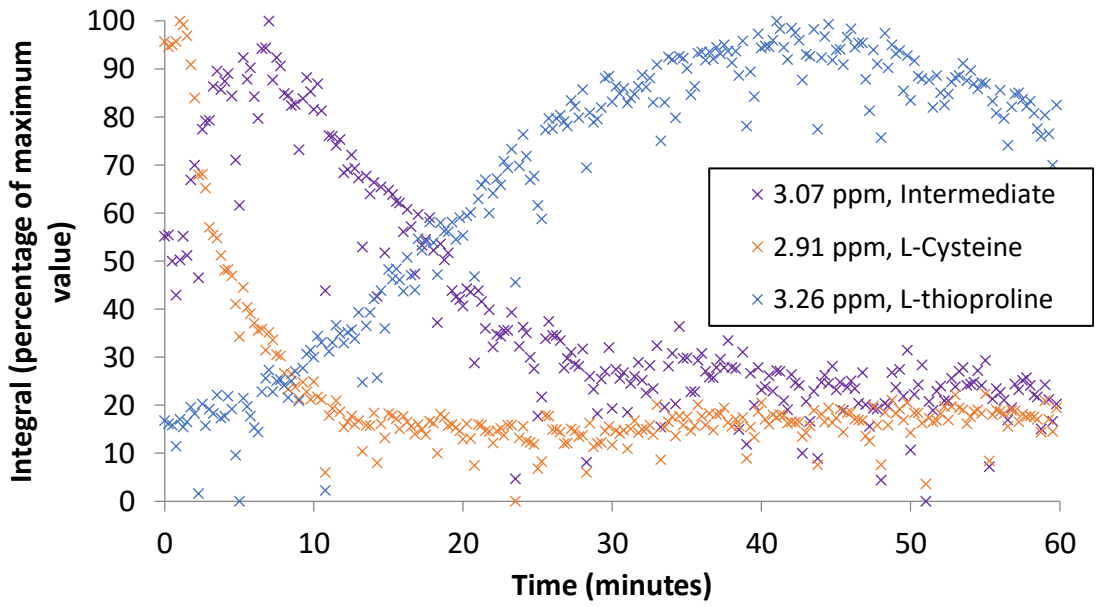

Figure 4-6 NMR signals monitored in flow in H_2O solvent on 43 MHz instrument

As can be seen in Figure 4-3 and 4-4, the decay signal for cysteine follows the expected exponential decay profile, but the signal for thioproline does not follow that trend, with a markedly slower initial increase. Further investigation on a high field (500 MHz) instrument in D_2O allowed for the presence of an intermediate to be established, with a signal at 3.07ppm identified as belonging to that intermediate, accounting for the initially slower rate of thioproline formation. Figure 4-5 shows the results of this reaction in D_2O, conducted at the same concentration as the reactions monitored on the Spinsolve in an NMR tube.

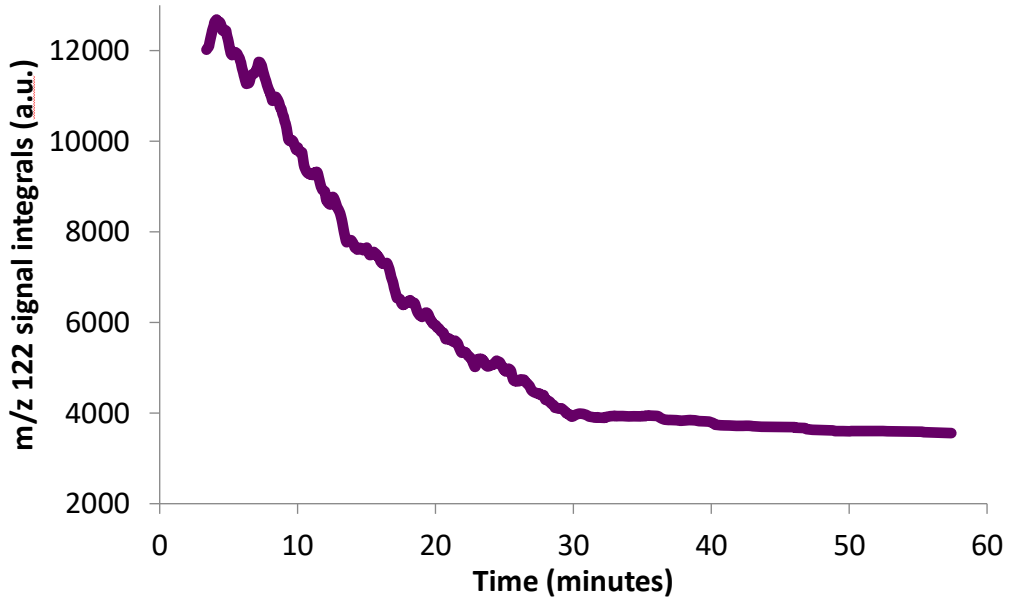

Figure 4-7- Positive ion ESI MS showing SIM for m/z 122 (cysteine $[M+H]^+$) for initial reaction

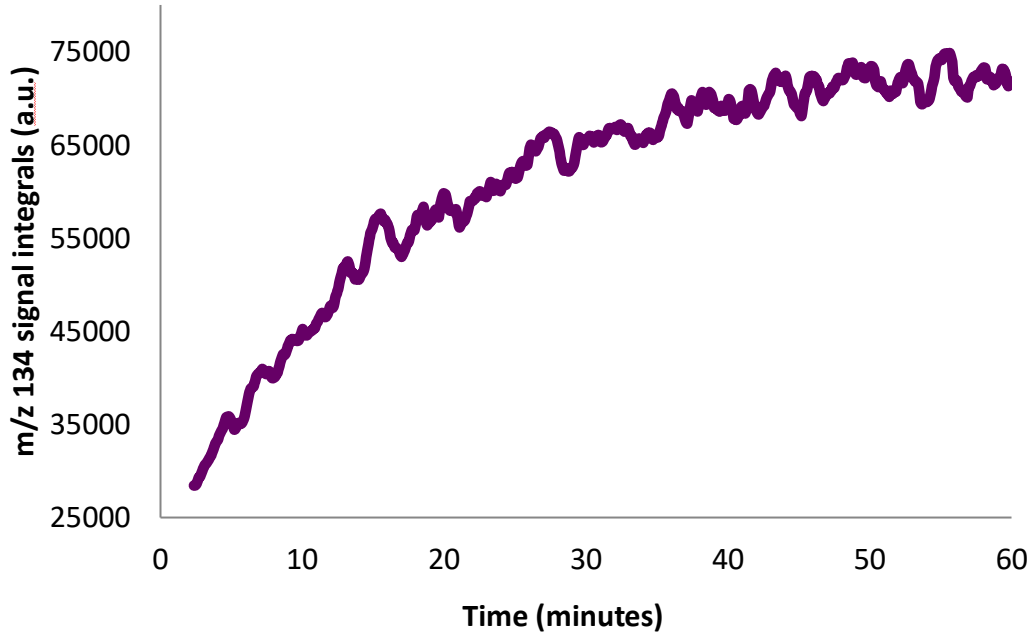

Figure 4-8- Positive ion ESI-MS showing SIM trace of m/z 134 (L-thioproline $[M+H]^+$) for initial reaction

The data for the SIM channels by ESI-MS shows good agreement with the NMR data for the depletion of Cysteine, though the thioproline profile is once again different from what would be expected.

Initially this was thought to be due to the intermediate, and so investigations were undertaken to try to monitor the intermediate by MS

A number of different conditions, make-up solvents, and additives (Table 4-1) were trialled to stabilise the intermediate in the MS, but none were successful in producing an intermediate signal over the observed *m/z* range (100-1000 mass units) in either positive or negative ionization mode, suggesting that any reaction intermediate produced does not ionise by ESI, is outside this mass range or produces a signal at the same *m/z* to the thioproline.

Table 4-1 Experiments attempted to resolve intermediate, reaction conditions kept the same each time (6 mg/mL cysteine in 20 mL water, equimolar formaldehyde, room temperature)

Make-up Solvent	Additives	Cone voltage changes
H_2O/ACN 50:50	None	Varied cone voltages from 5-30 V in 5 V increments
H_2O/ACN 10:90	None	Used standard 20 V cone voltage
MeOH	None	20V
H_2O/ACN 50:50	Sodium chloride 10 mM, sodium formate 10 mM, ammonium acetate 10 mM	20V

One other theory for a reaction intermediate that could reasonably explain the observed result is shown in Figure 4-10. It is reasonable that ionisation in positive mode would cause the loss of the OH group, effectively pushing the reaction to completion.

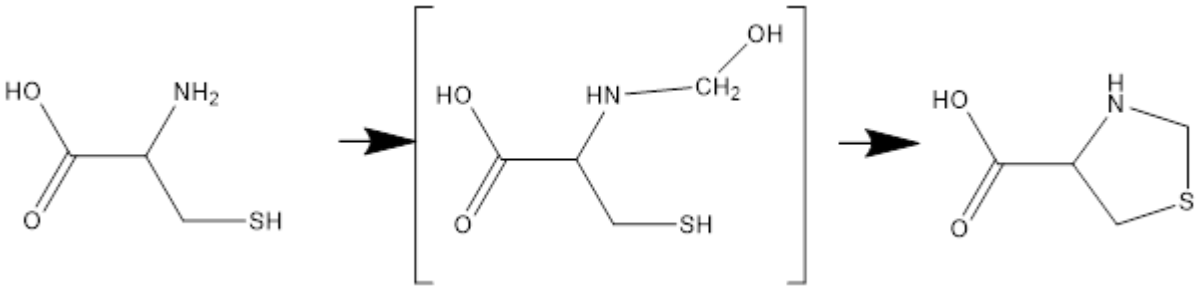

Figure 4-9- Proposed schematic for a reaction intermediate consistent with the absence of the intermediate in MS data.

This hypothesis is supported by the fact that the reaction in D_2O (Figure 4-5) showed a greater lifetime for the intermediate than was found for the online reaction which used H_2O as solvent (Figure 4-6), as it suggests that the protonation or, in the case of the experiment conducted in the high field instrument, deuteration, would be the rate limiting step in the consumption of the intermediate, and the presence of a pronounced kinetic isotope effect, providing one explanation for the slower formation and consumption of the intermediate in the deuterated condition, as the more massive deuterium causes reactions involving it to have a higher activation energy, would support that idea. It should, however, be noted that the reaction in deuterated solvent was done in an NMR tube, and it has been noted that container shape volume and agitation can produce significant differences in rates for reaction monitoring by NMR[99], which could provide an alternate explanation for this effect.

4.3.1 Effects of headspace on Cysteine consumption

Both data show the cysteine to have been consumed after 30 min. The reaction profiles for the cysteine consumption are in good agreement over the 30 min time frame despite the issues with ion suppression for the thioproline produced. However, despite achieving good agreement the

consumption rate neither corresponds to either first order nor to second order kinetics; the latter expected from the 1:1 reagent ratio used.

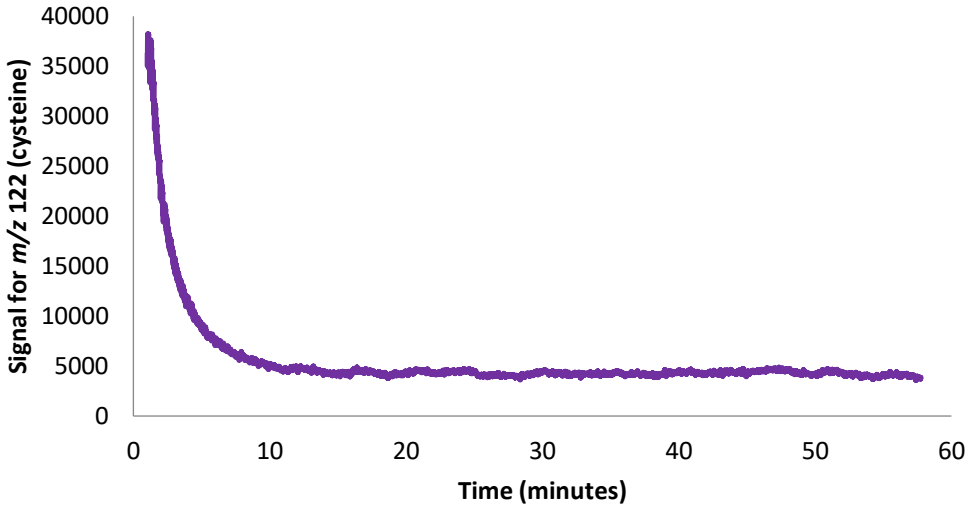

Figure 4-10 m/z 122 (cysteine) signal in the minimal headspace condition

This lack of conformity was hypothesised to be due to the gradual loss of the dissolved formaldehyde into the head space above the reaction, over the course of the reaction. This hypothesis was tested by comparing the rates of the reaction conducted in two different conditions. For the first experiment the reaction was conducted in a sealed round bottom flask in which the available headspace had been minimised (reaction media filled the vessel and headspace estimated at 2 mL). In a second experiment the same volume and concentration of reactants were placed in a round bottom flask with a volume of 25 cm^3. As can be seen in Figure 4-10, the reaction with the minimised headspace proceeded at a much faster rate and conformed to the expected 2^{nd} order kinetics.

This supports the hypothesis that an important component of the reaction is partitioning into the headspace. Given the reaction scheme shown in Figure 4-1, it is reasonable to expect formaldehyde

to be the component responsible, suggesting that the loss of dissolved formaldehyde to headspace is a significant factor in the progress of the reaction.

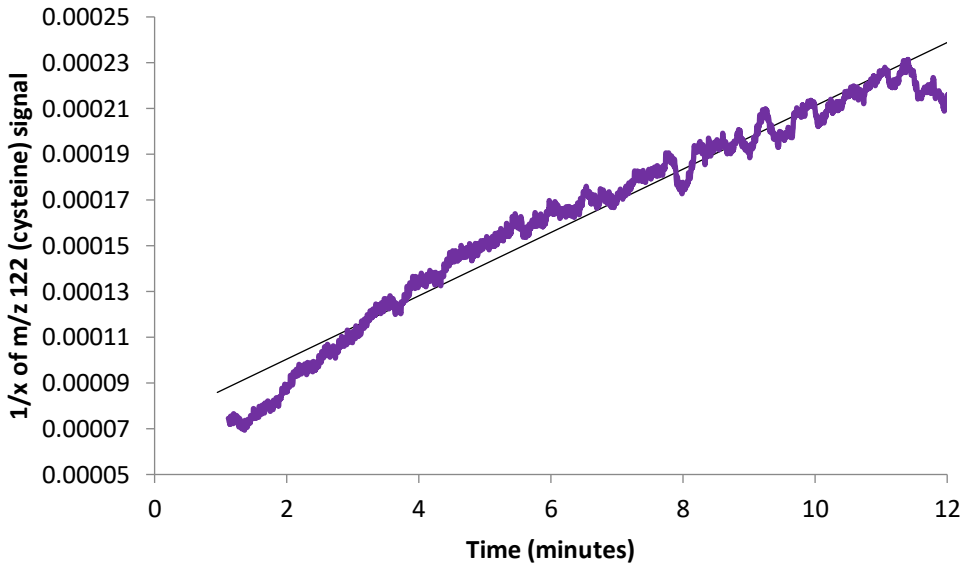

Figure 4-11 1/x of m/z 122 (cysteine) signal for minimal headspace condition over the reaction period. Fitted to straight line indicating 2nd order rate equation.

4.4 Exploring the differences in observed reaction rate between NMR and MS

Once this intermediate is accounted for, there remains a discrepancy between the decrease in the cysteine and the formation of the L-thioproline. If, as the literature mechanism shown in Figure 4-10 would suggest, the reaction is being pushed to completion in the ESI source, the sum of the NMR traces for the intermediate and product should match with the MS trace for the product. It was, as such, suspected that the MS signal for L-thioproline was being supressed.

4.4.1 Establishing the presence and extent of ion suppression

Suppression was explored experimentally by analysing a series of standard solutions containing a range of concentrations of cysteine representing 0-100% conversion of cysteine under reaction conditions while L-thioproline was fixed at a concentration corresponding to 50% conversion.

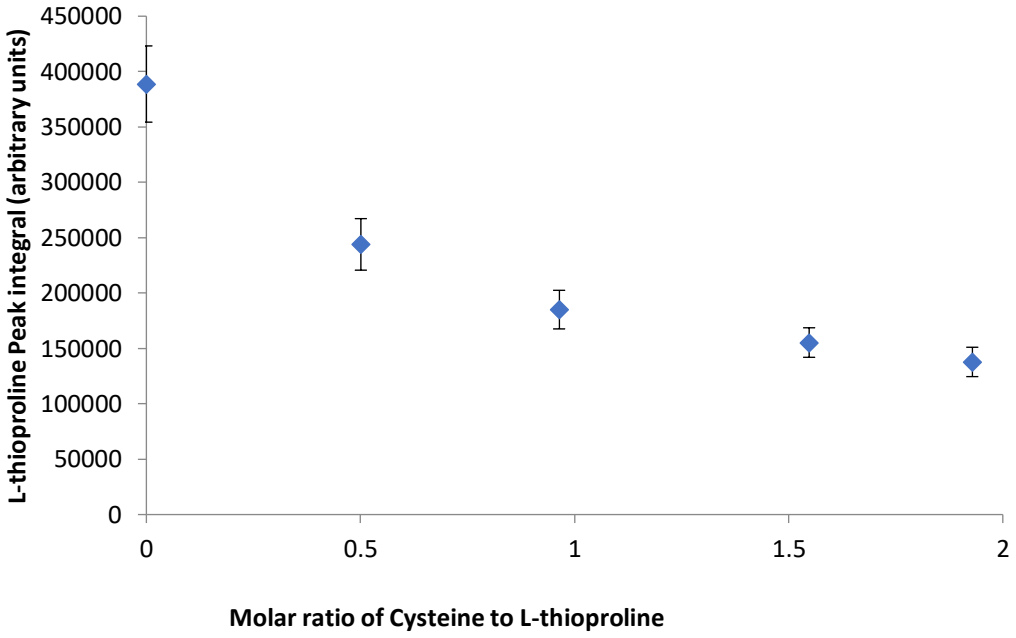

Figure 4-12 - Responses for fixed 0.25 mol dm^{-3} concentration of L-thioproline with varying cysteine concentrations.

The results (Figure 4-11) shows the signal intensity for 0.25 mol dm^{-3} thioproline in the absence of cysteine is 3.75 x10^{5} units, but by analysing thioproline in the presence of a 0.5 molar ratio of cysteine, and keeping the absolute concentration of thioproline at 0.25 mol dm^{-3} the thioproline signal in the MS drops to 2.25 x10^{5} units. At a molar ratio of 2:1 cysteine to thioproline the 0.25 mol dm^{-3} thioproline signal is significantly suppressed. For the inverse experiment to explore the effect of cysteine by L-thioproline (Figure 4-12) in the ESI MS, no such suppression was found, as shown in

Figure 4-11 where the signal intensity of 0.25 mol dm^{-3} cysteine remained constant as the thioproline was changed.

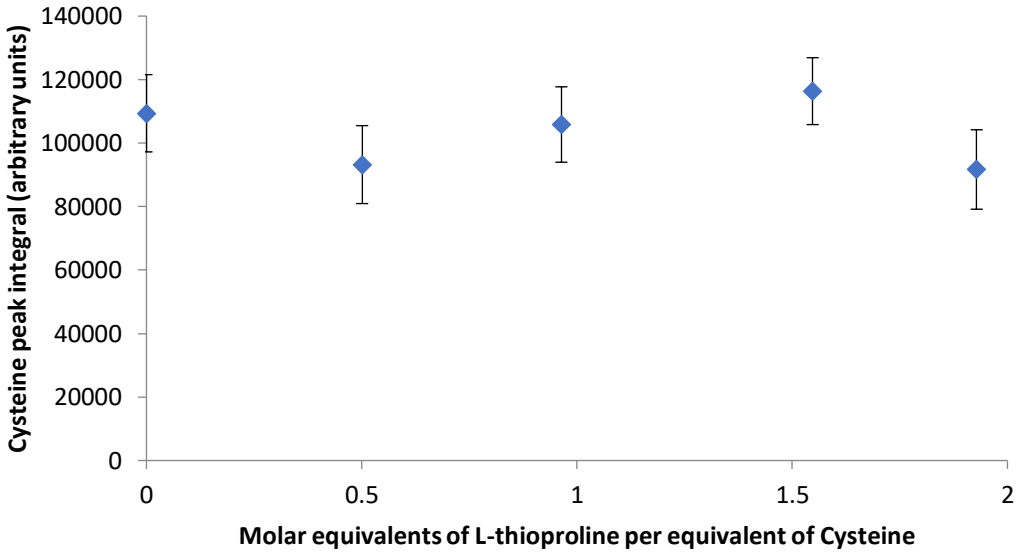

Figure 4-13-Responses for fixed concentration of 0.25 mol dm^{-3} cysteine with varying L-thioproline concentrations

Having established the occurrence of suppression during the ESI process, the degree of suppression in the on-line experiment was examined by reference to the NMR signal, with the aim of using established a method to use one on-line analytical instrument (in this case the NMR) to determine and correcting for systematic errors produced by another on-line analytical instrument (in this case the ESI MS). For the reaction understudy herein, an experiment was conducted such that a fixed concentration of an isotopologue of the suppressed species, in this case 1mg/mL ^{13}C labelled l-thioproline synthesised from labelled formaldehyde (Sigma Aldrich), was spiked into the reaction mixture in the bulk (round bottomed flask). All other reagents were kept at the same concentration.

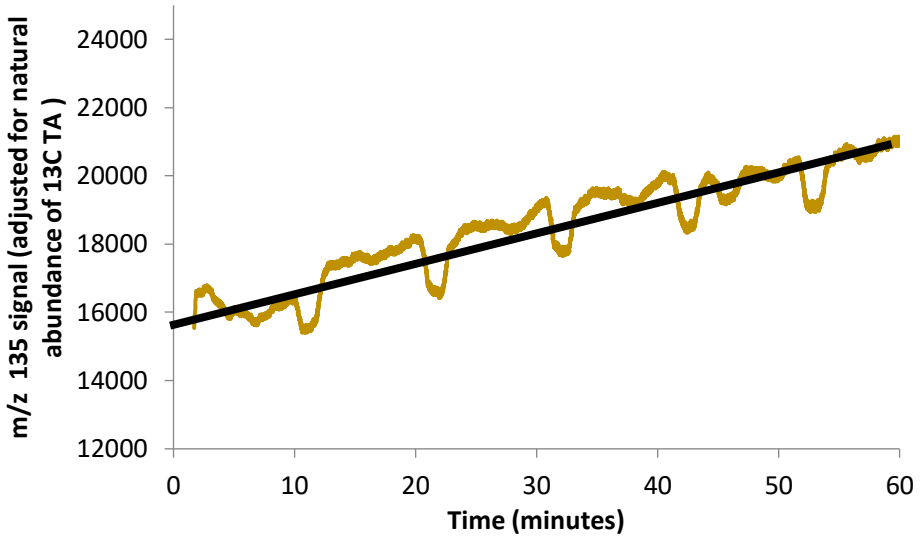

Figure 4-14- m/z 135 (^{13}C labelled L-Thioproline) signal, corrected for the formation of ^{13}C L-thioproline in the reaction due to natural abundance. Monitoring conducted on G2S Synapt (Waters), periodic dips due to lockspray baffle interrupting flow

A baseline response for the labelled compound at a fixed 0.125 µg/mL concentration (equivalent to a concentration in the reaction mixture of 1 mg/mL) was first established by running it into the instrument with no other compounds present through a syringe pump at 0.5 mL/min, and then the same concentration of labelled compound was added to the reaction vessel containing 16mL of 6 mg/mL formaldehyde to which was added 4mL of 15 mg/mL formaldehyde solution . The signal for the labelled compound Figure 4-13 can be seen to steadily increase as the cysteine in the reaction is consumed. This monitoring was conducted on the G2S Synapt due to issues with instrument availability and the desire to ensure that the signals for the labelled and unlabelled compounds were fully resolved from one another. By applying a correction factor (Equation 9) generated from the labelled signal to the observed unlabelled L-thioproline signal, a corrected trace for the L-thioproline can be generated and is shown in Figure 4-13.

$$Signal\ intensity\ (corrected) =$$

$$Observed\ Signal\ intenstiy\ \times \frac{Labelled\ signal\ intensity\ observed}{Labelled\ signal\ intensity\ reference}$$

Equation 4- Correction factor for MS suppression in labelled compound doping experiment.

The corrected ESI MS data was found to be in good agreement with the NMR data. In order to give a comparable signal, a synthetic trace was created by subtracting the cystine signal at time t from the maximum cysteine signal, as the NMR signal normally used to monitor L-thioproline would be affected by the doping of the ^{13}C labelled L-thioproline into the reaction. The resulting trace, (Figure 4-13) demonstrates the validity of the NMR as a tool for identifying and providing a basis for correction for suppression in on-line MS, without the need for the use of labelled compounds.

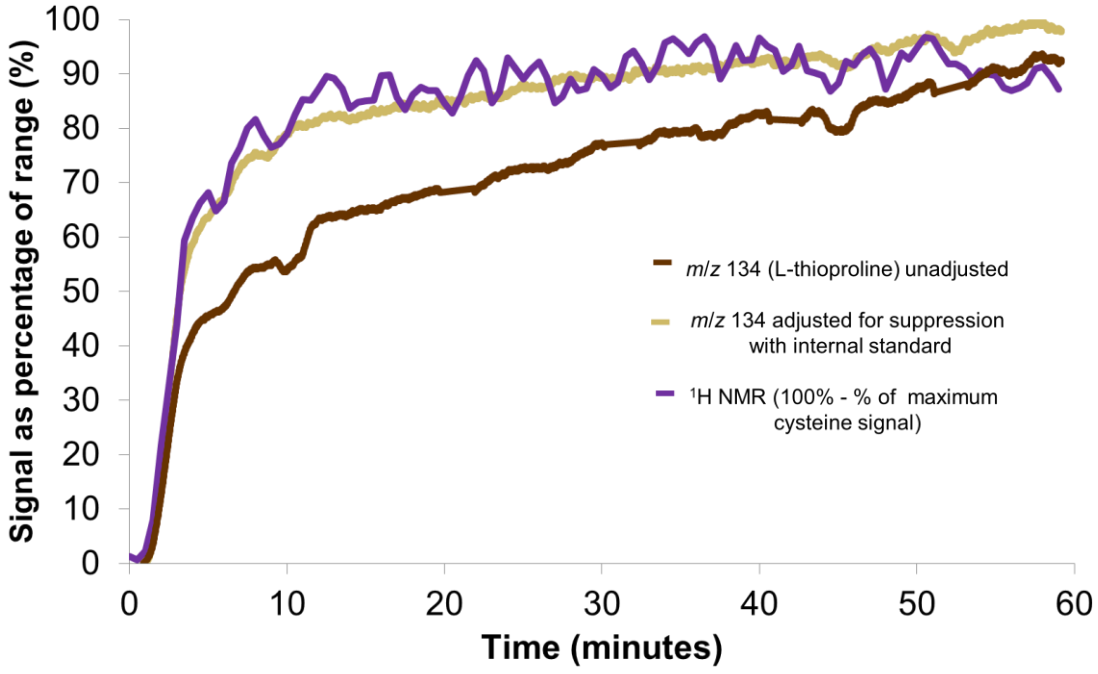

Figure 4-15- Uncorrected MS, Corrected MS and NMR traces for the reaction conducted with the ^{13}C labelled l-thioproline present.

4.5 Selected Ion flow tube MS monitoring of formaldehyde consumption

Formaldehyde in aqueous solution is a notoriously difficult compound to directly monitor by ESI MS as it does not ionise by ESI without derivatisation[100]. In NMR, formaldehyde proves difficult to monitor as it exists in an equilibrium with methylene glycol ($HOCH_2OH$) and polyoxymethylene glycol ($HO(CH_2O)_nH$, where n>1) [101], making the NMR signals very difficult to track in aqueous solution as they are near to the water OH signal, which is orders of magnitude larger than any of the formaldehyde signals and thus obscures those signals.

Measuring formaldehyde was not strictly necessary to monitor reaction progress, as both cysteine consumption and thioproline formation could be successfully observed online, however an experiment was undertaken to give oversight of the formaldehyde. In this experiment the change in formaldehyde abundance in the reaction vessel was monitored with a Syft Technologies Voice200ultra Selected Ion Flow Tube (SIFT) MS (Anatune Ltd., Cambridge UK), which has been noted for its ability to analyse formaldehyde in headspace. As the technique is inherently quantitative once the count rates are established for a particular combination of analyte and reagent ion[102], and formaldehyde was already in the libraries provided by the manufacturer, immediate quantitation of formaldehyde in headspace was possible.

While a measurable quantity of formaldehyde was detected in the headspace of the sealed 10 mL vials in which the reaction was conducted at room temperature with 4mL of 6 mg/mL cysteine solution and 0.2 mL of 15 mg/mL formaldehyde solution. When monitored in real-time, the formaldehyde signal showed gradual increase in time as shown in Figure 4-15. This is in contrast to expectations given reaction scheme 1, suggesting that the dissolution of formaldehyde into the headspace was significantly slower than the reaction, as if the reaction was slower one would expect the headspace concentration to follow the decrease in dissolved formaldehyde, and that the return to the equilibrium expected in a fixed headspace as per Henry's Law was not rapid enough to allow headspace monitoring to serve as a useful means of monitoring reaction progress. Henry's law is

given in equation 10, where C is the solubility of a gas in a given solvent at a fixed temperature in M, k is Henry's law constant in M/atm and P_{gas} is the partial pressure of the gas in atm,

Equation 5 - Henry's law equation for gas partioning

$$C = kPgas$$

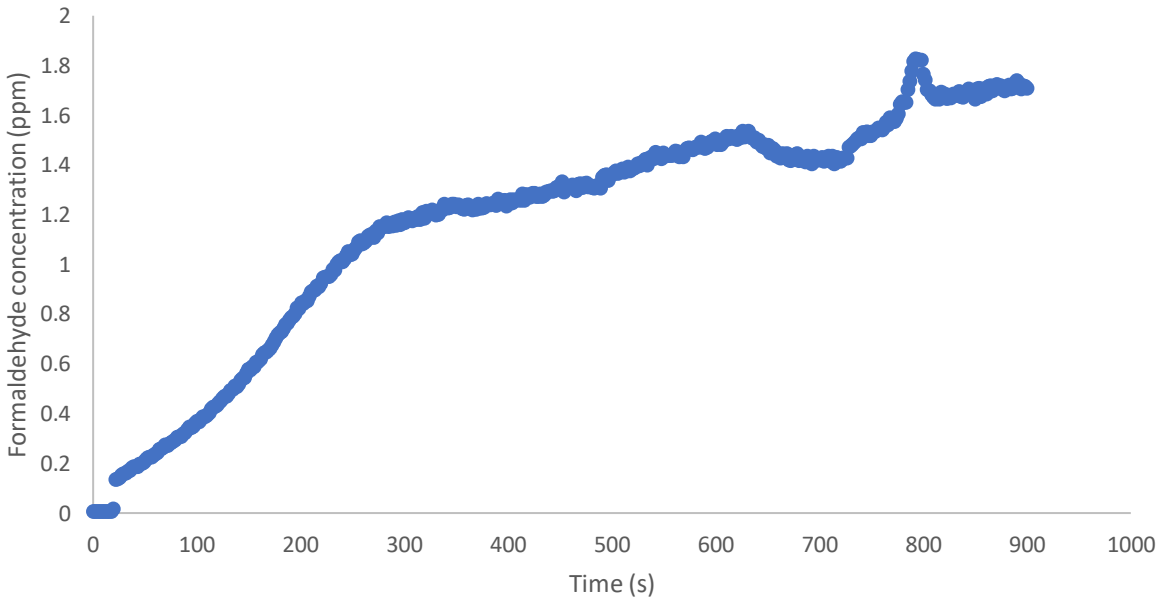

Figure 4-16 Formaldehyde concentration in headspace of cysteine-formaldehyde reaction as monitored by SYFT using H_3O+ reagent ion.

4.6 Conclusion

Ion suppression has been shown to be a significant issue in reaction monitoring using this system, and the capability of the system in identifying the presence of ion suppression has been established. The results herein demonstrate the importance of ensuring that a secondary system or some other form of validation is undertaken whenever mixtures of more than one compound are to be analysed simultaneously, a vital concern for any real time MS-based reaction monitoring system, as without chromatography, it is essential that the presence and degree of ion suppression be determined before any meaningful information can be extracted reliably from data produced. It is however notable that this is not the common use of the QDa or similar systems, which are used primarily as detectors for HPLC systems, and thus will not routinely encounter a situation where multiple species are being ionised simultaneously and quantitation is expected (as such a situation would represent a failure of the HPLC method to do its job).

A more general point in favour of the combined system is demonstrated through the detection of this issue, in that the use of two techniques which monitor chemicals in fundamentally different ways creates a much more fault-tolerant system, as erroneous results such as those produced through suppression are much more easily identified and corrected for in the presence of another monitoring technique that cannot have an identical problem.

5 Suppression of interfering solvent signals in ^{1}H NMR

5.1 Abstract

Inherent in ^{1}H NMR reaction monitoring is the issue of interfering signals from solvents. Almost all solvents in routine use contain at least one hydrogen environment, and those solvents are generally present in a much greater abundance than solutes. This can result in solvent signals that are several orders of magnitude larger than the signals of interest for a given reaction, and which must thus be suppressed to allow monitoring of the reaction. A number of *in-silico* techniques as well as a common pulse-sequence based techniques were investigated for solvent signal suppression in flow reaction monitoring.

This is a particular issue with low field instruments, as both solvents which generate singlet peaks such as water and those which generate split signals such as ethanol will occupy a greater ppm width on the spectrum, in the former case because the approximately Lorentzian peak shape of the signal has a broad base of a consistent width in Hz, representing a larger portion of the spectrum in a low field instrument, and in the latter case this broadening also occurs but is exacerbated by the wider splitting.

5.2 Issues arising from solvent signals in reaction monitoring by ^{1}H NMR

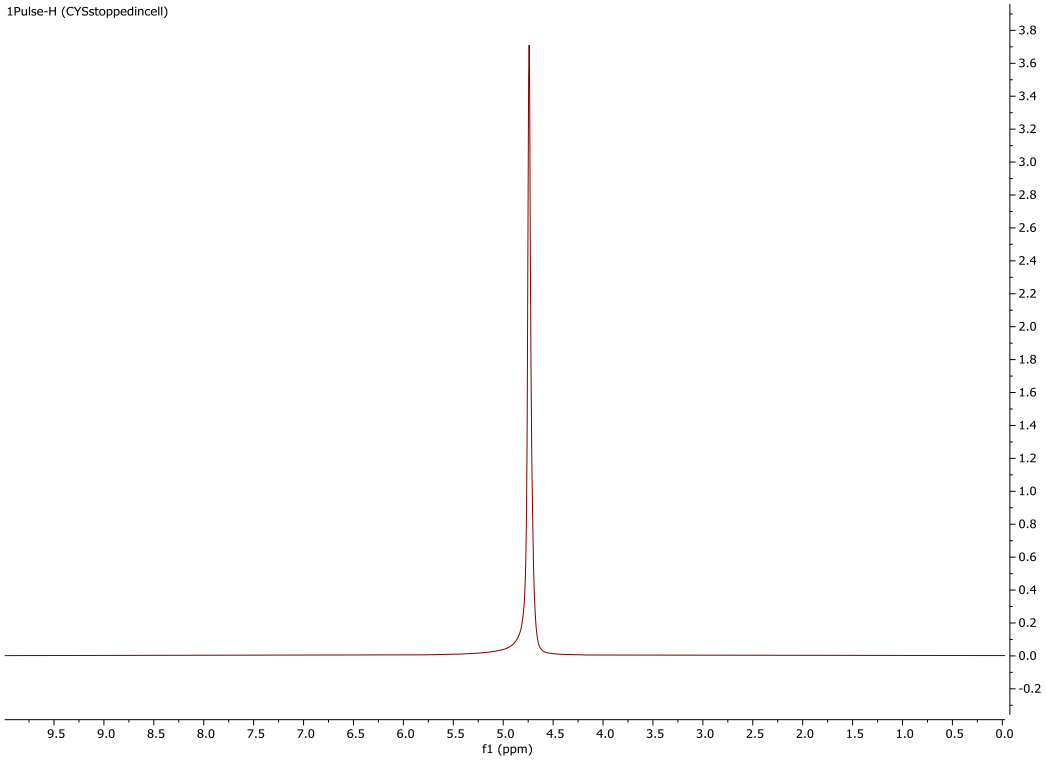

Figure 5-1 - NMR spectrum (^{1}H 43 MHz, H_2O) of 6mM cysteine zoomed out to show the full height of the water signal

The issue of solvent signals in NMR reaction monitoring arises from the relative abundance of solvent as compared to solute in most reactions. As ^{1}H peak integral is proportional to concentration, the result is that solvent signals for reactions in solvents containing at least one hydrogen atom are often many orders of magnitude larger than analyte signals, and thus any analyte signals in the vicinity of the solvent signals are likely to be rendered impossible to extract meaningful data from with regards to reaction progress as they are wholly or partially covered by the much larger solvent signal, meaning even minor fluctuations in the strength or lineshape of the solvent signal would result in relatively large changes in integration values for the analyte signals. Furthermore, dynamic range is limited by the analogue to digital converter in the instrument, meaning that if gain is set relatively low (in order to accommodate the very strong solvent signal), the weaker analyte signals will suffer from poor signal to noise ratios, while if gain is set high so as to

provide better signal to noise on the weaker signals, the operator risks the initial parts of the FID overflowing the converter and producing artificial signals in the final spectrum

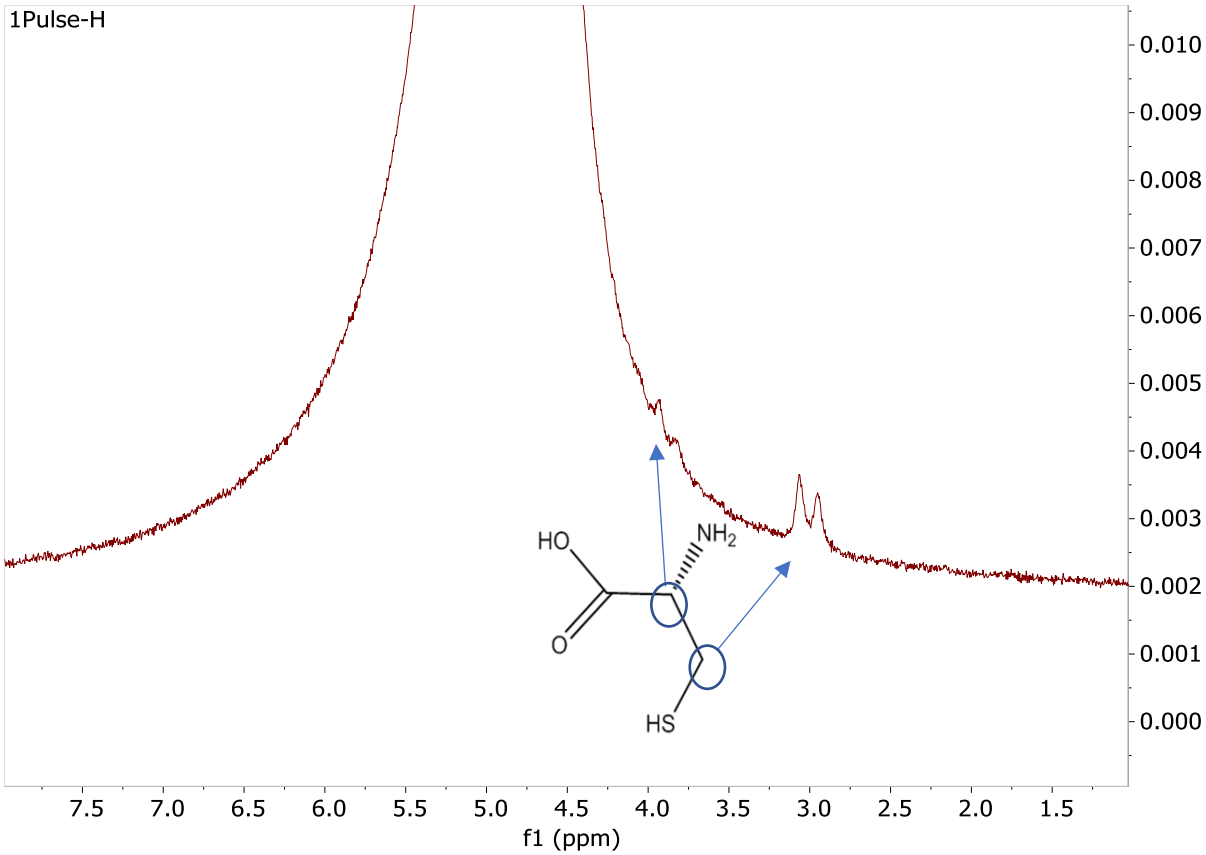

Figure 5-2 Solvent region of NMR spectrum (^1H 43 MHz, H_2O) of 6mM cysteine, note the doublet analyte signals at 3.1 and 3.8 ppm, the latter barely visible due to the distortion of the solvent signal.

Figure 5-1 shows a typical example, a sample of cysteine at a 6 mg/mL concentration in water, the starting concentration for the cysteine-formaldehyde reaction discussed in chapter 4. While deuterated solvents are commonly used to avoid this issue in NMR, it is not practical to do so in a reaction monitoring context as that would require the reaction to be conducted in far more expensive deuterated solvents, far outweighing any cost savings that could possibly be achieved by better monitoring and control of the reaction. The signal for the water at 4.8 ppm in Figure 5-2 reaches a height 1100 times greater than those of the analyte, and the analyte signals at 3.1 and 3.8 ppm subject to significant interference due to the base of the water signal being spread over a range of around 5 ppm.

5.3 Software based solvent signal suppression

MestreNova version 11.1 (Mestrelab Research S.L.) has functionality for signal suppression post acquisition, using 3 main algorithms: convolution, wavelets and the Whittaker smoother.

5.3.1 Application of a convolution algorithm to suppress solvent signals

The convolution post-processing method of signal suppression is based on the principle that the solvent signal will produce a high amplitude, low frequency signal in the FID, while analyte signals are expected to be of lower amplitude and higher frequency. As such, a periodic 'moving average' of the FID may be taken, producing a function which represents a good approximation of what the FID would look like if it contained only the solvent signal and no analyte signals. This is achieved by convolution of the FID and a rectangular function, followed by extrapolation of the FID back to the start of the acquisition and forward to the end (as a moving average of fixed size cannot be applied to the very start or very end of a dataset)[103]. This 'solvent only' FID is then subtracted from the original FID to give an FID which in theory contains only the signals from the non-solvent analytes.

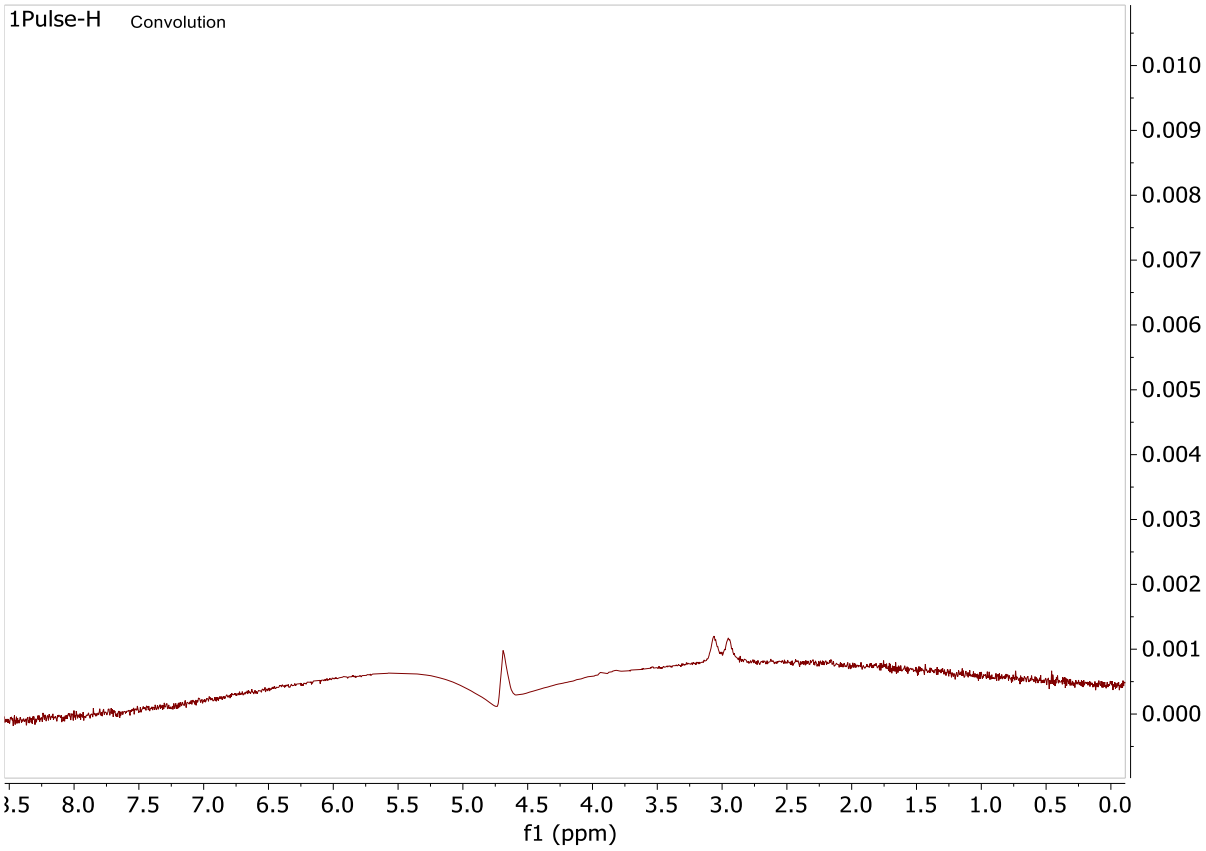

Figure 5-3 ^{1}H NMR spectrum from Figure 5-1 after the application of convolution signal suppression postprocessing. Note the doublet analyte signal at 3.0 ppm, and the near total suppression of the analyte signal at 3.8 ppm

As seen in Fig 5-2, the convolution method is reasonably successful in removing even extremely large solvent signals, in this case reducing signal height from 3.66 units to less than 0.0015, though the suppression effect is somewhat weighted towards the centre of the signal, which, as it is extremely broad, means some residual effect on base line remains to be corrected. Convolution almost entirely removes the effect of the solvent signal on the 3.1 ppm cysteine doublet, but fails to resolve the 3.8 ppm doublet from the solvent signal and thus near totally suppresses it, as its frequency is close to that of the solvent signal, demonstrating a drawback of the convolution technique when it comes to signals that are wholly or partially within the range covered by the signal to be suppressed.

5.3.2 Suppression of solvent signals by wavelets based algorithm

The wavelets suppression method offered as part of the MestreNova software package is a discrete wavelet transformation based method developed based on the work of Günther *et al*.[104] The Fourier transform converts time domain data to frequency domain data by, in effect, expressing it as a series of sin(x) and cos(x) terms. As these terms are inherently of infinite duration (in that sin(x) or cos(x) will never tend to zero and remain at zero), it is impossible for a Fourier transform to find the frequency at an exact moment in time, with it having instead to return the frequency range over a set period. Wavelet transforms seek to overcome this issue by instead expressing the time domain signal as the sum of a series of functions with limited duration, in that they tend quickly to zero and remain there. The time domain data is deconstructed into a sum of a number of these 'wavelets', transforming into a wavelet domain rather than the frequency mimicking domain provided by the Fourier transform, in this case using Daubechies wavelets[105] to express the time domain data. The use of numerous scaled domains to express the signal allows for those domains which correspond to low frequency (on resonance) signals in the time domain NMR signal to be suppressed, in effect suppressing the signals close to the solvent signal. The suppression can be tuned by selection of the wavelet used, and the number of dyadic levels (the scaled domains) to be suppressed.

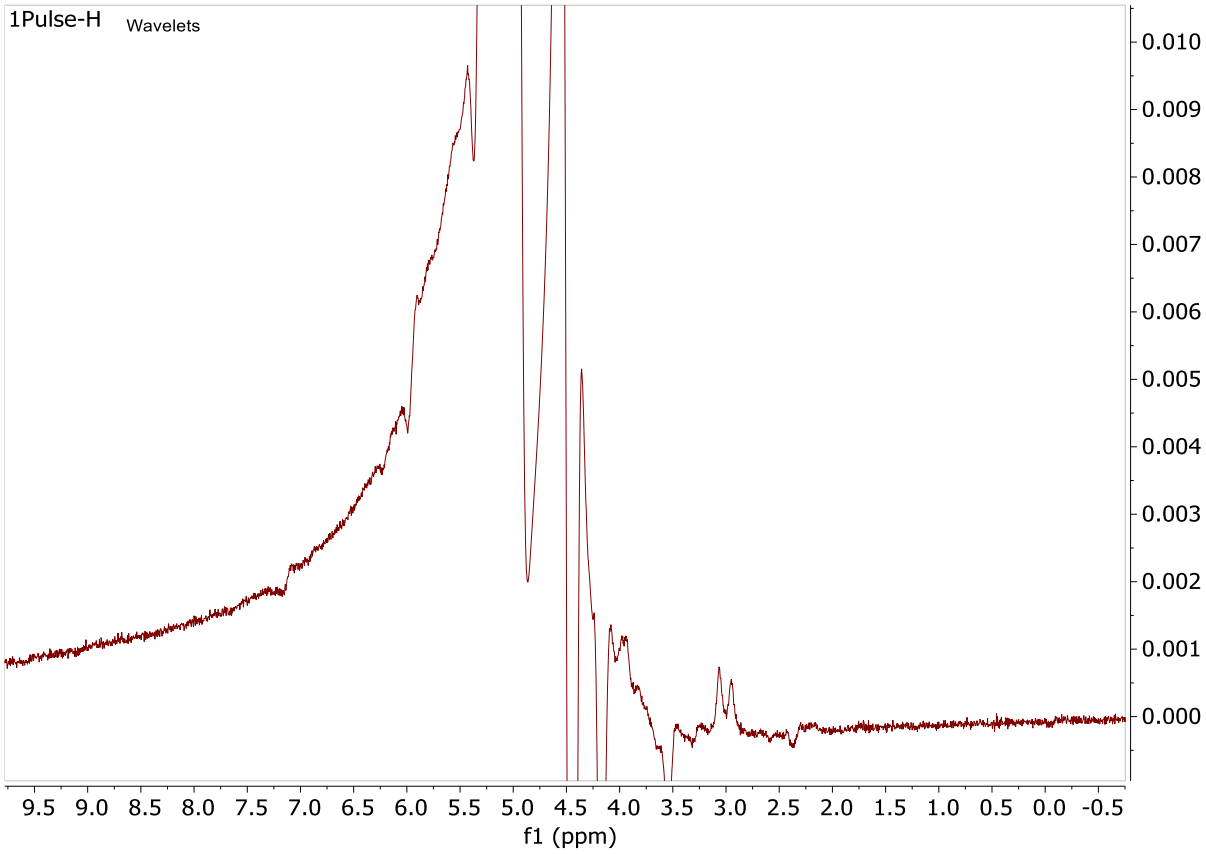

Figure 5-4 Cysteine NMR spectrum (^1H, 43 MHz, H_2O) from Figure 5-1 after the application of suppression by wavelets, 4 dyadic levels, wavelet of Daubechies coefficient 12 used.

The resulting suppression struggles to deal with the large, broad water signal produced by conducting measurements in aqueous solvent, though it does clearly resolve the signal at 3.1 ppm with relatively little baseline effect as compared to the convolution-based method.

5.3.3 Suppression of solvent signals by algorithm based on the Whittaker smoother

The Whittaker smoother operates based on a system of penalized least squares, wherein the result is a weighted combination of two goals, namely accuracy to the original data (Fidelity) and accuracy to a straight line (smoothness)[106]. A sum of squares is used to calculated each parameter, with a final line calculated by finding the series of points which minimises Q in the equation 5.3 in which F is the sum of squares difference to the original data (Fidelity), S is the sum of squares difference to the smooth line (smoothness) and λ is a user-set parameter to allow for the tuning of smoothness as against fidelity by the operator.

Equation 5-1 Whittaker Smoother parameter

$$Q = F + \lambda S$$

However, the signal suppression algorithm based on the Whittaker smoother as implemented in MestreNova does not allow for user set λ values.

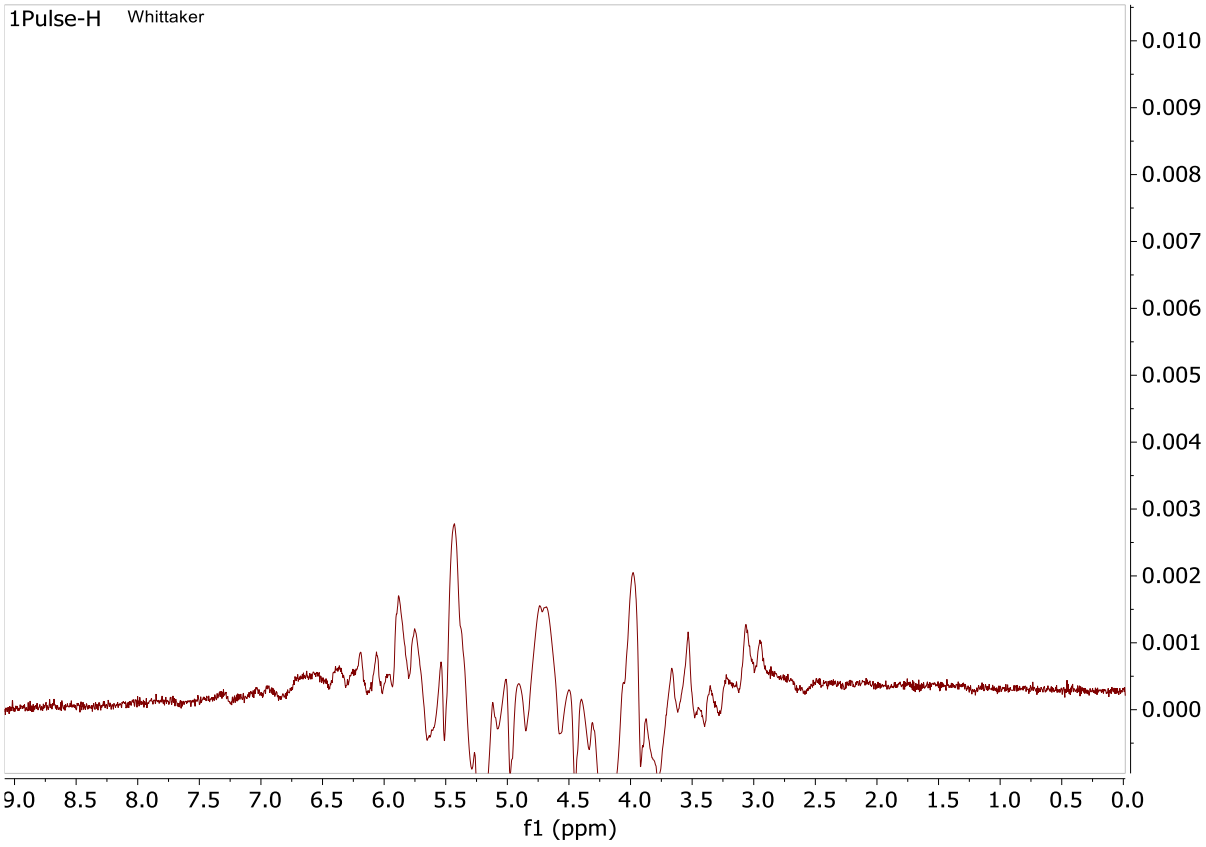

Figure 5-5 Cysteine NMR spectrum (^1H, 43 MHz, H_2O) from Figure 5-1 after the application of Whittaker smoother postprocessing

The resulting suppression, as can be seen in Fig 5-4, produces a broad and complex signal in the suppressed region, with the effects of the solvent signal localised to a greater degree than in the wavelets or convolution methods. The trade-off for this is that the signals within the suppressed region, which include both the 3.1 ppm and 3.8 ppm cysteine signals are more heavily affected by

the remains of the solvent signal, making monitoring of those signals less likely to produce useful data.

5.4 Pulse sequence based solvent suppression

Presaturation has been chosen as an example of pulse sequence based suppression as it is both the most widely used solvent suppression method[107] and one of the simplest pulse sequence based suppression methods, relying on just two fairly simple pulses.

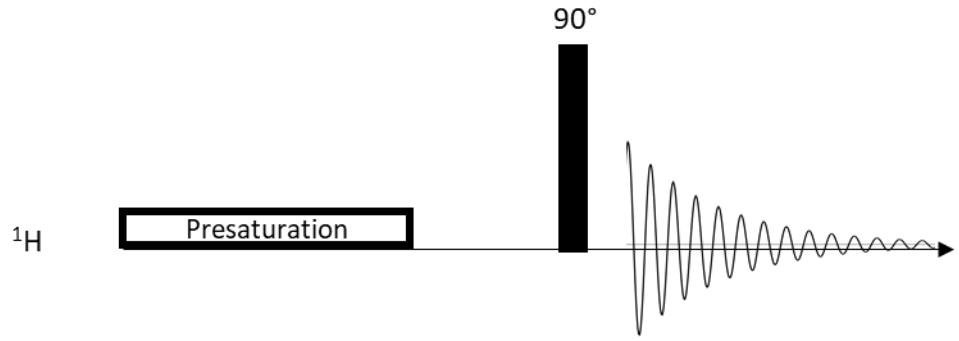

Figure 5-6 Presaturation pulse sequence diagram

As shown in Fig 5-5, the first is a long, low power selective RF pulse on the solvent resonance for a time period in the order of the solvent T_1, which serves to selectively saturate those protons, in theory to the point that there is no net magnetisation for protons in such environments (in that the populations of the excited and ground states are equal) followed by a standard 90° excitation pulse which excites the entire spectrum, resulting in no signal from the saturated region, but normal signal for protons remote from the targeted signal[108].

The net effect of this is to saturate the signals on the solvent resonance, forcing their magnetisation out of the xy plane (as shown in Fig 5-6) and thus significantly reduce the signal observed for that region in the spectrum, as the protons no longer significantly interact with the receiver coil.

The key variable for tuning of presaturation is the amplitude of the initial presaturation pulse, as this must balance between sufficient power to saturate the solvent signal out and avoiding saturating nearby signals.

A number of experiments were performed using 6 mg/mL aqueous cysteine, analytically relevant concentration and solvent for the reaction reported in this thesis (Chapter 4). Various pre-saturation amplitudes were examined. It was found that the water signal was so intense that even moderate suppression resulted in total loss of any nearby signals. The issue is illustrated in Fig 5-7, where the spectrum taken from a non-flowing sample (within the flow cell apparatus, but with the pump stopped) shows a significant water signal remaining while the cysteine signals (and indeed all analyte signals for several ppm on either side) entirely absent.

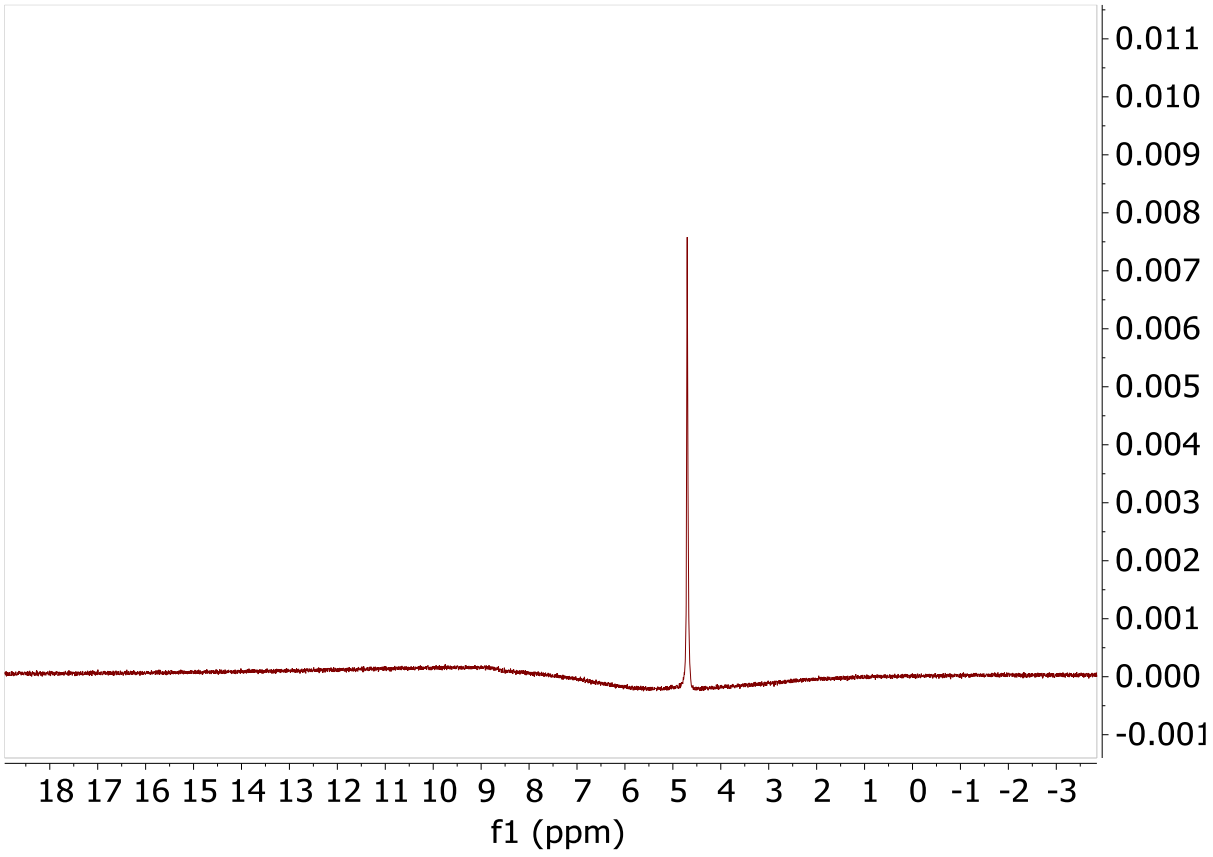

Figure 5-7 Presaturation spectrum for aqueous cysteine, -16 dB presat pulse. Note the signifcant baseline depression around the remaining water signal, showing how widely the spectrum has been impacted.

After experimentation with the suppression both in flow and on stationary samples, it was decided to discontinue the attempt, as no useful level of suppression could be achieved in either case without the obliteration of the signals of interest.

One important point to note about pulse-sequence based suppression methods is that, unlike those methods which rely on post-hoc manipulation of the data, they do not allow for changes in methodology after the fact, and so it is much more important to optimise the pulse sequences for the specific conditions being used prior to any attempt to monitor a reaction.

5.5 Conclusions

The fundamental issue of the breadth of solvent signals, arising in part from a limited number of available shims in the Spinsolve instrument, underlies all the attempts made in this chapter to mitigate the problem of solvent suppression, and given the inherent issues with attempting to apply pulse sequences to a 'moving target' of flowing reaction mixture, these techniques, and indeed those involving more complex pulse sequences such as those reported by Gouilleux[109] represent a mitigation of the problem at best. For the purposes of this work, it was concluded that the convolution based software method represented the best available method of mitigating the solvent signal, but that consideration of the presence and position of solvent signals was likely to remain a major point of concern in deciding which reactions the system was capable of monitoring, and that establishing the presence of monitoring signals clearly separated from the solvent region should be a primary concern for anyone wishing to use the system to monitor a reaction, with the suppression methods serving to support good experimental design in this regard rather than as a solution to the issue of solvent signals.

.

6 Monitoring electrophilic fluorination reactions.

6.1 Abstract

For the first time a small footprint MS and low field ^{19}F NMR were combined to investigate and provide kinetic information on a reaction. To achieve this goal a custom ^{19}F reaction monitoring script based upon the existing Magritek ^{1}H reaction monitoring script was created and the practical limits of ^{19}F reaction monitoring on the Spinsolve were investigated. Validation was provided on-site at AstraZeneca Macclesfield by 470 MHz ^{19}F NMR equipped with a Bruker InsightMR flow system.

6.2 Advantages of ^{19}F for reaction monitoring by on-line NMR

Reaction monitoring by ^{19}F NMR offers a number of potential advantages over ^{1}H NMR for a small footprint instrument. First and foremost, there is the advantage of simplicity, as it is extremely rare for there to be a large number of fluorine environments in a single reaction, while ^{1}H reaction monitoring will often deal with a dozen or more proton environments per molecule involved. This simplicity makes separation of signals of interest, and therefore identification, far easier, resulting in a greatly simplified spectrum from which to select trackable reactant and product peaks. Secondly there is the advantage that the vast majority of solvents do not contain fluorine, and as such do not produce an ^{19}F NMR signal. This means that the issues with solvent suppression methods dealt with in chapter 5 are completely avoided, with only a very small number of solvents causing any trouble whatsoever. Thirdly, the chemical shift range of ^{19}F is much larger than that of protons, with shifts covering a range of hundreds of ppm, making the likelihood of overlapping signals much lower even where multiple fluorine signals are present, making the likelihood of having a well resolved signal to monitor much greater.

From the perspective of reaction monitoring on a Spinsolve, another key aspect of ^{19}F NMR is that the frequencies involved are close enough to those used in ^{1}H NMR that on a 1T magnet such as that used by the Spinsolve, it is not necessary to retune the probe or provide a separate probe channel to acquire ^{19}F. The proton optimised probe can be used to acquire ^{19}F spectra without any additional hardware or operator maintenance requirements. A potential drawback is that ^{19}F signals occur over a much wider frequency range than those in ^{1}H NMR, with signals for organofluorine compounds occurring over a range of about 300 ppm, which can lead to issues with signal resolution when acquiring over a large range. Also, while there are generally fewer ^{19}F environments in a given compound than there would be proton environments in a usual ^{1}H spectrum, the potential for coupling between ^{1}H and ^{19}F nuclei can still produce complex peaks.

6.3 Sensitivity of ^{19}F for reaction monitoring by small footprint on-line NMR

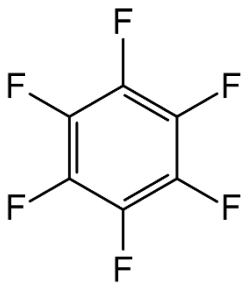

Figure 6-2 Hexafluorobenzene (C_6F_6)

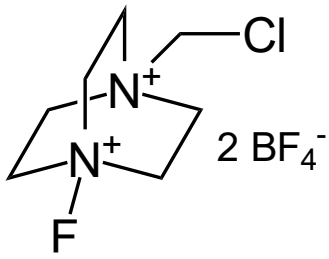

Figure 6-1 SelectFluor

The sensitivity of the Spinsolve's ^{19}F experiments was determined using serial dilutions of C_6F_6 (Figure **6-1**), a standard compound used for ^{19}F sensitivity experiments, in acetonitrile. A serial dilution in acetonitrile of concentrations from 100 µL/mL down to 1.25 µL/mL were conducted in a standard NMR tube, with a limit of detection being established as below 6.25 µL/mL as shown in Figure 6-1, equivalent to a 325 µM concentration of fluorine as each mole of C_6F_6 (**6-1**) contains 6 moles of fluorine.

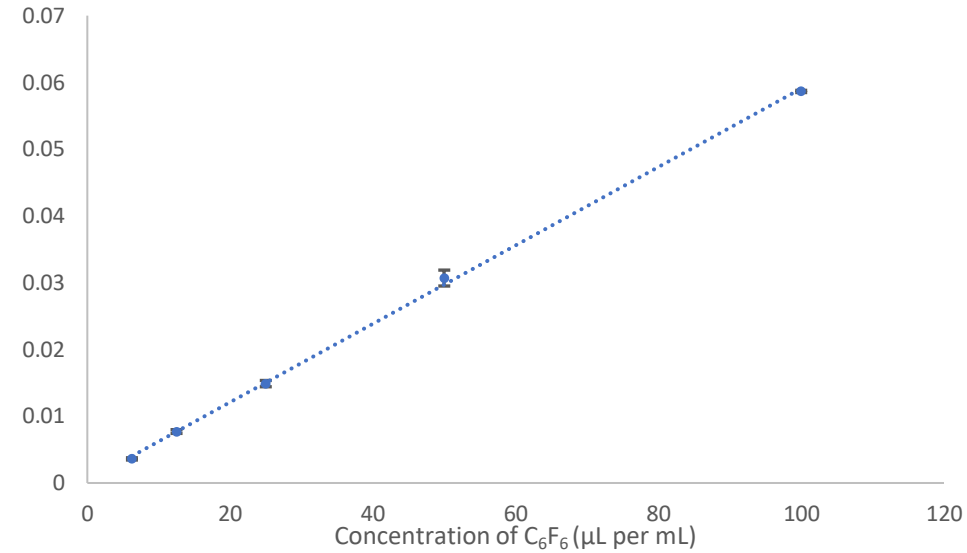

*Figure 6-3. ^{19}F NMR (40 MHz, acetonitrile, non-flow) signal integrals for C_6F_6 (**6-1**) signal (-156 ppm). Error bars indicate 1 standard deviation from 5 repeat measurements.*

The 1.25 µL/mL sample did not produce a signal which could be distinguished from the background and is thus not included in Figure 6-3.

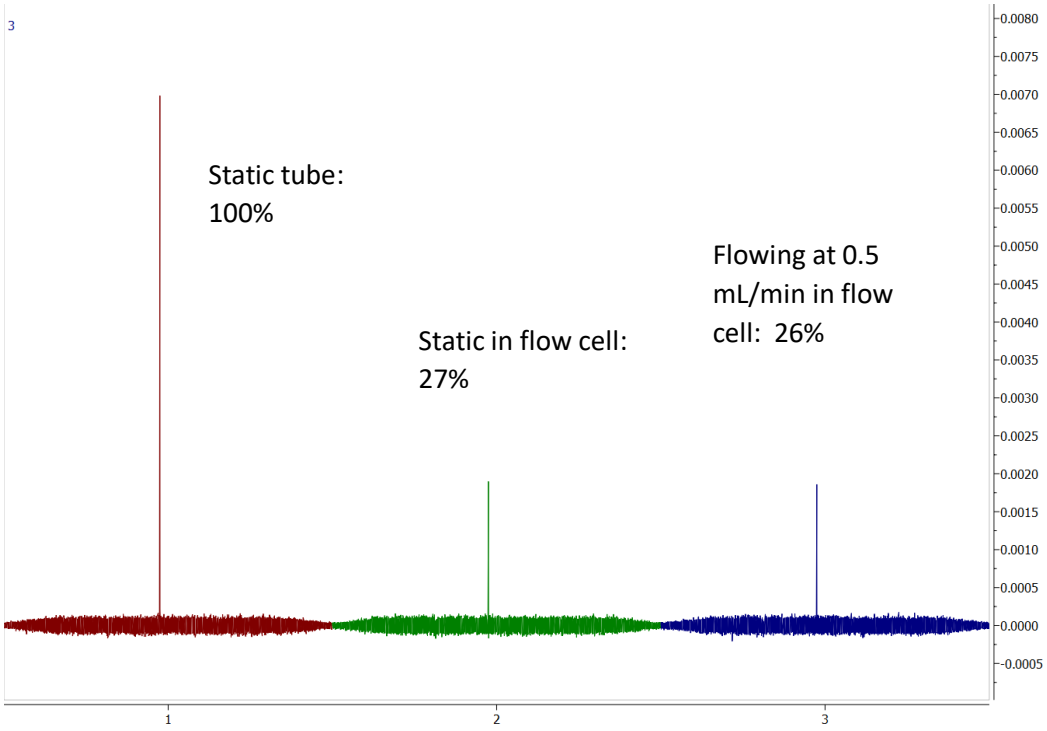

*Figure 6-4. ^{19}F NMR (40 MHz, acetonitrile) signal for 160 mM solution of SelectFluor (**6-2**) in (1) a standard NMR tube, (2) stationary in the NMR flow tube and (3) in flow at 0.5 mL/min in the NMR flow tube.*

The effect of the flow cell on ^{19}F sensitivity was tested using a solution of SelectFluor, a common electrophilic fluorinating reagent (Figure **6-2**) which was first measured in a standard NMR tube (signal 1 in Figure 6-4), and then pumped through the NMR flow cell with at 0.5 mL/min. As shown in Figure 6-4 the flow cell produced a significantly smaller signal, a 73% decrease in signal height from the NMR tube (signal 1) to the static sample in the flow cell (signal 2), though the difference between the signals taken with a static sample in the flow tube (signal 2) and while flowing at 0.5 mL/min (signal 3) showed only a very slight (3%) decrease due to the flow removing some sample from the measurement volume between pulse and acquisition.

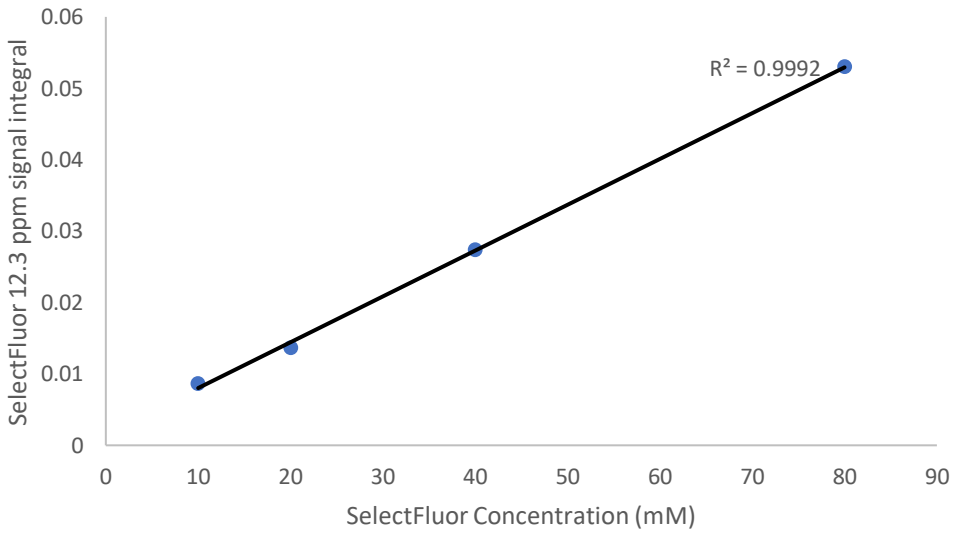

Figure 6-5 Dilution series of SelectFluor, signal integrals ^{19}F NMR (40 MHz, acetonitrile, 0.5 mL/min flow)

A series of dilutions of SelectFluor were then analysed to determine the concentration range over which reactions with singly fluorinated electrophilic fluorinating reagents could be monitored, using a range of concentrations beginning at the highest level which would be likely to be encountered in a reaction of interest, diluting down until the signal could no longer be clearly distinguished from the noise. The lowest concentration shown in Figure 6-4 (10 mM) achieved a signal-to-noise ratio of 8.03, which represents a good signal-to-noise ratio, above the generally acceptable level of 3. The

data shown in Figure 6-5 clearly shows that singly fluorinated compounds could be analysed by flow measurement on the Spinsolve (Magritek), to an approximate lower limit of 10 mM.

An issue which arose during this experiment was the requirement for manual phase correction on spectra at lower concentrations.

Phase correction is a process designed to compensate for issues which arise from detector layout in NMR dectectors. In order to allow the direction of rotation of magnetisation to be distinguished, is necessary to include signals from more than one point orthogonal to the net magnetisation direction (z) in the FT (as signals recorded at a single point would be unable to distinguish between a clockwise and anticlockwise rotation). These two inputs are the passed to the FT as 'real' and 'imaginary' inputs. The 'real' output of the FT is then taken as the spectrum, and should, assuming that there is no error in the phase difference between the two signals, result in a spectrum producing maximally positive signals. However, as the phase error increases, the peaks become increasingly close to the baseline, reaching a minimum at 90° out of phase and then increasing to a negative peak of the same magnitude as the correctly phased peak at 180° out of phase.

As the signals in this case appeared out of phase by very close to 90°, they were, without correction, nearly buried in the baseline, meaning that the software based automatic phase correction methods normally employed did not reliably pick up on the presence of the signals. However, as can be seen in figure 6-5, the requirement for manual phasing does not appear to introduce significant error into the integral values, though this potential error source should still be borne in mind when dealing with data from these spectra.

6.4 Fluorination of Dibenzoylmethane

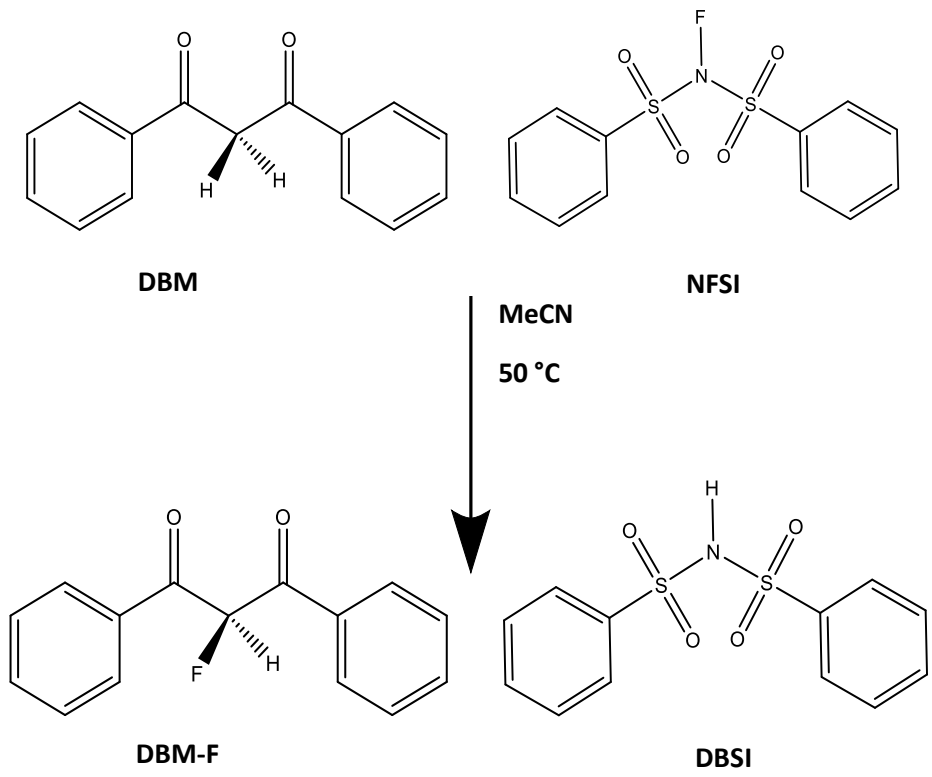

Figure 6-6. Reaction between dibenzoyl methane and N-fluorobenzene Sulfonimide

N-fluorobenzenesulfonimide (**NFSI**) reacts with dibenzyolmethane (**DMB**) in acetonitrile in a stoichiometric fashion to give the singly fluorinated product (**DBM-F**) according to the reaction given in Figure 6-5. The reaction was selected as it was under investigation by a colleague at Durham, provided a simple A+B -> C+D reaction which would occur over a timescale that was readily monitorable with the QDa and Spinsolve at the concentrations of fluorine established to produce detectable signals in flow for the Spinsolve[110], could be conducted at easily accessible temperatures, is not air or moisture sensitive and can be safely conducted in an NMR situated outside a fumehood.

6.5 ^{19}F NMR monitoring of Dibenzoylmethane fluorination

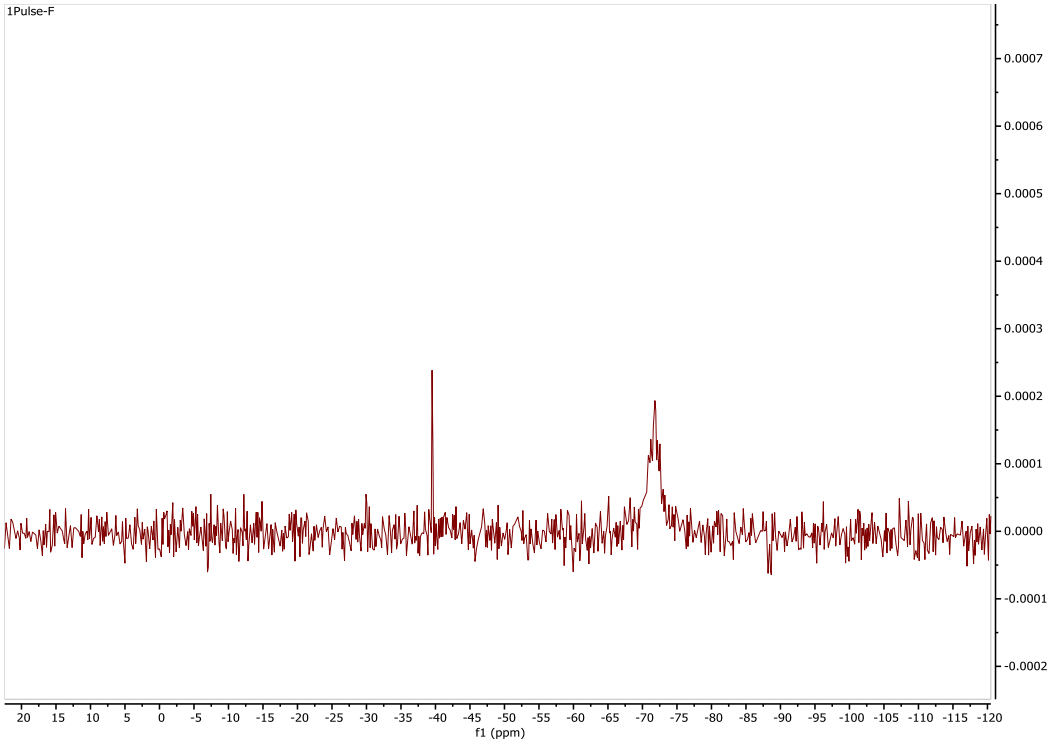

Figure 6-7 ^{19}F NMR Spectrum (40MHz, acetonitrile, 0.5 mL/min flow) for NFSI and DBM-F taken from a reaction in flow.

In ^{19}F NMR, NFSI produces a singlet signal at -37 ppm, while DBM-F gives a multiplet signal at -72 ppm, due to the coupling of the adjacent proton to the fluorine. It is possible to conduct broadband decoupling to avoid this on typical high field NMR instruments where a separate proton channel is available, but as the Spinsolve uses the same channel for proton and ^{19}F experiments, relying on the fact that the frequency range for ^{19}F is sufficiently close to that for ^{1}H at the magnetic field strength used in the Spinsolve to allow the detector which was designed and optimised for ^{1}H NMR performance to be used for ^{19}F without any retooling. The absence of the decoupling means that the signal-to-noise ratio for the doublet DBM-F signal is inherently poorer as the signal is spread over a lager frequency range, giving random noise a bigger impact. The singlet signal at -37 ppm was selected for monitoring as it presented the easiest target, being a large singlet well away from any other signals, present at the start of the reaction to allow for easy determination of the section of the spectrum to integrate across for the analysis.

The reaction was monitored on the Spinsolve using a 0.5 mL/min flow rate. While the Spinsolve software does provide a ^{19}F pulse program, there is no script provided in the versions of the software available to apply the ^{19}F pulse program to automated reaction monitoring. To enable ^{19}F reaction monitoring, the existing ^{1}H reaction monitoring script was adapted. The modifications from the original macro were confined largely to changing instances where the original macro referred out to the ^{1}H pulse program to instead run the pulse ^{19}F pulse sequence and altering constants to those appropriate for ^{19}F. The result enables spectra to be collected in an automated fashion, with the user defining the number of spectra, time per spectrum, number of individual acquisitions to be averaged to give each spectrum and time per acquisition, much as the original proton version of the script did.

For validation purposes, the reaction was also monitored using the Bruker InsightMR flow instrument equipped with a 11.75 T (^{1}H 500 MHz, ^{19}F 470 MHz) superconducting magnet and dedicated flow cryoprobe (courtesy AstraZeneca), which was able to achieve much higher sensitivity for ^{19}F than the Spinsolve. The reaction was monitored in-flow at 50 °C, using a flow system as described in chapter 2.3.4.

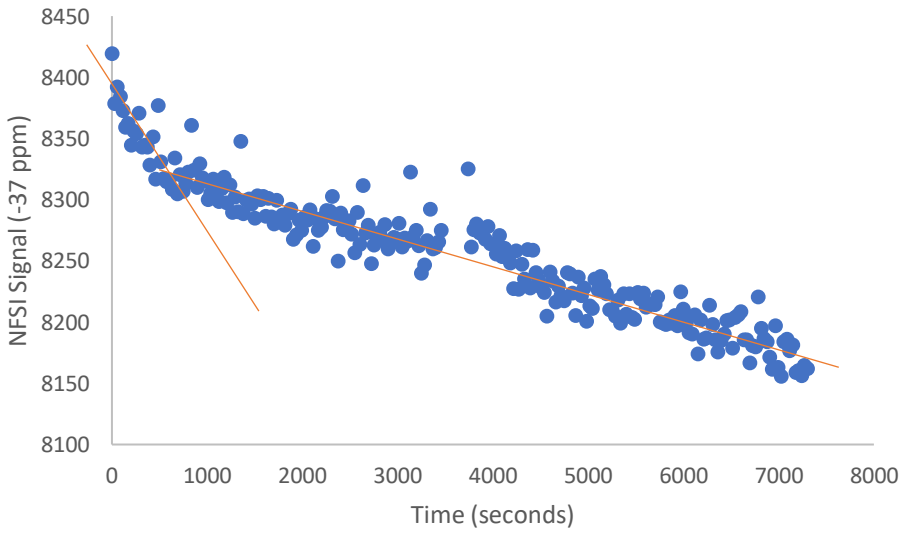

Figure 6-8. (^{19}F NMR, 40MHz, acetonitrile, 0.5 mL/min flow) Signal at -37 ppm (NFSI) for NFSI/DBM reaction

The resulting data as shown in Figure 6-6, shows a rapid initial decay for approximately the first 500 seconds followed by a straight region from approximately 500 seconds to the end of the reaction, suggesting a zero-order reaction, as rate does not vary with the concentration of either reactant. It is hypothesised that this zero-order rate is due to the reaction being diffusion limited, resulting in a rate which depends on the ability of the NFSI and DBM to mix in solution rather than the concentrations of either component. The initial decrease is hypothesised to be due to the relatively large volume of transfer line in the Bruker flow system, as the system was primed with a solution of NFSI, with the DBM then added to the bulk solution. The initial rate would thus represent the flushing of the cell, while the zero-order rate would be representative of the progression of the reaction at the concentrations used. The is also a short discontinuity at around 3500 seconds due to a known software bug in the timings of the Bruker InsightMR software used for monitoring, which unfortunately caused the monitoring to briefly pause mid-experiment. Unfortunately, due to limited time on the instruments at AstraZeneca and a number of runs interrupted by similar bugs, this run represented the best data that could be collected.

6.6 MS monitoring of Dibenzoylmethane fluorination

Tracking the reaction by MS was initially problematic due to the difficulty of obtaining signals for anything other than NFSI, though it was possible to obtain good signals for NFSI, DBM and DBM-F by adding 10 ug/mL NaCl to the 50/50 MeCN/H_2O make-up solvent used. As a result, the sodiated ions were tracked for all compounds. Initial experiments were performed using the G2S Synapt to benefit from the high mass resolution and accuracy across the mass range. This enabled clear and confident identification of the peaks at *m/z* 265.0639 $[DBM\text{-}F+Na]^+$ with a 0.8 ppm error and *m/z* 337.9928 corresponding to $[NFSI+Na]^+$ with 1.5 ppm error.

Following clear identification of diagnostic peaks, the reaction was moved to the QDa, also in flow. While peaks corresponding to the sodiated compounds could be observed, they were at a S:N of less than 3:1, and as such were judged to be insufficient for monitoring.

6.7 Combined NMR and MS monitoring of Dibenzoylmethane fluorination

A combined reaction monitoring was conducted using a version of the combined system with the Spinsolve (Magritek) connected to a Synapt G2S (Waters), for the reasons discussed in chapter 6.6. The system was in all other respects the same as that described in Chapter 3.5.

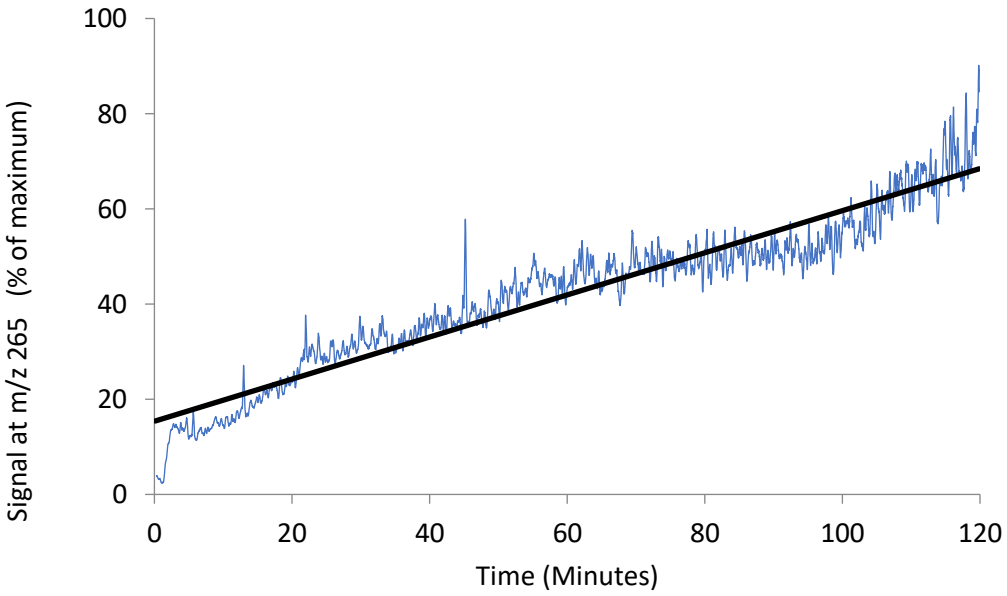

Figure 6-9 EIC of m/z 265 $[DBM\text{-}F+Na]^+$ for combined monitoring reaction

The resulting data supported the zero order reaction shown by the high field NMR, and it was possible to extract information on the rate giving a rate constant for $[DBM\text{-}F+Na]^+$: k = 0.467 ± 0.001 % signal intensity s^{-1}.

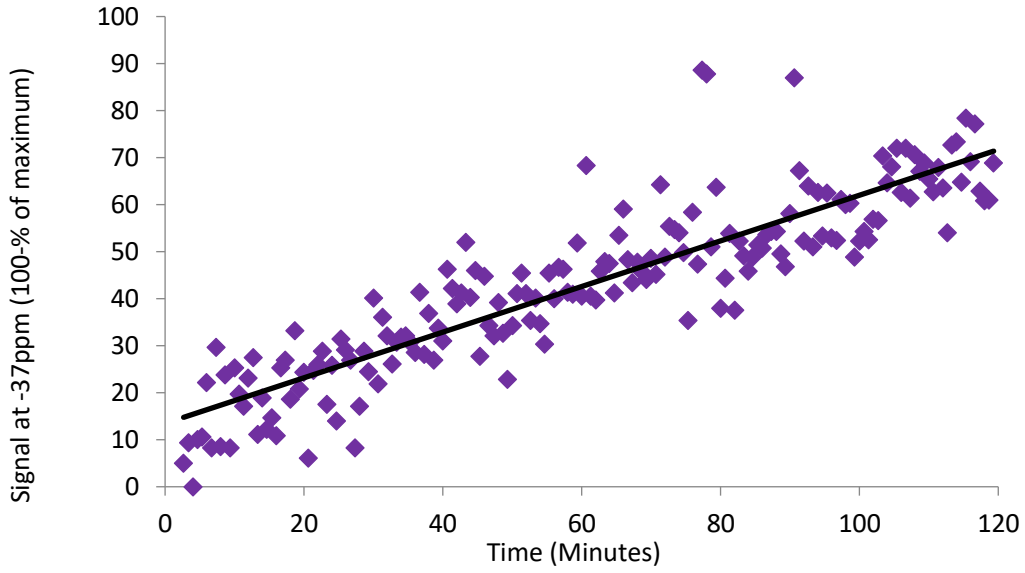

Figure 6-10 100% - normalised signal integral at -37 ppm (NFSI) for reaction monitored using benchtop ^{19}F 40 MHz NMR

Using the ^{19}F NMR signal for NFSI, a comparable reaction profile (Figure 6-8) was obtained from the Spinsolve by normalising the data to 100% and then subtracting the value from 100%,this was done because the doublet signal for DBM-F was significantly affected by noise on the Spinsolve, being a doublet and spread over a larger ppm range, the large J values more common in ^{19}F being exacerbated by the fact that on a 40 MHz instrument they translate to a larger ppm value than on a 470 MHz instrument. A point in favour of the Spinsolve is the absence of the significant initial decay that was seen in the first 500 seconds for the larger Bruker Insight system (Figure 6-6), as the smaller instrument and lack of significant external field means that the loop used can be much smaller, meaning lower internal volume and less time between reaction start and the reaction mixture being introduced to the measurement volume, in this case less than 1 minute. Applying this method the result gives k = 0.485 ± 0.018 % peak area s^{-1} , which agrees with the results from MS within the margin of error of the regression.

6.8 Conclusions

The use of ^{19}F NMR on the Spinsolve benchtop instrument as a means of reaction monitoring has been demonstrated, with a script developed to allow automated ^{19}F reaction monitoring. This has shown both the capability of the Spinsolve system in this regard and the significant limitations with regard to sensitivity that arise in this application. The system has been shown to be capable of providing monitoring which validates an second system, in this case monitoring by MS, but the utility of this instrument for ^{19}F reaction monitoring without some significant progress on either the physical hardware of the benchtop instrument or the pulse programs and shimming used to deploy that hardware appears limited.

7 Transportable MS instrumentation for in-situ analysis of toxicological analytes

7.1 Chapter Abstract

The in-situ analysis of toxicological compounds represents a useful area of application for transportable instrumentation, as there are many scenarios in which the provision of rapid data on-site can significantly aid the work of emergency services and others. In this work, the ability of ASAP MS to analyse drug samples was validated with LC-MS, and a prototype single quadrupole ASAP MS instrument was evaluated for its ability to detect and characterise toxicological samples, to differentiate mixtures of different drug compounds and to be used in a non-laboratory environment with minimal supporting infrastructure.

7.2 Development of a transportable mass spectrometer for field-based applications.

7.2.1 Applications for transportable analytical instrumentation

There are a variety of potential applications for transportable MS instrumentation, ranging from environmental studies checking the levels of compounds of interest in waterways to explosives testing[111] through to analysis of suspected drug samples for the emergency services, who may need rapid information on unknown substances in order to react safely to a situation. It is, for example, vital for paramedics to know what a white powder found in the possession of an unconscious person might be in order to properly treat that person and to avoid the risk of injury to the paramedics.

In this work, the application being focused upon is the analysis of suspected drug compounds, to which end we have collaborated with Durham Constabulary, Manchester Metropolitan Police and the Loop, a charity which provides drug analysis services in city centres and at music festivals.

The provision of rapid, on-site testing with rapid feedback to interested parties is a desirable goal for such services, as at events like music festivals there is a limited benefit to providing information to interested parties days or weeks after they bring a sample to be tested. The provision of rapid analytical information in conjunction with a brief intervention by healthcare staff has been shown to produce significant effects on the behaviour of service users[112], with a test at a music festival in the UK in 2016 resulting in 21.3% of service users handing in their remaining drugs for destruction by the police, while a further 17.1% of service users expressed an intention to modify their behaviour to reduce risk (either by taking smaller doses, spacing doses out more or by throwing the drugs away themselves). The music festival in question also reported a 95% reduction in drug related hospital admissions in the year of the testing pilot scheme as compared to the previous year in which no on-site drug analysis had been available.

In addition to the provision of advice, one of the key concerns for a drug analysis service is the mis-selling of drugs, wherein a drug, often one of the 'new psychoactive substances' which are entering the market, is sold as a different drug, often with similar psychoactive properties. This can cause significant health risks as the interactions, effective dosages, lethal dosages and duration of effect can vary significantly for even closely related analogues of drug molecules[113].

7.2.2 Current analytical approaches

The large variety of services available in different countries, ranging from government run laboratories to volunteer testing services mean that a wide variety of analytical techniques are used for identification of drugs. These services can be broadly categorised into 'on-site' and 'off-site' testing facilities, where on-site tests are conducted outside of a traditional laboratory setting. The off-site methods use the full gamut of analytical instrumentation, with GC-MS and LC-MS as well as NMR favoured for their ability to provide detailed analytical information. However the on-site services are necessarily much more limited in their ability to deploy equipment to venues like music

festivals, town centres and nightclubs, and as such rely more heavily on light-based spectroscopy, with FT-IR instruments predominating[114], backed up by colorimetric reagent testing using reagent kits available to the general public and mass loss testing. Mass loss analysis is a very approximate quantitation of an active compound in a tablet, achieved by weighing the tablet, washing with methanol, drying and reweighing it, working on the assumption that only the active compound is soluble in methanol.[115]

While these techniques have the advantage of being deployable with relatively little infrastructure, requiring only standard power sockets and a reasonably stable surface on which to put the instrument, they lack specificity, in the case of mass loss due to the solubility of many non-psychoactive substances in methanol, in the case of reagent testing due to the inherently non-specific nature of the reagents, which will react with numerous chemically similar compounds rather than exclusively with the substance of interest, and with the FT-IR due to the exclusive reliance on library based search methods which are easily fooled by chemically similar compounds.

7.3 Characterisation of drug samples by ASAP Mass spectrometry

7.3.1 Validation of ASAP-MS with LC-MS

ASAP is a direct analysis method of ionisation and was chosen for this application due to the speed of analysis, with samples able to be analysed in 3 minutes or less, and that the sample is analysed without any treatment, although all tablets in this study were crushed to provide a uniform powder and avoid the very real problem that illegal drug tablets can have variability in distribution of active ingredient throughout the tablet. 1 mg of powdered sample was diluted in 1 mL methanol and analysed by ASAP ionisation using a QToF mass spectrometer (LCT Premier, Waters Corp). The mass spectrometry method was built such that during one experiment, the cone voltage was increased stepwise in four stages (15 eV, 30 eV, 50 eV and 70 eV), each stage lasting 45 seconds. At each stage, the melting point tube was removed and dipped into the sample vial to refresh the sample loading.

These cone voltage settings were chosen to approximate the CID collision energies used in established LC tandem mass spectrometry based toxicology screening assays which rely on library matching to identify target compounds. Figure 7-2 gives the sample chromatograms showing the introduction of analyte at each cone voltage, and Figure 7-3 shows the spectra of each peak. Samples for LC/MS were first diluted 1000 times before a 3 nL injection into a 0.4 mL/min flow.

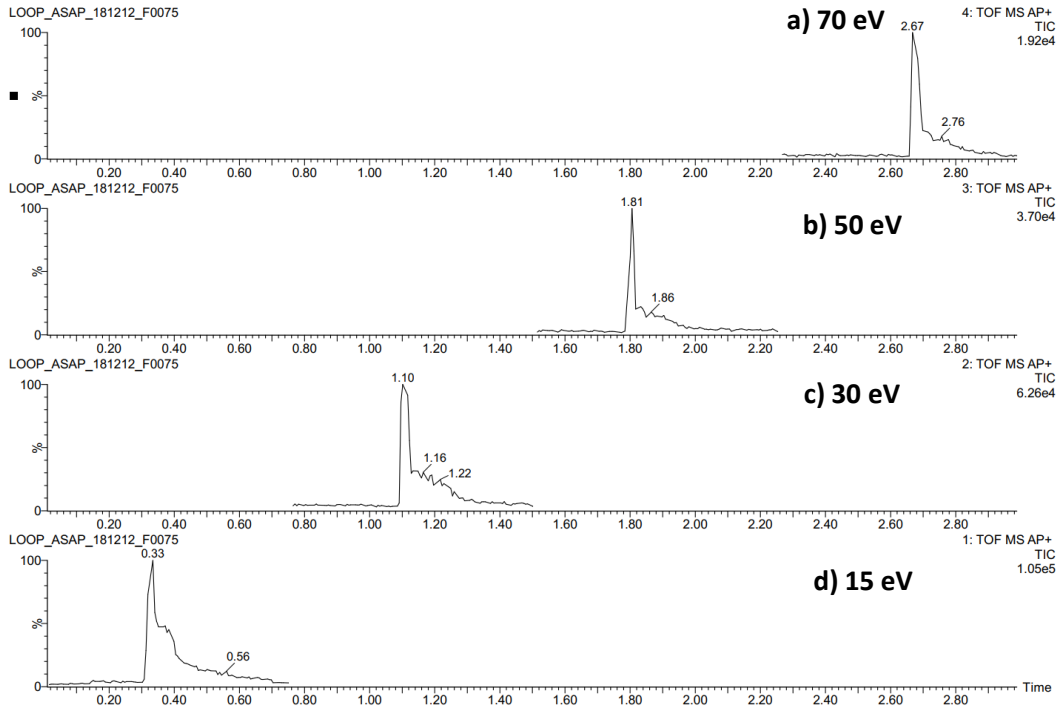

Figure 7-1 Total ion chromatograms for sample F0075 as fresh sample is dipped and placed into the ASAP ion source for each of the 4 cone voltage settings examined.

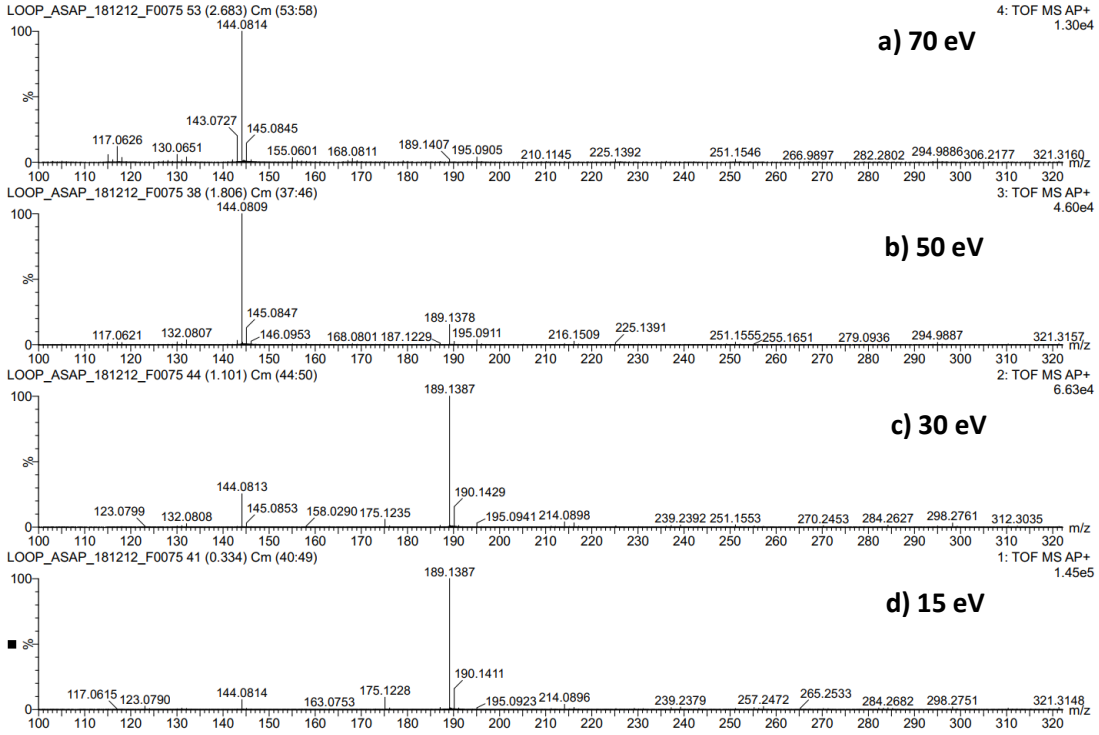

Figure 7-2 Mass spectra for F0075, summed over most intense regions of the chromatograms (shown in Figure 7-2) at each cone voltage setting.

The sample, a white powder, gives a strong response by ASAP at all 4 cone voltages as can be seen in Figure 7-1, with some tailing as expected in ASAP as the sample on the melting point tube fully evaporates, but the signal rapidly falls away and there is no carryover between sample introductions, facilitating a time efficient analysis. The 15 eV cone voltage (Figure 7-2 **d**), aimed at minimising any dissociation, produced a signal at *m/z* 189.1387, which corresponds to $[C_{12}H_{17}N_2]^+$ with 2.5 ppm error. This is in agreement with the belief that this compound is N,N-Dimethyltryptamine. As the cone voltage increases (Figure 7-2 **b**-**d**), there is clear evidence of dissociation, with a peak at 144.0814 becoming more intense until between 30 and 50 eV it becomes the base peak in the spectrum. This peak corresponds to $[C_{10}H_{10}N]^+$ with an 0.7 ppm error, consistent with the $[M+H-NMe_2]^+$ signal commonly used as an MRM transition when quantifying this compound in toxicological studies[116]

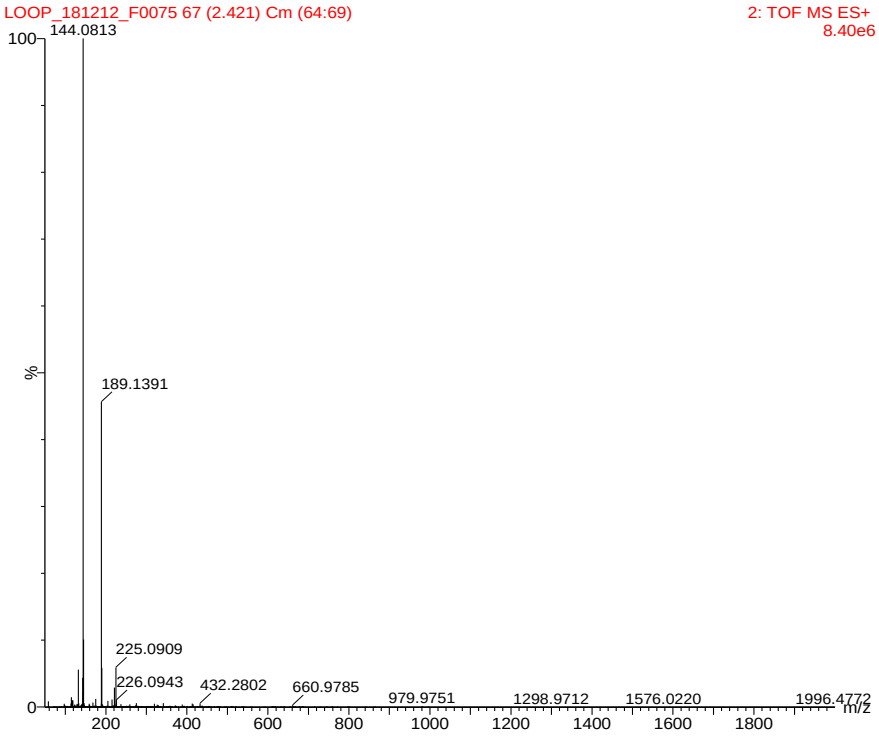

Figure 7-3 Spectrum from LCMS analysis of sample F0075

Figure 7-3 shows the spectrum for the peak corresponding to N,N-Dimethyltryptamine in the LCMS method, with the signal at 144.0813 corresponding to $[C_{10}H_{10}N]^+$ with 0ppm error and the signal at 189.1391 corresponding to $[C_{12}H_{17}N_2]^+$ with 0.5 ppm error, confirming the identification of the compound.

Table 7-1 summary of results from testing event in Durham city centre

Sample ID	Believed identity as given by the submitter	Identity determined by MS	Identity determined by FT-IR	Appearance
F0075	'DMT' (N,N-Dimethyltryptamine)	N,N-Dimethyl Tryptamine (By both ASAP and LCMS)	N,N-Dimethyltryptamine	Off-white powder
F0076	'MDMA' (3,4-Methylenedioxymethamphetamine)	3,4-Methylenedioxymethamphetamine (By both ASAP and LCMS)	3,4-Methylenedioxymethamphetamine	Pill
F0077	'MDMA' (3,4-Methylenedioxymethamphetamine)	3,4-Methylenedioxymethamphetamine (By both ASAP and LCMS)	3,4-Methylenedioxymethamphetamine	Pill with 'Beats' logo.
F0078	Cocaine	Cocaine (by both ASAP and LCMS)	Cocaine	White powder
F0084	'N,N-DMT' (N,N-Dimethyltryptamine)	DMT (by both ASAP and LCMS)	DMT	Off-white powder

F0085	MDMA (3,4-Methylenedioxymethamphetamine)	3,4-Methylenedioxymethamphetamine (by both ASAP and LCMS)	3,4-Methylenedioxymethamphetamine	Pill
F0086	Ketamine	2-Fluorodeschloroketamine by both ASAP and LCMS	Ketamine (low confidence score on library search)	White powder
F0087	LSD (Lysergic acid diethylamide)	Lysergic acid diethylamide by LCMS, no determination possible by ASAP	Not possible due to sample format	Sample submitted on blotter paper
F0091	'MDMA' (3,4-Methylenedioxymethamphetamine)	Chloroquine by ASAP and LCMS	Chloroquine	Off-white crystals
F0092	'4-HO-MET' (4-hydroxy-N-methyl-N-ethyltryptamine)	4-hydroxy-N-methyl-N-ethyltryptamine by ASAP and LCMS	Not possible due to sample format	Sample submitted as a portion of a gummy bear.
F0093	'4-AcO-DMT' (4-Acetoxy-N,N-dimethyltryptamine)	4-Acetoxy-N,N-dimethyltryptamine by ASAP and LCMS	Not possible due to sample format	Sample submitted as a portion of a gummy bear.

F0095	LSD (Lysergic acid diethylamide)	No LSD present, 25D-NBOMe, a NPS hallucinogen, was identified	No determination possible due to sample format	Sample submitted on blotter paper
F0112	Ketamine	Ketamine by both ASAP and LCMS	Ketamine	White powder.
F0113	'Speed' (Amphetamine)	Caffiene and one unknown compound.	Caffeine	Brown granules
F0114	Cocaine	Cocaine by LCMS and ASAP	Unknown.	White powder
F0116	Ketamine	Creatine by LCMS, ASAP inconclusive.	Creatine	White powder, poorly soluble
F0119	Heroin (Diacetylmorphine)	Caffeine, paracetamol, diacetylmorphine and noscapine by both ASAP and LCMS	Caffeine, paracetamol and diacetylmorphine	Yellowish crystals
F0120	Heroin (Diacetylmorphine)	Caffeine, paracetamol, diacetylmorphine and noscapine by both ASAP and LCMS	Caffeine, paracetamol and diacetylmorphine	Yellowish crystals

18 samples, selected as a subset of those collected over 2 one-day public testing events held at St. Nicholas Church in Durham city centre, analysed by FT-IR in a temporary onsite lab set up in the church attic, with the subset of samples deemed interesting (a selection of common street drugs were chosen, as well as any unusual samples or ones which were not amenable to the onsite FT-IR). Subsamples were then dissolved in 1 mL methanol before being transported with police escort to the Durham Chemistry department for analysis by ASAP-MS. There was only opportunity to do one analysis per sample before the samples were removed by the police for destruction. As can be seen in Table 7-1, in most cases, the ASAP-MS was able to provide the same characteristic ions as the LC-MS, with the notable exception of sample F0087, a small piece of blotting paper with LSD on it.

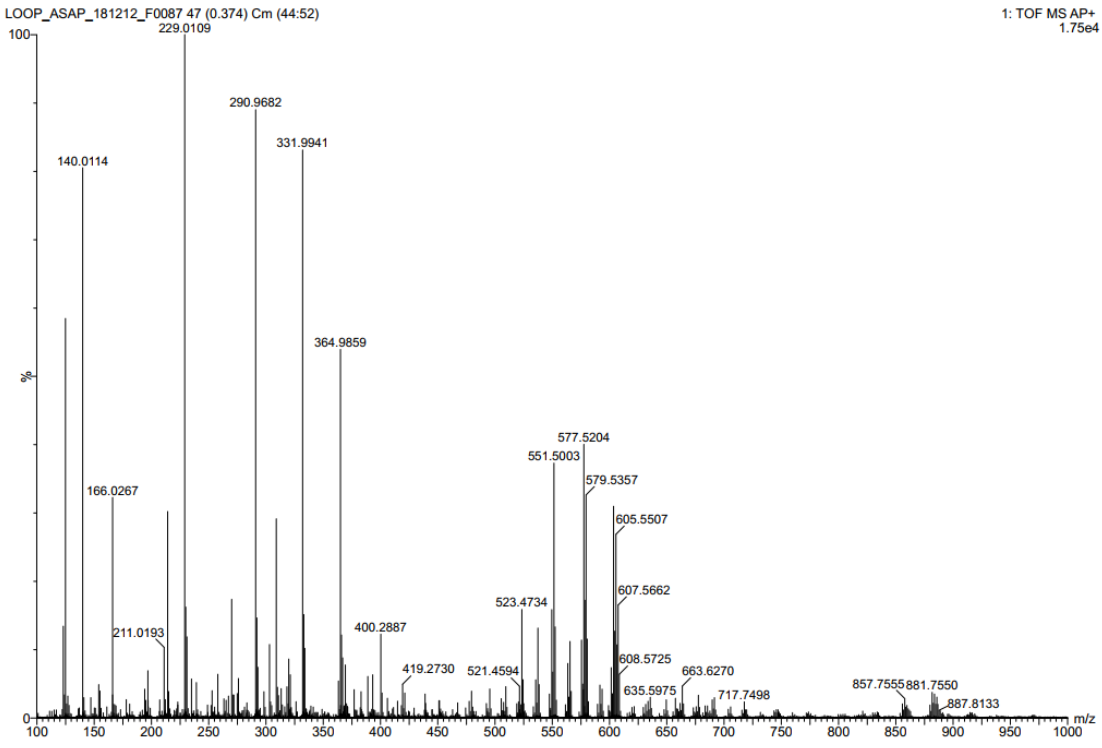

Figure 7-4 15 eV ASAP spectrum for sample F0087, blotting paper submitted as LSD. No signals for LSD could be observed.

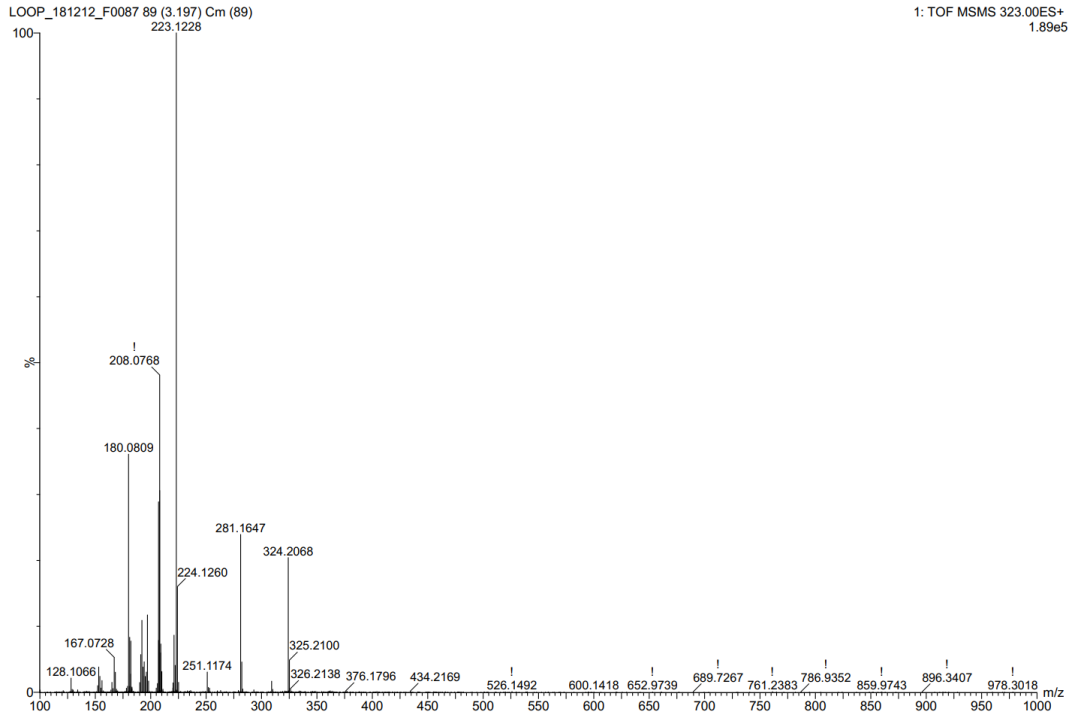

Figure 7-5 LC MSMS spectrum for sample F0087, blotting paper submitted as LSD. Signals for LSD and fragments are clearly seen.

This sample was not tested by FT-IR as the blotting paper is not amenable to such measurement, as the strong signals from both the paper and the grease thereupon interfere with library matching, while on the ASAP instrument the solution, after the blotting paper had been soaked in methanol to dissolve the drug, gave an extremely crowded spectrum (Figure 7-2) with a large number of peaks, none of which could be related back to LSD.

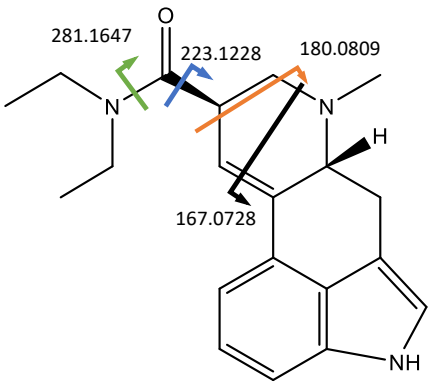

Figure 7-6 Structure of LSD, with fragments indicated.

The LC-MS spectrum of sample F0087 (Figure 7-3) shows a clear signal for LSD $[M+H]^+$ at *m/z* 324.2068 and a number of fragments at *m/z* 281.1574, 223.1228, 180.0809 and 167.0728 as shown in Figure 7-5 , as well as a fragment in 208.0768 which is consistent with MRM transitions normally used in toxicology[117]. The LCMS analysis is able to separate the LSD from the various oils, dyes and general grease and dirt from the blotting paper substrate that has been handled by the producer and submitter (and the supply chain between). In this case, there is too much background signal from ASAP ionisation supressing the ions of interest to allow for analysis.

Sample F0086 was proposed to be ketamine by the submitter. There was tentative support for this proposal following FT-IR analysis using a Bruker Alpha FTIR with an ATR attachment. The FTIR library match using the TICTAC spectral library (Tictac Communications Ltd.) was 638 and the threshold for accepting FTIR identification is 600. The low score was initially accounted for as being due to the low ketamine content in the sample provided and the presence of impurities.

When analysed by ASAP MS there was no signal for ketamine expected at *m/z* 238 with product ions at *m/z* 220, *m/z* 207 and *m/z* 179. Instead a very strong signal was observed at *m/z* 222.124, without the expected chlorine isotope pattern. As the cone voltage increased, product ions appeared at *m/z* 204.1203, *m/z* 191.0889 and *m/z* 163.0914.

It was noted that this pattern matched the expected fragmentation pattern for ketamine, Figure 7-6 a), though 16 mass units lighter in every case, suggesting a similar structure, with potential substitution of the chlorine present in ketamine with fluorine. Furthermore, the accurate mass for the main peak in the LCMS method at *m/z* 222.1299 matched $[C_{13}H_{17}NOF]^+$ with a deviation of 2.5 ppm.

a)

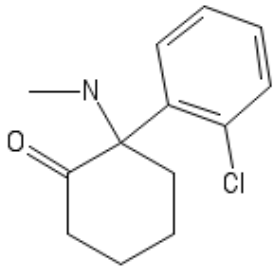

b)

Figure 7-7 Structures of a) Ketamine, a common psychoactive substance and b) 2-fluorodeschloroketamine, a new psychoactive substance.

This evidence allowed us to suggest an identity the unknown sample as 2-fluorodeschloroketamine, Figure 7-6 b), a known NPS which had not been previously detected in the UK, demonstrating the value of MS instrumentation to provide up to date information for the emergency services as to the drugs in circulation. The FTIR misidentified the sample as 2-fluorodeschloroketamine was not present in the library being used, and the similarity of its structure to ketamine meant that the bonds present were similar enough to give a score for ketamine that was at the lower end of what was deemed acceptable for identification.

Figure 7-8 A gummy bear of the type used as a dosage form for samples F0092 and F0093, identified as 4--hydroxy-N-methyl-N-ethyltryptamine and 4-Acetoxy-N,N-dimethyltryptamine respectively

Samples F0092, F0093 and F0095 are notable in that the ASAP MS was able to determine the drugs present in samples which came in formats not compatible with the FT-IR instruments normally used, as samples F0092 and F0093 came in the form of gummy bears, as shown in figure 7-7, while sample F0095 came as a piece of blotting paper with a printed design. These dosage forms were not compatible with the FT-IR as the strong background signals from the paper and the sugar and gelatin filled gummy substance respectively would significantly impair the ability of the FT-IR to pick up signals for the active compound. The samples were introduced to the mass spectrometers by first placing a small portion of the dosage form in methanol to allow the drug compound to be dissolved and then diluting the solution further for LCMS and dipping the melting point tube directly into the methanol solution for the ASAP.

The ability to analyse samples that are not in the form of pills or powders is of great use especially for the diverse dosage forms of NPS drugs.

Another notable result was the analysis of two samples of 'heroin', both of which gave strong signals for caffeine, paracetamol, and the expected diacetylmorphine in ASAP, LCMS and FTIR. However in addition to these, the LCMS and ASAP were able to detect signals which matched Noscapine (see appendix 2), an alkaloid derived from the opium poppy. The ability to detect even minor components in complex mixtures is an important feature for the MS instruments in this application.

7.3.2 Transportable ASAP MS

Having established that ASAP ionisation is well suited to the application of identifying drug compounds from a range of formats, this study moved back to exploring approaches for making this technology transportable. To this end a prototype single quadrupole ASAP MS instrument (Waters, Corp.) was trialled with a variety of toxicological standards, with a view to use as a transportable MS instrument for in-situ analysis of toxicological samples. The method developed on the ASAP-QToF MS was replicated such that the same four cone voltages, 15 eV, 30 eV, 50 eV and 70 eV were used, with the notable difference that the 4 voltages were cycled rather than being run sequentially, allowing for all 4 to be applied to the same sample introduction, facilitating much quicker analysis and allowing multiple replicates for each sample.

Typically, ASAP ionisation uses a supply of nitrogen (99.9% grade nitrogen flowing at 8 L/min). As discussed in section 2.1.3, the nitrogen is ionised by the corona discharge, and in turn transfers a charge to the volatilised analyte. In order to make the instrument more transportable, the nitrogen supply for the ASAP source was replaced with a small (147mm x 86mm x 38 mm) light (575 g) diaphragm pump (Boxer GmBh). This was able to operate from a standard UK 13 amp mains socket and provided sufficient air flow to facilitate ionisation. Figure 7-9 shows the results for a 50 µg/mL solution of 3,4-Methylenedioxymethamphetamine using (a) dedicated high-grade dry nitrogen supply and (b) using the diaphragm pump to supply ambient air from the local environment. 3,4-Methylenedioxymethamphetamine produces, as may be seen in Figure 7-9 a) i), a $[M+H]^+$ ion at *m/z* 194, with less intense peaks at *m/z* 163 $[M+H\text{-}NHMe]^+$, *m/z* 135 $[M+H\text{-}C_3H_8N]^+$ *m/z* 105 $[M+H\text{-}C_5H_{10}NO_2]^+$ and *m/z* 77 $[C_6H_5]^+$

When nitrogen was used the base peak intensity from the average of 10 scans is $5.84x10^5$. When switching to air this rose to $6.66\ x10^5$ for the same amount of sample loaded on to the tip. It should

be noted that in these studies, to ensure repeatable sample loading, 2 µL was pipetted on to the melting point tube for analysis, and this loading was done triplicate per analysis.

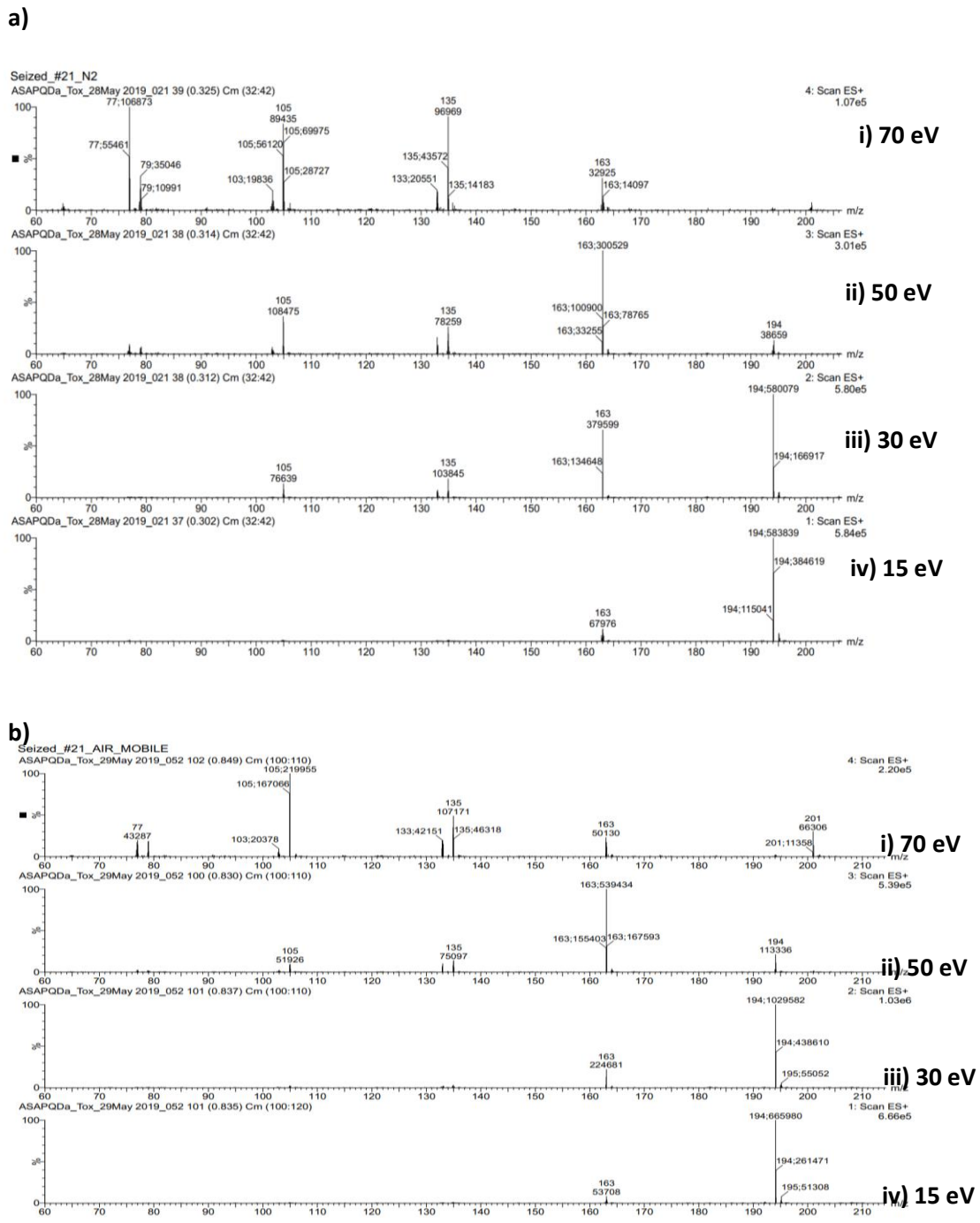

Figure 7-9 Spectra obtained for 3,4-Methylenedioxymethamphetamine analysed (a) in the clean environment of a mass spectrometry laboratory with a high-grade dry nitrogen supply (left) and (b) in a non-laboratory environment with air supplied by diaphragm pump (right)

The increase in signal with air is proposed to be due to the increase in protic solvent in the ionisation region. The laboratory nitrogen is dry, but the limited water vapour (or residual solvent vapour from the sample loading) is still sufficient to direct the ionisation mechanism to protonation. In switching to air drawn in from a damp, non-air conditioned environment, the high levels of moisture provide an excellent source from which to proton transfer to the volatilised analyte.

Close comparison of the analyses performed in nitrogen with air show that the level of background chemcial noise is greater for the experiments performed in air, with the baseline TIC in the 15 eV mode reaching 5.65×10^5 counts in nitrogen as compared to 2.73×10^6 in the non-laboratory air condition.

It is also relevant to note that the total time from powering on the instrument to pumping down, self-calibrating and being ready to analyse samples was less than 10 minutes, demonstrating the rapid deployability of this instrument in a non-laboratory setting.

The source of this chemical noise is thought to be a combination of environmental molecules drawn in with the air plus some contamination from a rubber hose connecting the gas supply from the pump to the mass spectrometer.

While the increased background represents a disadvantage, this is somewhat mitigated by the increased signal for the analytes of interest, but it is important that in future work with this or similar systems the effects of environmental changes be closely monitored, especially with regards to their effect on the capability of library search-based analysis of spectra.

7.3.3 Mixture analysis

The issue of adulteration of one drug with another is one that presents significant health dangers, with drugs often being sold either accidentally contaminated with other drugs or deliberately ‘cut’ with a cheaper drug to increase the profits to the seller. The contamination of heroin and cocaine with fentanyl, a highly potent synthetic opioid has been linked to significant numbers of drug related

deaths in the USA[118] and is an area of growing concern for health services and police in the UK. To investigate the capabilities of the small footprint instrument to analyse mixtures, 50 µg/mL standards of different compounds were mixed at different ratios as shown in Table 7-2.

Table 7-2 Results of mixture experiments

Mixture (Minor/Major)	1:1	1:10	1:100	1:1000
Fentanyl/Cocaine	✓	✓	✓	×
Fentanyl/Diacetylmorphine	✓	✓	✓	✓
Fentanyl/Caffeine	✓	✓	×	×
Paramethoxy-N-methylamphetamine/3,4-Methylenedioxymethamphetamine	✓	✓	×	×
Ketamine/Monosodium glutamate	✓	✓	×	×
Amphetamine/Caffeine	✓	✓	×	×
Cocaine/Benzocaine	✓	✓	✓	×

Fentanyl was notably detectable at a 1 to 1000 ratio with diacetylmorphine (heroin), the drug it is most commonly found to be a contaminant of, which is an encouraging result as it would present a significant advance in the ability to rapidly and reliably detect fentanyl contamination in heroin in-situ, which could be of significant help to first responders when dealing with an unknown substance. The suppression of the fentanyl signal by caffeine, however, represents an area of concern as caffeine has been commonly found to be cut with heroin and could therefore serve to mask fentanyl signals. It should be emphasised that these tests were run with dilute standards of the compounds of interest, as it was not practical to secure samples of the controlled substances as solids, and as such it is likely that in a real field deployment of the technology, a higher concentration would be

introduced to the instrument, meaning that these results serve to indicate potential rather than as an assessment of the limits of the instrument when it comes to mixture analysis.

7.3.4 Library searching

The ability to automatically detect the components of both simple and mixed samples was thus a desirable feature for an instrument in the proposed application to have, and to this end a simple library search system was developed in google sheets, whereby the peak list for each cone voltage could be pasted into the sheet, a variable thresholding equation applied to remove background noise by zeroing out peaks below a user-determined multiple of the average with a graphical representation used to allow the user to vary the multiple to select a reasonable number of signals for analysis, and the remaining signals searched against a database of known signals.

The library search would then assign a score based on the presence of the molecular ion, which was found to be present in every substance analysed and the number of other signals present for a given compound, modified by the frequency at which those signals appeared in the library so that a common fragment like $[C_6H_5]^+$ would contribute far less to the score for a given result than a more uncommon fragment. The result was a system which produced scores for each of a library of compounds, allowing for easy identification of any of the compounds in a sample.

In order to allow the identification of multiple compounds at differing concentrations, a second stage whereby the signals for an already identified compound could be removed from the spectrum (by setting the intensity at those values to zero) the thresholding process repeated with the new spectrum and the library search rerun with the new set of signals.

This method was shown to be able to detect mixtures of cocaine and fentanyl as shown in Figure 7-8, with it able to detect both compounds from the spectrum of 1 part fentanyl in 100 parts cocaine, matching the results when analysed by eye.

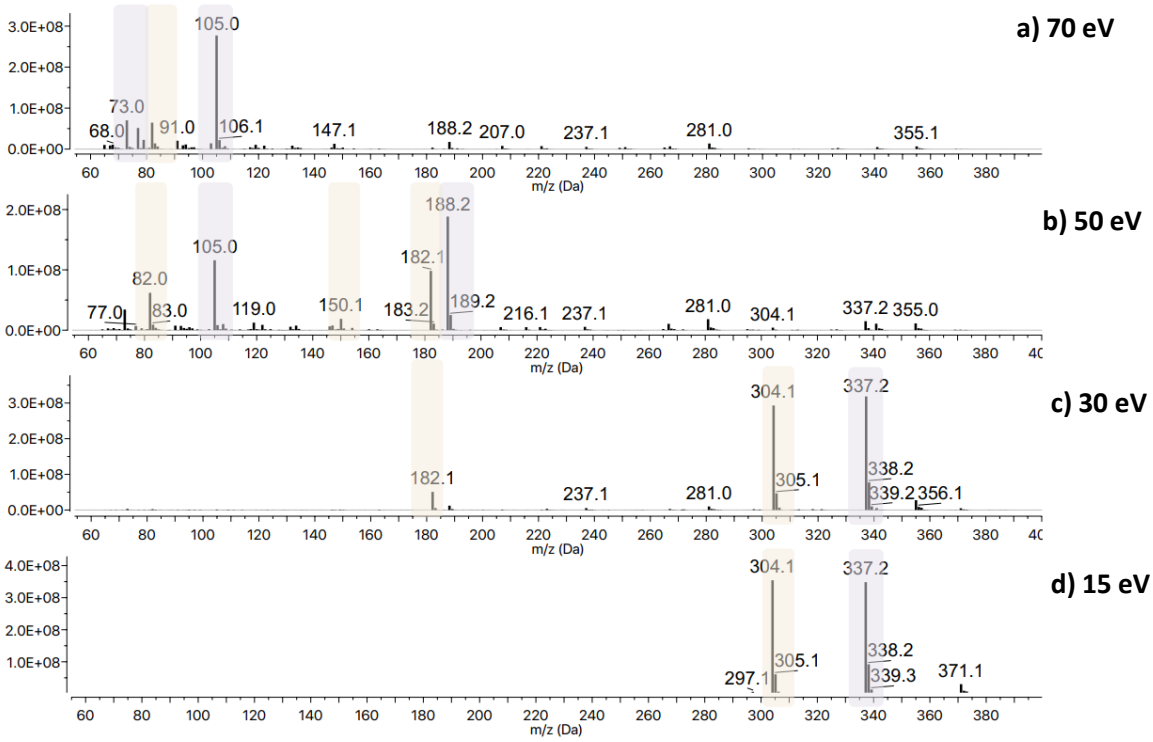

Figure 7-10 Spectrum of a cocaine:fentanyl mixture, signals identified as arising from fentanyl highlighted in purple, signals identified as arising from cocaine highlighted in gold.

7.4 Conclusion

This chapter provides significant evidence to suggest that ASAP MS, and in particular transportable ASAP MS, represents a good prospect for further research into in-situ identification of drugs.

For 'street' drugs and drugs hauls seized by the authorities, it has been shown that known drugs can be identified by ASAP-MS with ease. In addition, the extent of the information provided by this mass spectrometry approach enables new drugs to be characterised in the field and potential identification of these compounds to be suggested, providing rapid information for emergency services and allowing easy identification of samples of interest for full characterisation.

As well as showing the capability of the technique for analysing samples of interest, the deployability of the single quadrupole instrument and its ability to work outside of a laboratory setting without a nitrogen supply have been demonstrated. This capability, along with the rapid setup reported and the ability shown to detect drug compounds in mixed samples make it promising candidate for a deployable system to be added to the toolkit of techniques used in field testing environments.

8 Conclusion

The concept of a combined, on-line MS and NMR reaction monitoring system based around the use of benchtop instruments has been explored, and the fundamental idea behind using orthogonal techniques on smaller, less individually capable instruments to provide a more robust overall system than could be managed with a more capable (and significantly more expensive) single instrument has been borne out overall.

Nevertheless, the inherent issues of the techniques involved, while each to some degree compensated for by the merits of the other, remain and these techniques do not by any means represent a panacea for the problem of reaction monitoring. They do, however, represent significant additions to the toolkit of any chemist hoping to be able to rapidly characterise reactions in situ, as they allow for a drop-in system which is capable of quickly providing reliable information on the progress of a reaction.

The use of 19F NMR for reaction monitoring on the benchtop, while limited by sensitivity issues in this particular instrument, represents a promising avenue for further research as the instrumentation continues to be developed, as it has the potential to expand the range of reactions to which the benchtop NMR may be applied.

The use of transportable ASAP-MS on a single quadrupole instrument for the identification of drug compounds also presents a promising area for further development, both in the use of ASAP-MS in this specific application and more generally in that the ability to have a deployable ambient MS instrument running without nitrogen or other infrastructure has great potential for expanding the analytical capabilities of mobile laboratory setups in general. The rapid setup, minimal infrastructure requirements, simple sample loading and rapid data acquisition available with such a system make for a compelling package, as they would produce rich data suitable for expert interrogation, but are

also amenable to automated analysis against libraries to provide a non-expert user with a rapid identification of known compounds.

In summation, small footprint MS and NMR have been shown, when paired together, to provide a powerful analytical tool, which, once validated has potential beyond that which has been explored in this work.

9 Future work

There remains much to be done in the area of small footprint MS and NMR monitoring, with rapid developments being made in the available equipment in both fields, the potential to expand the capabilities of a combined monitoring setup is significant.

Of particular interest on the NMR side is the development of small footprint instruments geared towards other nuclei, in particular those for ^{13}C and ^{31}P which have become available in recent years. The ^{13}C instrument would present an interesting case for investigation as a reaction monitoring instrument, though its utility may be limited by the low natural abundance of ^{13}C (1.107 % as compared to the 99.985% of ^{1}H), which would likely necessitate longer single experiment times. ^{31}P, by contrast, has a 100% natural abundance, and would be limited mainly by the requirement for its presence in the reaction to begin with, though for phosphorus containing reactions it would appear to be an attractive target. Care must be taken, however, to avoid direct comparison of signal integrals between signals in ^{31}P, as the signal integral does not depend solely on the concentration of the ^{31}P nucleus in a given chemical environment as it does for ^{1}H.

Improvements are also being made in the available field strength for benchtop NMR, with 80 MHz models now being offered and manufacturers working towards the goal of variable temperature NMR on benchtop instruments, which will by necessity mean overcoming many of the temperature control issues discussed in this work. These improvements will expand the applicability of the system to a greater range of reactions.

On NMR solvent suppression, further work on pulse sequences would be highly desirable, success has been reported in on-line suppression using more complex solvent suppression sequences, in particular a WET-180-NOESY pulse sequence, and it would be useful to investigate the capabilities of this sequence relative to software-based signal suppression and investigate its impact on the instrument duty cycle over a reaction monitoring experiment.

Improvements to the pump setup could also be made, with lower dead volume pumps potentially allowing for significant reductions in the time between sample extraction and analysis, and thus giving not only a closer representation of the conditions in the reaction but also access to even earlier stages of the reaction, as the present limiting factor on this score is the requirement to get the reaction mixture though the system, and a large portion of the dead volume is due to the pump internals.

A custom switching valve would also be a desirable addition, with the ability to vary the split ratios beyond those available on the MRA, as the system has often been operated at the practical limits of the dilutions available, and while makeup solvent flow rate can be increased to increase the dilution, the flow rate required to achieve dilutions beyond the 1:8000 used in this work quickly become impractical.

With regards to the use of transportable instrumentation for in-situ toxicological analysis, much work remains to be done in the field. This work is intended to serve as a proof of principle for the use of the small footprint ASAP instrument in this field, but much work must be done to build up libraries, refine the instrument design to integrate the air pump as a part of the instrument running off of the instrument power supply and controlled by the user through the instrument control software rather than the manually adjusted pump running from a 12V power supply that was used in this work, and to establish the capabilities of the instrument for quantitation of the active ingredients in drugs as well as the detection and profiling of non-active compounds which could potentially be a means for the providence of street drugs to be tracked and profiled, giving law enforcement groups useful information on what is being supplied where.

10 Bibliography

1 D. C. Hassell and E. M. Bow, *Appl. Spectrosc.*, 1998, **52**, 18A-29A.
2 L. L. Simon, H. Pataki, G. Marosi, F. Meemken, K. Hungerbühler, A. Baiker, S. Tummala, B. Glennon, M. Kuentz, G. Steele, H. J. M. Kramer, J. W. Rydzak, Z. Chen, J. Morris, F. Kjell, R. Singh, R. Gani, K. V. Gernaey, M. Louhi-Kultanen, J. O'Reilly, N. Sandler, O. Antikainen, J. Yliruusi, P. Frohberg, J. Ulrich, R. D. Braatz, T. Leyssens, M. von Stosch, R. Oliveira, R. B. H. Tan, H. Wu, M. Khan, D. O'Grady, A. Pandey, R. Westra, E. Delle-Case, D. Pape, D. Angelosante, Y. Maret, O. Steiger, M. Lenner, K. Abbou-Oucherif, Z. K. Nagy, J. D. Litster, V. K. Kamaraju and M.-S. Chiu, *Org. Process Res. Dev.*, 2015, **19**, 3–62.
3 I. Marziano, D. C. A. Sharp, P. J. Dunn and P. A. Hailey, *Org. Process Res. Dev.*, 2000, **4**, 357–361.
4 Online UV-visible spectroscopy and multivariate curve resolution as powerful tool for model-free investigation of laccase-catalysed oxidation. - Abstract - Europe PMC, http://europepmc.org/article/med/18157664, (accessed 9 August 2020).
5 M. Assirelli, W. Xu and W. Chew, *Org. Process Res. Dev.*, 2011, **15**, 610–621.
6 A. Ray, T. Bristow, C. Whitmore and J. Mosely, *Mass Spectrom. Rev.*, 2018, **37**, 565–579.
7 V. Sans, L. Porwol, V. Dragone and L. Cronin, *Chem. Sci.*, 2015, **6**, 1258–1264.
8 C. for D. E. and Research, PAT — A Framework for Innovative Pharmaceutical Development, Manufacturing, and Quality Assurance, http://www.fda.gov/regulatory-information/search-fda-guidance-documents/pat-framework-innovative-pharmaceutical-development-manufacturing-and-quality-assurance, (accessed 11 August 2019).
9 L. Olsson, U. Schulze and J. Nielsen, *TrAC Trends Anal. Chem.*, 1998, **17**, 88–95.
10 M. R. Walsh and M. A. LaPack, *ISA Trans.*, 1995, **34**, 67–85.
11 K. D. Cook, K. H. Bennett and M. L. Haddix, *Ind. Eng. Chem. Res.*, 1999, **38**, 1192–1204.
12 R. C. Johnson, N. Srinivasan, R. G. Cooks and D. Schell, *Rapid Commun. Mass Spectrom.*, 1997, **11**, 363–367.
13 R. C. Johnson, R. G. Cooks, T. M. Allen, M. E. Cisper and P. H. Hemberger, *Mass Spectrom. Rev.*, 2000, **19**, 1–37.
14 K. F. Hansen, S. Gylling and F. R. Lauritsen, *Int. J. Mass Spectrom. Ion Process.*, 1996, **152**, 143–155.
15 K. M. Jensen, M. H. Jensen and R. P. Cox, *FEMS Microbiol. Ecol.*, 1996, **20**, 101–109.
16 K. D. Duncan, E. P. B. McCauley, E. T. Krogh and C. G. Gill, *Rapid Commun. Mass Spectrom.*, 2011, **25**, 1141–1151.
17 C. R. Blakley and M. L. Vestal, *Anal. Chem.*, 1983, **55**, 750–754.
18 Guenther. Hambitzer and Joachim. Heitbaum, *Anal. Chem.*, 1986, **58**, 1067–1070.
19 K. J. Volk, R. A. Yost and A. Brajter-Toth, *Anal. Chem.*, 1992, **64**, 21A-33A.
20 Michael. Barber, R. S. Bordoli, G. J. Elliott, R. Donald. Sedgwick and A. N. Tyler, *Anal. Chem.*, 1982, **54**, 645–657.
21 R. M. Caprioli, *Biochemistry*, 1988, **27**, 513–521.
22 M. Dole, R. L. Hines, L. L. Mack, R. C. Mobley, L. D. Ferguson and M. B. Alice, *Macromolecules*, 1968, **1**, 96–97.
23 The Nobel Prize in Chemistry 2002, https://www.nobelprize.org/prizes/chemistry/2002/fenn/facts/, (accessed 13 July 2020).
24 V. W. S. Lee, Y.-L. Chen and L. Konermann, *Anal. Chem.*, 1999, **71**, 4154–4159.
25 P. Dell'Orco, J. Brum, R. Matsuoka, M. Badlani and K. Muske, *Anal. Chem.*, 1999, **71**, 5165–5170.

26 J. Brum, P. Dell'Orco, S. Lapka, K. Muske and J. Sisko, *Rapid Commun. Mass Spectrom.*, 2001, **15**, 1548–1553.
27 T. W. T. Bristow, A. D. Ray, A. O'Kearney-McMullan, L. Lim, B. McCullough and A. Zammataro, *J. Am. Soc. Mass Spectrom.*, 2014, **25**, 1794–1802.
28 T.-Y. Chen, J.-Y. Lin, J.-Y. Chen and Y.-C. Chen, *J. Am. Soc. Mass Spectrom.*, 2010, **21**, 1547–1553.
29 T.-Y. Chen, C.-S. Chao, K.-K. T. Mong and Y.-C. Chen, *Chem. Commun.*, 2010, **46**, 8347–8349.
30 X. Yan, E. Sokol, X. Li, G. Li, S. Xu and R. G. Cooks, *Angew. Chem. Int. Ed.*, 2014, **53**, 5931–5935.
31 D. S. Cho, S. C. Gibson, D. Bhandari, M. E. McNally, R. M. Hoffman, K. D. Cook and L. Song, *Rapid Commun. Mass Spectrom.*, 2011, **25**, 3575–3580.
32 N. Holmes, G. R. Akien, R. J. D. Savage, C. Stanetty, I. R. Baxendale, A. J. Blacker, B. A. Taylor, R. L. Woodward, R. E. Meadows and R. A. Bourne, *React. Chem. Eng.*, 2016, **1**, 96–100.
33 D. Fabris, *Mass Spectrom. Rev.*, 2005, **24**, 30–54.
34 L. A. Colnago, F. D. Andrade, A. A. Souza, R. B. V. Azeredo, A. A. Lima, L. M. Cerioni, T. M. Osán and D. J. Pusiol, *Chem. Eng. Technol.*, 2014, **37**, 191–203.
35 J. J. Grimaldi and B. D. Sykes, *Rev. Sci. Instrum.*, 1975, **46**, 1201–1205.
36 D. A. Foley, E. Bez, A. Codina, K. L. Colson, M. Fey, R. Krull, D. Piroli, M. T. Zell and B. L. Marquez, *Anal. Chem.*, 2014, **86**, 12008–12013.
37 D. A. Foley, J. Wang, B. Maranzano, M. T. Zell, B. L. Marquez, Y. Xiang and G. L. Reid, *Anal. Chem.*, 2013, **85**, 8928–8932.
38 D. A. Foley, A. L. Dunn and M. T. Zell, *Magn. Reson. Chem.*, 2016, **54**, 451–456.
39 J. C. Edwards, *Magn. Reson. Chem.*, 2016, **54**, 492–493.
40 Application of Quantitative 19F and 1H NMR for Reaction Monitoring and In Situ Yield Determinations for an Early Stage Pharmaceutical Candidate | Analytical Chemistry, https://pubs.acs.org/doi/10.1021/ac202287y, (accessed 31 August 2020).
41 A. Chanda, A. M. Daly, D. A. Foley, M. A. LaPack, S. Mukherjee, J. D. Orr, G. L. Reid, D. R. Thompson and H. W. Ward, *Org. Process Res. Dev.*, 2015, **19**, 63–83.
42 A. W. Owen, E. A. J. McAulay, A. Nordon, D. Littlejohn, T. P. Lynch, J. S. Lancaster and R. G. Wright, *Anal. Chim. Acta*, 2014, **849**, 12–18.
43 I. A. Buryakov, *J. Anal. Chem.*, 2011, **66**, 674.
44 R. A. Crocombe, *Appl. Spectrosc.*, 2018, **72**, 1701–1751.
45 E. de Hoffmann and V. Stroobant, *Mass Spectrometry: Principles and Applications*, John Wiley & Sons, 2013.
46 M. Barber, R. S. Bordoli, R. D. Sedgwick and A. N. Tyler, *J. Chem. Soc. Chem. Commun.*, 1981, 325–327.
47 K. Tanaka, H. Waki, Y. Ido, S. Akita, Y. Yoshida, T. Yoshida and T. Matsuo, *Rapid Commun. Mass Spectrom.*, 1988, **2**, 151–153.
48 Michael. Karas, Doris. Bachmann and Franz. Hillenkamp, *Anal. Chem.*, 1985, **57**, 2935–2939.
49 D. J. Weston, R. Bateman, I. D. Wilson, T. R. Wood and C. S. Creaser, *Anal. Chem.*, 2005, **77**, 7572–7580.
50 Z. Takáts, J. M. Wiseman, B. Gologan and R. G. Cooks, *Science*, 2004, **306**, 471–473.
51 A. Cappiello, G. Famiglini, F. Mangani and P. Palma, *Mass Spectrom. Rev.*, 2001, **20**, 88–104.
52 F. H. Field, *Acc. Chem. Res.*, 1968, **1**, 42–49.
53 J. Mosely, .
54 C. N. McEwen, R. G. McKay and B. S. Larsen, *Anal. Chem.*, 2005, **77**, 7826–7831.

55 C. Petucci and J. Diffendal, *J. Mass Spectrom.*, 2008, **43**, 1565–1568.
56 D. M. Garcia, S. K. Huang and W. F. Stansbury, *J. Am. Soc. Mass Spectrom.*, 1996, **7**, 59–65.
57 F. Hillenkamp, M. Karas, R. C. Beavis and B. T. Chait, *Anal. Chem.*, 1991, **63**, 1193A-1203A.
58 R. Zenobi and R. Knochenmuss, *Mass Spectrom. Rev.*, 1998, **17**, 337–366.
59 M. K. and and R. Krüger, Ion Formation in MALDI, https://pubs.acs.org/doi/pdf/10.1021/cr010376a, (accessed 13 July 2020).
60 R. Knochenmuss, *Analyst*, 2006, **131**, 966–986.
61 N. B. Cech and C. G. Enke, *Mass Spectrom. Rev.*, 2001, **20**, 362–387.
62 D. C. Taflin, T. L. Ward and E. J. Davis, *Langmuir*, 1989, **5**, 376–384.
63 L. Konermann, E. Ahadi, A. D. Rodriguez and S. Vahidi, *Anal. Chem.*, 2013, **85**, 2–9.
64 J. V. Iribarne, *J. Chem. Phys.*, 1976, **64**, 2287.
65 M. Wilm, *Mol. Cell. Proteomics MCP*, , DOI:10.1074/mcp.M111.009407.
66 H. Metwally, Q. Duez and L. Konermann, *Anal. Chem.*, 2018, **90**, 10069–10077.
67 R. Juraschek, T. Dülcks and M. Karas, *J. Am. Soc. Mass Spectrom.*, 1999, **10**, 300–308.
68 P. Kebarle and L. Tang, *Anal. Chem.*, 1993, **65**, 972A-986A.
69 M. Karas, U. Bahr and T. Dülcks, *Fresenius J. Anal. Chem.*, 2000, **366**, 669–676.
70 T. M. Annesley, *Clin. Chem.*, 2003, **49**, 1041.
71 J. L. Sterner, M. V. Johnston, G. R. Nicol and D. P. Ridge, *J. Mass Spectrom.*, 2000, **35**, 385–391.
72 R. Bonfiglio, R. C. King, T. V. Olah and K. Merkle, *Rapid Commun. Mass Spectrom.*, 1999, **13**, 1175–1185.
73 R. King, R. Bonfiglio, C. Fernandez-Metzler, C. Miller-Stein and T. Olah, *J. Am. Soc. Mass Spectrom.*, 2000, **11**, 942–950.
74 J. F. J. Todd, *Pure Appl. Chem.*, 1991, **63**, 1541–1566.
75 J. S. Brodbelt and J. J. Wilson, *Mass Spectrom. Rev.*, 2009, **28**, 390–424.
76 J. S. Brodbelt, L. J. Morrison and I. Santos, *Chem. Rev.*, 2020, **120**, 3328–3380.
77 A. R. Johnson and E. E. Carlson, *Anal. Chem.*, 2015, **87**, 10668–10678.
78 The role of electron capture dissociation in biomolecular analysis - Cooper - 2005 - Mass Spectrometry Reviews - Wiley Online Library, https://onlinelibrary.wiley.com/doi/abs/10.1002/mas.20014, (accessed 31 August 2020).
79 M.-S. Kim and A. Pandey, *PROTEOMICS*, 2012, **12**, 530–542.
80 D. F. Smith, D. C. Podgorski, R. P. Rodgers, G. T. Blakney and C. L. Hendrickson, *Anal. Chem.*, 2018, **90**, 2041–2047.
81 J. V. Olsen, L. M. F. de Godoy, G. Li, B. Macek, P. Mortensen, R. Pesch, A. Makarov, O. Lange, S. Horning and M. Mann, *Mol. Cell. Proteomics*, 2005, **4**, 2010–2021.
82 G. Hopfgartner, I. V. Chernushevich, T. Covey, J. B. Plomley and R. Bonner, *J. Am. Soc. Mass Spectrom.*, 1999, **10**, 1305–1314.
83 M. Guilhaus, D. Selby and V. Mlynski, *Mass Spectrom. Rev.*, 2000, **19**, 65–107.
84 M. Guilhaus, *J. Mass Spectrom.*, 1995, **30**, 1519–1532.
85 T. Wang, C. Chu, H. Hung, G. Kuo and C. Han, *Rev. Sci. Instrum.*, 1994, **65**, 1585–1589.
86 S. Guan and A. G. Marshall, *J. Am. Soc. Mass Spectrom.*, 1996, **7**, 101–106.
87 T. Kim, A. V. Tolmachev, R. Harkewicz, D. C. Prior, G. Anderson, H. R. Udseth, R. D. Smith, T. H. Bailey, S. Rakov and J. H. Futrell, *Anal. Chem.*, 2000, **72**, 2247–2255.
88 P. J. Hore, *Nuclear Magnetic Resonance*, Oxford University Press, 2nd edn., 2015.
89 F. Bloch, *Phys. Rev.*, 1946, **70**, 460–474.
90 R. K. Harris, E. D. Becker, de M. S. M. Cabral, R. Goodfellow and P. Granger, *Pure Appl. Chem.*, 2001, **73**, 1795–1818.
91 Waters QDa technical manual, *Waters Corp.*

92 Waters Introduces SYNAPT G2-S Mass Spectrometer, Combining Revolutionary StepWave Ion Optics With Ion Mobility Technology Taking Performance to New Level : Waters, https://www.waters.com/waters/newsDetail.htm?locale=en_us&id=134622528&cid=134528064, (accessed 13 July 2020).
93 *Waters Corporation.* .
94 H. C. Brown, O. H. Wheeler and K. Ichikawa, *Tetrahedron*, 1957, **1**, 214–220.
95 R. Earl. Davis and J. Ann. Gottbrath, *J. Am. Chem. Soc.*, 1962, **84**, 895–898.
96 G. R. Fulmer, A. J. M. Miller, N. H. Sherden, H. E. Gottlieb, A. Nudelman, B. M. Stoltz, J. E. Bercaw and K. I. Goldberg, *Organometallics*, 2010, **29**, 2176–2179.
97 Waters Webinar transcript, https://www.waters.com/webassets/cms/events/docs/us_events/2015_us_events/LiveQDaQ_A_transcriptNov12.pdf, accessed 18/02/2021
98 A. L. Van Geet, *Anal. Chem.*, 1968, **40**, 2227–2229.
99 D. A. Foley, A. L. Dunn and M. T. Zell, *Magn. Reson. Chem. MRC*, 2016, **54**, 451–456.
100 Y.-G. Zhao, Y. Zhang, F.-L. Wang, N. Chen, C.-Y. Lou, K. Zhang, M.-C. Jin and Y. Zhu, *Anal. Methods*, 2017, **9**, 4234–4239.
101 I. Hahnenstein, H. Hasse, C. G. Kreiter and G. Maurer, *Ind. Eng. Chem. Res.*, 1994, **33**, 1022–1029.
102 D. Smith and P. Španěl, *Mass Spectrom. Rev.*, 2005, **24**, 661–700.
103 C. J. Craven and J. P. Waltho, *J. Magn. Reson. B*, 1995, **106**, 40–46.
104 U. L. Günther, C. Ludwig and H. Rüterjans, *J. Magn. Reson.*, 2002, **156**, 19–25.
105 I. Daubechies, *Ten Lectures on Wavelets*, Society for Industrial and Applied Mathematics, Philadelphia, PA, USA, 1992.
106 C. Cobas, *Magn. Reson. Chem.*, 2018, **56**, 1140–1148.
107 A. Ross, G. Schlotterbeck, F. Dieterle and H. Senn, in *The Handbook of Metabonomics and Metabolomics*, eds. J. C. Lindon, J. K. Nicholson and E. Holmes, Elsevier Science B.V., Amsterdam, 2007, pp. 55–112.
108 D. I. Hoult, *J. Magn. Reson. 1969*, 1976, **21**, 337–347.
109 B. Gouilleux, B. Charrier, S. Akoka and P. Giraudeau, *Magn. Reson. Chem.*, 2017, **55**, 91–98.
110 N. Rozatian, I. W. Ashworth, G. Sandford and D. R. W. Hodgson, *Chem. Sci.*, 2018, **9**, 8692–8702.
111 T. P. Forbes and E. Sisco, *Analyst*, 2018, **143**, 1948–1969.
112 F. C. Measham, *Int. J. Drug Policy*, 2019, **67**, 102–107.
113 C. V. Giné, I. F. Espinosa and M. V. Vilamala, *Drug Test. Anal.*, 2014, **6**, 819–824.
114 M. J. Barratt, M. Kowalski, L. Maier and A. Ritter, *Drug Policy Model. Program Bull.*
115 Discussions with Loop Senior Scientist
116 S. A. Barker, J. Borjigin, I. Lomnicka and R. Strassman, *Biomed. Chromatogr.*, 2013, **27**, 1690–1700.
117 S. S. Johansen and J. L. Jensen, *J. Chromatogr. B Analyt. Technol. Biomed. Life. Sci.*, 2005, **825**, 21–28.
118 Products - Data Briefs - Number 356 - January 2020, https://www.cdc.gov/nchs/products/databriefs/db356.htm, (accessed 27 August 2020).

Appendix 1: Mass Rate Attenuator settings

Setting number	Cycle Frequency (Hz)	Transfer volume (uL)
4	0.227	0.022
12	0.227	0.022
13	0.303	0.022
22	0.303	0.022
23	0.303	0.022
24	0.385	0.022
25	0.385	0.022
26	0.455	0.022
34	0.455	0.022
35	0.556	0.022
36	0.588	0.022
37	0.588	0.022
38	0.769	0.022
39	0.769	0.022
45	0.769	0.022
46	0.769	0.022
47	0.769	0.022
48	1.111	0.022
49	1.111	0.022
50	1.111	0.022
51	1.429	0.022
55	1.429	0.022
56	1.429	0.022
57	1.429	0.022
58	1.429	0.022
59	2.000	0.022
1	0.500	0.100
5	0.500	0.100
6	0.625	0.100
7	0.667	0.100
14	0.667	0.100
15	0.667	0.100
16	0.667	0.100
17	0.833	0.100
27	0.833	0.100
28	1.000	0.100
29	1.000	0.100
30	1.250	0.100
40	1.250	0.100
41	1.250	0.100
42	1.250	0.100
43	1.667	0.100
44	1.667	0.100
52	1.667	0.100
53	1.667	0.100
54	2.000	0.100
2	0.833	0.300
3	0.833	0.300
8	0.833	0.300
9	1.111	0.300
10	1.111	0.300
11	1.111	0.300
18	1.111	0.300
19	1.429	0.300
20	1.667	0.300
21	1.667	0.300
31	2.222	0.300
32	2.222	0.300
33	2.222	0.300

Appendix 2- Summary of analysed drugs from city centre testing

Sample ID	Believed identity as given by the submitter	Identity determined by MS	Identity determined by FT-IR	ASAP MS signals (*m/z*)	LC-MS signals (G2S Synapt)	Notes on sample
F0075	'DMT' (N,N-Dimethyl Tryptamine)	N,N-Dimethyl Tryptamine (By both ASAP and LCMS)	N,N-Dimethyl Tryptamine	189.1387 $[M+H]^+$ (15 eV, 30 eV, 50 eV) 144.0814 $[M+H-NMe_2]^+$ (15 eV, 30 eV, 50 eV, 70 eV)	189.1392 $[M+H]^+$ 144.0814 $[M+H-NMe_2]^+$	Off-white powder
F0076	'MDMA' (3,4-Methylenedioxymethamphetamine)	3,4-Methylenedioxymethamphetamine (By both ASAP and LCMS)	3,4-Methylenedioxymethamphetamine	194.1183 $[M+H]^+$ (15 eV, 30 eV, 50 eV, 70 eV), 163.0762 $[M+H-NHMe]^+$ (15 eV, 30 eV, 50 eV, 70 eV), 135.0454 $[M+H-C_3H_8N]$ (15 eV, 30 eV, 50 eV, 70 eV) 105.0702 $[M+H- C_5H_{10}NO_2]$ (15 eV, 30 eV, 50 eV, 70 eV)	194.1185 $[M+H]^+$ 163.0765 $[M+H-NHMe]^+$ 135.0452 $[M+H-C_3H_8N]$ 105.0704 $[M+H- C_5H_{10}NO_2]$	Pill

Appendix 2- Summary of analysed drugs from city centre testing

Sample ID	Believed identity as given by the submitter	Identity determined by MS	Identity determined by FT-IR	ASAP MS signals (*m/z*)	LC-MS signals (G2S Synapt)	Notes on sample
F0077	'MDMA' (3,4-Methylenedioxymethamphetamine)	3,4-Methylenedioxymethamphetamine (By both ASAP and LCMS)	3,4-Methylenedioxymethamphetamine	194.1170 $[M+H]^+$ (15 eV, 30 eV, 50 eV, 70 eV), 163.0758 $[M+H-NHMe]^+$ (15 eV, 30 eV, 50 eV, 70 eV), 135.0427 $[M+H-C_3H_8N]$ (15 eV, 30 eV, 50 eV, 70 eV), 105.0699 $[M+H- C_5H_{10}NO_2]$ (15 eV, 30 eV, 50 eV, 70 eV)	194.1176 $[M+H]^+$ 163.0759 $[M+H-NHMe]^+$ 135.0448 $[M+H-C_3H_8N]$ 105.0700 $[M+H- C_5H_{10}NO_2]$	Pill with 'Beats' logo.
F0078	Cocaine	Cocaine (by both ASAP and LCMS)	Cocaine	304.1555 (30 eV, 50 eV, 70 eV) $[M+H]^+$ 182.1188 (30 eV, 50 eV, 70 eV) $[M+H-C_7H_6O_2]^+$	304.1553 $[M+H]^+$ 182.1183 $[M+H-C_7H_6O_2]^+$	White powder
F0084	'N,N-DMT' (N,N-Dimethyl Tryptamine)	DMT (by both ASAP and LCMS)	DMT	189.1401 $[M+H]^+$ (15 eV, 30 eV, 50 eV) 144.0809 $[M+H-NMe_2]^+$ (15 eV, 30 eV, 50 eV, 70 eV)	189.1391 $[M+H]^+$ 144.0816 $[M+H-NMe_2]^+$	Off-white powder

Appendix 2- Summary of analysed drugs from city centre testing

Sample ID	Believed identity as given by the submitter	Identity determined by MS	Identity determined by FT-IR	ASAP MS signals (*m/z*)	LC-MS signals (G2S Synapt)	Notes on sample
F0085	MDMA (3,4-Methylenedioxymethamphetamine)	3,4-Methylenedioxymethamphetamine (by both ASAP and LCMS)	3,4-Methylenedioxymethamphetamine	194.1208 $[M+H]^+$ (15 eV, 30 eV, 50 eV, 70 eV), 163.0785 $[M+H-NHMe]^+$ (15 eV, 30 eV, 50 eV, 70 eV), 135.0444 $[M+H-C_3H_8N]$ (15 eV, 30 eV, 50 eV, 70 eV), 105.0703 $[M+H- C_5H_{10}NO_2]$ (15 eV, 30 eV, 50 eV, 70 eV)	194.1181 $[M+H]^+$ 163.0763 $[M+H-NHMe]^+$ 135.0448 $[M+H-C_3H_8N]$ 105.0700 $[M+H- C_5H_{10}NO_2]$	Pill
F0086	Ketamine	2-Fluorodeschloroketamine by both ASAP and LCMS	Ketamine (low confidence score on library search)	222.1242 $[2\text{-FDCK+H}]^+$ (15 eV, 30 eV, 50 eV, 70 eV) 204.1203 $[2\text{-FDCK+H-F}]^+$ (50 eV, 70 eV) 191.0889 (30 eV, 50 eV, 70 eV) 163.0914 (30 eV, 50 eV, 70 eV) 109.0448 (50 eV, 70 eV)	222.1299 $[2\text{-FDCK+H}]^+$ 204.1189 $[2\text{-FDCK+H-F}]^+$ 191.0874 163.0923 109.0455	White powder

Appendix 2- Summary of analysed drugs from city centre testing

Sample ID	Believed identity as given by the submitter	Identity determined by MS	Identity determined by FT-IR	ASAP MS signals (*m/z*)	LC-MS signals (G2S Synapt)	Notes on sample
F0087	LSD (Lysergic acid diethylamide)	Lysergic acid diethylamide (by LCMS, no determination possible by ASAP due to sample contamination, probably due to inks and or finger oil residues in the blotter paper)	Not possible due to sample format	Large numbers of peaks with no clear relation to the LSD. Peaks seen in LCMS could not be found at any voltage.	324.2068 223.1229 208.0768 180.0809 167.0728 See figure 7-4 for fragments.	Sample submitted on blotter paper
F0091	'MDMA' (3,4-Methylenedioxymethamphetamine)	Chloroquine by ASAP and LCMS	Chloroquine	320.1884 $[M+H]^+$ (15 eV, 30 eV, 50 eV, 70 eV) 247.0995 (50 eV, 70 eV) $[M+H-NEt_2]$	320.1894 $[M+H]^+$ 247.0999 $[M+H-NEt_2]$ 160.5988 $[M+H-C_{10}H_{12}N_2]$	Off-white crystals
F0092	'4-HO-MET' (4-hydroxy-N-methyl-N-ethyltryptamine)	4-hydroxy-N-methyl-N-ethyltryptamine by ASAP and LCMS	Not possible due to sample format	219.1504($[M+H]^+$ (15 eV, 30 eV, 50 eV, 70 eV) 160.0759 $[M+H-C_3H_9N]$ 30 eV, 50 eV, 70 eV)	219.1495 $[M+H]^+$ 160.0761 $[M+H-C_3H_9N]$	Sample submitted as a portion of a gummy bear.

Appendix 2- Summary of analysed drugs from city centre testing

Sample ID	Believed identity as given by the submitter	Identity determined by MS	Identity determined by FT-IR	ASAP MS signals (*m/z*)	LC-MS signals (G2S Synapt)	Notes on sample
F0093	'4-AcO-DMT' (4-Acetoxy-N,N-dimethyltryptamine)	4-Acetoxy-N,N-dimethyltryptamine by ASAP and LCMS	Not possible due to sample format	247.1469 $[M+H]^+$ (15 eV, 30 eV, 50 eV, 70 eV) 205.1353 $[M+H-NMe_2]$ (30 eV, 50 eV, 70 eV) 160.0771 $[M+H-AcO-NMe_2]^+$ (50 eV, 70 eV)	247.1433 $[M+H]^+$ 160.0769 $[M+H-AcO-NMe_2]^+$	Sample submitted as a portion of a gummy bear.
F0095	LSD (Lysergic acid diethylamide)	No LSD present, 25D-NBOMe, a NPS hallucinogen, was identified	No determination possible due to sample format	316.1910 (15 eV, 30 eV, 50 eV, 70 eV) 193.1227 (30 eV, 50 eV, 70 eV) 178.1003 (50 eV, 70 eV)	316.1910 193.1228 178.0993	Sample submitted on blotter paper
F0112	Ketamine	Ketamine by both ASAP and LCMS	Ketamine	238.1003 $[M+H]^+$ (15 eV, 30 eV, 50 eV, 70 eV) 220.0892 $[M+H-H_2O]^+$ (30 eV, 50 eV, 70 eV) 207.0577 $[M+H-CH_3NH]^+$ (30eV, 50 eV, 70 eV) 178.0628 Ring contraction after loss of $NHCH_3$ (50 eV, 70 eV)	238.0996 $[M+H]^+$ 220.0892 $[M+H-H_2O]^+$ 207.0577 $[M+H-CH_3NH]^+$ 178.0628 Ring contraction after loss of $NHCH_3$	White powder.

Appendix 2- Summary of analysed drugs from city centre testing

Sample ID	Believed identity as given by the submitter	Identity determined by MS	Identity determined by FT-IR	ASAP MS signals (*m/z*)	LC-MS signals (G2S Synapt)	Notes on sample
F0113	'Speed' (Amphetamine)	Caffeine and one unknown compound.	Caffeine	195.0871 Caffeine $[M+H]^+$ (30 eV, 50 eV, 70 eV) 138.0669 $[M+H\text{-}OCNCH_3]^+$ (50 eV, 70 eV)	195.0924 Caffeine $[M+H]^+$ 138.0669 $[M+H\text{-}OCNCH_3]^+$	Brown granules
F0114	Cocaine	Cocaine by LCMS and ASAP	Unknown.	304.1557 $[M+H]^+$ (15 eV, 30 eV, 50 eV, 70 eV) 182.1186 $[M+H\text{-}OCOC_6H_5]^+$ (30 eV, 50 eV, 70 eV)	304.1555 $[M+H]^+$ 182.1186 $[M+H\text{-}OCOC_6H_5]^+$	White powder
F0116	Ketamine	Creatine by LCMS, ASAP inconclusive.	Creatine	Large numbers of signals, none characteristic of Ketamine or Creatine.	132.0775 Creatine $[M+H]^+$	White powder, poorly soluble

Appendix 2- Summary of analysed drugs from city centre testing

Sample ID	Believed identity as given by the submitter	Identity determined by MS	Identity determined by FT-IR	ASAP MS signals (*m/z*)	LC-MS signals (G2S Synapt)	Notes on sample
F0119 **F0119 (cont.)**	Heroin (Diacetylmorphine)	Caffeine, paracetamol, diacetylmorphine and noscapine by both ASAP and LCMS	Caffeine, paracetamol and diacetylmorphine	152.0712 Paracetamol $[M+H]^+$ (15 eV, 30 eV, 50 eV, 70 eV) 195.0859 Caffeine $[M+H]^+$ (15 eV, 30 eV, 50 eV, 70 eV) 138.0667 Caffeine $[M+H\text{-}OCNCH_3]^+$ (70 eV) 370.1646 Heroin $[M+H]^+$ (15 eV, 50 eV, 70 eV) 414.1554 Noscapine $[M+H]^+$ (15 eV 30 eV, 50 eV, 70 eV)	152.0711 Paracetamol $[M+H]^+$ 195.0884 Caffeine $[M+H]^+$ 138.0667 Caffeine $[M+H\text{-}OCNCH_3]^+$ 370.1664 Heroin $[M+H]^+$ 414.1559 Noscapine $[M+H]^+$	Yellowish crystals

Appendix 2- Summary of analysed drugs from city centre testing

Sample ID	Believed identity as given by the submitter	Identity determined by MS	Identity determined by FT-IR	ASAP MS signals (*m/z*)	LC-MS signals (G2S Synapt)	Notes on sample
F0120	Heroin (Diacetylmorphine)	Caffeine, paracetamol, diacetylmorphine and noscapine by both ASAP and LCMS	Caffeine, paracetamol and diacetylmorphine	152.0719 Paracetamol $[M+H]^+$ (15 eV, 30 eV, 50 eV, 70 eV) 195.0877 Caffeine $[M+H]^+$ (15 eV, 30 eV, 50 eV, 70 eV) 138.0669 Caffeine $[M+H\text{-}OCNCH_3]^+$ (50 eV, 70 eV) 370.1655 Heroin $[M+H]^+$ (15 eV, 30 eV, 50 eV, 70 eV) 414.1555 Noscapine $[M+H]^+$ (15 eV 30 eV, 50 eV, 70 eV)	152.0721 Paracetamol $[M+H]^+$ 195.0933 Caffeine $[M+H]^+$ 138.0671 Caffeine $[M+H\text{-}OCNCH_3]^+$ 370.1763 Heroin $[M+H]^+$ 414.1628 Noscapine $[M+H]^+$	Yellowish crystals